Mapping relative risk to seabirds from offshore wind energy developments in Danish waters

Technical Report from DCE – Danish Centre for Environment and Energy no. 331 2024

AARHUS
UNIVERSITY
DCE – DANISH CENTRE FOR ENVIRONMENT AND ENERGY

Mapping relative risk to sea-birds from offshore wind energy developments in Danish waters

Technical Report from DCE – Danish Centre for Environment and Energy No. 331 2024

Saana Isojunno[1]
Lindesay Scott-Hayward[1]
Claus Lunde Pedersen[2]
Heidi Thomsen[2]
Jordan Chetcuti[2]
Morten Frederiksen[2]
Thomas Bregnballe[2]
Jacob Sterup[2]
Rasmus Due Nielsen[2]
Monique McKenzie[1]
Ib Krag Petersen[2]

[1] CREEM, School of Mathematics and Statistics, University of St Andrews
[2] Aarhus University, Department of Ecoscience

AARHUS
UNIVERSITY
DCE – DANISH CENTRE FOR ENVIRONMENT AND ENERGY

Data sheet

Series title and no.:	Technical Report from DCE – Danish Centre for Environment and Energy No. 331
Category:	Scientific advisory report
Title:	Mapping relative risk to seabirds from offshore wind energy developments in Danish waters

Author(s):	Saana Isojunno[1], Lindesay Scott-Hayward[1], Claus Lunde Pedersen[2], Heidi Maria Thomsen[2], Jordan Chetcuti [2], Morten Frederiksen [2], Thomas Bregnballe [2], Jacob Sterup [2], Monique MacKenzie[1], Ib Krag Petersen[2]
Institution(s):	[1] CREEM, School of Mathematics and Statistics, University of St Andrews [2] Aarhus University, Department of Ecoscience.

Publisher:	Aarhus University, DCE – Danish Centre for Environment and Energy ©
URL:	https://dce.au.dk/en
Year of publication:	January 2025
Editing completed:	January 2025
Referee(s):	Anthony David Fox
Quality assurance, DCE:	Jesper Fredshavn and Camilla Uldal
External comments:	Find comments here
Financial support:	Energistyrelsen.
Please cite as:	Isojunno, S., Scott-Hayward, L., Pedersen, C.L., Thomsen, H.M., Chetcuti, J., Frederiksen, M., Bregnballe, T., Sterup, J., MacKenzie, M. Petersen, I.K. 2024. Mapping relative risk to seabirds from offshore wind energy developments in Danish waters. Aarhus University, DCE – Danish Centre for Environment and Energy, 101 pp. Technical Report No. 331

Abstract: Based on 243 days of aerial Distance Sampling line transect surveys of birds in Danish marine areas over the past 24 years we developed this risk assessment algorithm for birds and offshore wind farm development. The assessment was based on abundance estimates from 17 marine bird species and their susceptibility towards offshore wind farm development. Using habitat, displacement and collision risk layers we classified the Danish marine areas in least and greatest risk of impacts to marine birds.

Keywords:	Seabird, offshore wind farm, spatial planning, sensitivity analysis, risk assessment, risk ranking.
Front page photo:	Flying long-tailed ducks in snow. Photo by Rasmus Due Nielsen.
ISBN:	978-87-7156-929-2
ISSN (electronic):	2244-999X
Number of pages:	101

Contents

Executive summary

The aim of this work was to develop a spatial planning tool to identify sensitive marine areas where seabirds would be most at risk from future offshore wind energy developments. Conversely, the aim was to identify areas where future development would have the least impact on seabirds.

Sensitivity mapping approaches and outcomes vary widely and so it is important to define the outcomes of such assessments. A more nuanced approach, using sensitivity mapping for the selection of areas for future development, should help decrease risks to seabirds and, by avoiding the most sensitive areas, reduce the consenting risk for developers.

We developed an approach to sensitivity mapping with the objective to rank Danish marine areas according to high vs low relative species risk. Relative species risks were quantified with respect to explicit assessment targets based on species conservation status. We considered three sources of risk (hazards): habitat alteration, displacement, and collision. The susceptibility of each species to each of these hazards was informed by published literature. In a precautionary approach, relative species risks to each hazard were combined by taking the maximum across each species, and across the three hazards. This means that for each mapped grid cell (1 x 1 km) the ranking combines the most vulnerable species to each hazard (defined by multiple parameters), and the highest-ranking areas across the three hazards. This produced a map of highest-ranking areas in Danish marine areas from which we can determine the most and least sensitive marine areas for future offshore wind development.

The initial implementation of the algorithm, presented here, used aerial survey data to estimate the distribution of seabirds. Most of this data was collected during the winter and spring months, which for migratory species is sufficient, but for resident species leaves a large temporal gap. We present some preliminary results of habitat use maps using GPS tracking data, which we plan to incorporate in the spatial risk-ranking approach in the future to improve temporal coverage. In addition, we also plan to incorporate migratory corridors which are important to improve the assessment of the collision risk hazard.

The framework presented here has potential to be developed into an interactive tool for users (rather than static maps) and is also generalizable so could include other taxa and hazards.

Resumé

Formålet med denne rapport var at udvikle et rumligt planlægningsværktøj der kan bruges til at identificere følsomme marine områder, hvor havfugle vil være mest udsatte for fremtidige udviklinger inden for havvindenergi. Endeligt var formålet at identificere marine områder, hvor fremtidig havvindudvikling vil have den mindste påvirkning på havfugle.

Tilgangene og resultaterne inden for følsomhedskortlægning kan variere betydeligt. Det er derfor vigtigt at definere resultaterne af sådanne vurderinger, så det bliver klart, hvordan valget af områder til fremtidig udvikling kan mindske/øge risici for havfugle i en bestemt forvaltnings- og politisk kontekst.

Nærværende rapport udviklede en tilgang til følsomhedskortlægning med det formål at rangere danske havområder efter høj vs. lav relativ artsrisiko. Den relative artsrisiko blev kvantificeret med hensyn til eksplicitte vurderingsmål baseret på arters bevaringsstatus og tre kilder til risiko (trusler): habitatændring, fortrængning og kollision. Den enkelte arts sårbarhed over for hver af disse trusler blev baseret på offentlig tilgængelig litteratur. Ved at benytte et forsigtighedsprincip blev de relative artsrisici for hver trussel kombineret ved at tage den maksimale risiko på tværs af hver art og de tre trusler. Dette betyder, at for hver kortlagt kvadrat (1 x 1 km) er rangeringen en kombination af den mest sårbare art for hver trussel (defineret ved flere parametre) og de højest rangerede områder på tværs af de tre trusler. Dette resulterede i et kort over de højest rangerede områder i danske havområder, hvorfra vi kan bestemme de mest og mindst følsomme marine områder for fremtidig havvindudvikling.

Den første implementering af algoritmen, som præsenteres her, anvendte data fra flyundersøgelser til at estimere havfuglenes udbredelsesområde. Størstedelen af disse data blev indsamlet i vinter- og forårsmånederne, hvilket er tilstrækkeligt for trækfugle, men efterlader et stort tidsmæssigt hul for ynglefugle. Derudover præsenteres nogle foreløbige resultater af habitatudnyttelseskort ud fra GPS-trackingdata, som vi planlægger at inkorporere i en fremtidig udgave af den rumlige risikorangeringsmetode. Dette vil kunne forbedre den tidsmæssige dækning. Derudover planlægger vi også at inkludere trækkorridorer, som er vigtige for at forbedre vurderingen af risikoen for kollision.

Den tilgang, der præsenteres her, har potentiale til at blive videreudviklet til et interaktivt værktøj til brugere (i stedet for statiske kort). Derudover er det muligt at generalisere den, så den kan inkludere andre arter og trusler.

Preface

Background for the report and relation to other activities

This report contributes to the project "*Environmental mapping and screening of the offshore wind potential in Denmark*" initiated in 2022 by the Danish Energy Agency. The project aims to support the long-term planning of offshore wind farms by providing a comprehensive overview of the combined offshore wind potential in Denmark. It is funded under the Finance Act 2022 through the programme "Investeringer i et fortsat grønnere Danmark" (Investing in the continuing greening of Denmark). The project is carried out by NIRAS, Aarhus University (Department of Ecoscience) and DTU Wind.

The overall project consists of four tasks defined by the Danish Energy Agency (https://ens.dk/ansvarsomraader/vindmoeller-paa-hav/planlaegning-af-fremtidens-havvindmoelleparker) :

- Sensitivity mapping of nature, environmental, wind and hydrodynamic conditions.
- Technical screening and assessment. to identify the most suitable areas for development of offshore wind energy in Danish marine areas.
- Assessment of potential cumulative effects from large-scale offshore wind development in Denmark and neighbouring countries.
- Assessment of barriers and potentials in relation to coexistence.

This report addresses one component of Task 1: sensitivity mapping. Specifically, it provides an overview of areas within Danish offshore regions that are likely to be particularly vulnerable to offshore wind farm development regarding birds and based on existing data. Other subjects within Task 1—such as fish, marine mammals, bats, benthic habitats, wind and hydrodynamics and ecosystem modelling — will be presented in separate reports in late 2024 and early 2025. A synthesis of all topics under Task 1 will be published in 2025.

The project has relied predominantly on historical data, with minimal new data collection. As a result, the sensitivity mapping is largely dependent on the availability and accessibility of pre-existing data across specific subject areas. From the outset, significant effort was made to incorporate all relevant data to comprehensively address the task requirements. However, certain existing datasets could not be accessed. Appendix 4 specifies the data sources used in the sensitivity mapping for seabirds and outlines additional existing data. It is important to recognise that sensitivity mapping serves as a dynamic tool, which can be updated as new data becomes available. Owing to the technical nature of the work in the report, all key terms are defined at their first use in the text and with a glossary in Appendix 1 for reference.

The project management teams at both AU and NIRAS have contributed to the description of the background for the report and the relation to other activities in the preface. The report and the work contained within are solely the responsibility of the authors.

Background to the sensitivity mapping approach

Sensitivity maps have been developed for a wide range of marine species, including seabirds and marine mammals, to inform spatial planning of offshore activities (Garthe & Hüppop, 2004; Furness et al., 2013; Bradbury et al., 2014; Certain et al., 2015; Kelsey et al., 2018; Best & Halpin, 2019; Verling et al., 2021; Fauchald et al., 2024). Sensitivity mapping exercises involve combining spatial distribution information from multiple species to indicate areas potentially sensitive to human activities. While algorithms vary, the contribution of each species is usually weighted by the level of concern for the population status and resilience, as well as the species susceptibility to hazards, such as displacement and collision risk. These weights are typically informed by multiple lines of heterogenous evidence (e.g., vital rates, habitat flexibility, flight manoeuvrability) and expressed on likert-scale or ordinal scores (e.g., low-to-high on a scale of 1-5). Besides sensitivity maps, such ordinal rankings are commonly used to generate semi-quantitative risk matrices in a "weight-of-evidence" approach to environmental risk assessment (Cox et al., 2005; Anthony Cox, 2008; Linkov et al., 2009). Such semi-quantitative approaches are widely used in broad-scale, strategic environmental risk assessments to screen and rank levels of concern for potential species impacts (Linkov et al., 2009; Tamis et al., 2016; Stelzenmüller et al., 2020). Risk-based approaches to environmental assessment are popular because they are consistent with risk management frameworks and administrative processes that require risk managers to consider both the likelihood and potential consequence of unwanted events (Gibbs & Browman, 2015; Verling et al., 2021). In this report, we express risk both relative to target protection levels for each species (hereafter, **relative species risk**), and then rank different areas in Danish marine waters by the highest relative species risk (hereafter, **spatially relative risk**). Sensitivity mapping exercises that aim to rank areas by combining species risks can be considered as spatially explicit risk-ranking algorithms (Box 1).

Box 1: Risk assessment. Broadly speaking, risk expresses the likelihood and consequence of unwanted outcome(s) (Appendix 1: Glossary). In environmental risk assessment, the unwanted outcome can be defined, for example, as unwanted health effects to individuals, or deterioration of population status. The likelihood and consequence of such changes can be estimated in absolute terms however, this is often impractical due to lack of necessary data, or time/cost constraints. Relativistic risk assessments, including risk-ranking and relative risk approaches, circumvent the estimation of absolute risk. Risk-ranking approaches aim to express risk in ordinal terms, which focus on the identification of lowest and highest risk scenarios. By contrast, relative risk approaches express risks with respect to a reference, benchmark level. Unlike categorical ranking of risk, continuous measures of relative risk allow magnitude comparisons between levels of risk.

While sensitivity maps for seabird species in offshore areas have been widely published, there is currently no agreed best-practice algorithms for generating these. Different authors have proposed different algorithms and arithmetic operations to combine vulnerability scores to weights, and how these species-specific weights and distribution data are then combined to produce overall sensitivity maps for the receptor group. For example, Certain et al. (2015) proposed a community vulnerability index, derived from Hill's diversity index (Hill, 1973), that could be interpreted as the number of equally abundant and fully vulnerable species to a given pressure type at a given location. The authors derived species-specific vulnerability to collision and displacement by scaling 10 ordinal scores, building upon previously published vulnerability and sensi-

tivity factors (e.g., Furness et al., 2013). A key conceptual advance was the consideration of "primary factors" that drive vulnerability or sensitivity of a population, and "aggravation factors" that mediate pre-existing vulnerability (Certain et al., 2015). However, no justification is provided for the proposed function to calculate species-specific vulnerability/sensitivity based on these factors. More generally, different arithmetic operations on ordinal scores carry different, often unarticulated, assumptions about their units, linearity, additivity and multiplicativity. When the calculation does not attempt to replicate the causal pathway of impact on each population, the outcome of the calculation, aiming to reflect the relative vulnerability of each species, may not scale linearly with potential population-level impacts.

To our knowledge, no published sensitivity mapping approaches have been quantitatively validated for seabirds. However, for seabird sensitivity to offshore wind development, the ranking of species-specific susceptibility to displacement and collision risk have been qualitatively scrutinized and refined by multiple research groups over the last two decades (Garthe & Hüppop, 2004; Furness et al., 2013; Bradbury et al., 2014; Certain et al., 2015; Kelsey et al., 2018; Fauchald et al., 2024). With accumulating empirical evidence and quantitative evidence syntheses (e.g., Avian Displacement Guidance Committee, 2024; Lamb et al., 2024) becoming available, there is substantial potential for an increasing degree of consensus on the expected impacts and level of concern for each species and key life history contexts.

In the present work, we develop a spatially explicit risk-ranking algorithm that aims to build on these existing sensitivity mapping approaches, while aiming to address some of the key caveats. With the proposed algorithm, we set out to achieve the following:

- Formulate explicit assessment objectives and target protections for each species.
- Produce maps that rank Danish marine areas according to high vs low species risk relative to the assessment targets
- Minimize the risk of impact on any species of concern; high risk for one species at any given location should not be compensated by a low risk for another species of equal conservation concern.
- As well as displacement and collision risk, consider the risk of habitat alteration through overlap with core use areas for each species.

Furthermore, we aimed, where possible, to move away from the qualitative treatment of quantitative data typical of previous sensitivity mapping approaches. To achieve this, we developed a quantitative assessment algorithm in which 1) input parameters for each species can be directly informed by empirical studies, 2) species-specific risks are quantified in a way that aim to replicate the causal pathways of impact on each population, and 3) uncertainty is propagated through the algorithm by re-sampling of the input parameters.

The developed spatial risk-ranking algorithm succeeded in achieving each of these objectives. The highest- and lowest-ranking areas and associated uncertainty are provided in Figure 2.7 in the Results section, we demonstrate the steps that were taken to produce this relative risk map, including the influence of key input parameters and assumptions. The Discussion provides further guidance on the interpretation of the map, with an emphasis on aspects of seabird sensitivity that are yet to be implemented in the algorithm, but pave way for further development and future iterations of the relative risk mapping approach.

Summary

To identify the most suitable areas for development of offshore wind energy in Danish marine areas, the Danish Energy Agency, in 2022, initiated a project to support the long-term planning of future offshore wind farms in Denmark. This report evaluates the relative risks to seabirds posed by offshore wind energy developments in Danish waters, focusing on habitat alteration, displacement, and collision risks.

Using a spatial risk-ranking algorithm, this report aims to identify the highest- versus lowest-sensitivity areas based on seabird distributions and abundances derived from aerial surveys conducted between 2000 and 2024. The algorithm combines species density distribution estimates with species-specific assessment targets and susceptibility to risks (habitat alteration, collision, displacement), producing maps highlighting zones where future offshore wind development could have relatively high impacts. Data on bird distributions and abundances were collected using the Distance Sampling line transect method (Buckland et al., 2001), comprising 243 aerial surveys conducted over 203 different days and covering more than 150,000 km of transects and more than 230,000 species detections. These surveys focused on capturing distributions of non-breeding birds. An overview of the data set is provided in Appendix 4.

Coastal and shallow areas showed the highest sensitivity in terms of potential habitat alteration and displacement risk in case of future wind energy development. These areas had high concentrations of divers, grebes and seaducks, and contained core habitats that wind farm structures and associated activities may disrupt. Seabirds susceptible to displacement, such as divers and some species of sea ducks, were particularly at risk, as these species tended to avoid areas around wind farms. These findings underscore the importance of protecting coastal and shallow areas with high seabird density, especially those designated as Special Protection Areas (SPAs).

Furthermore, offshore areas were identified as having higher relative collision risk, especially for species such as kittiwakes and other gull species, which are more prone to flying at heights within turbine blade sweep areas. The mapping identified particular offshore regions as high-risk zones for these species.

Additional data can provide extra information for the risk mapping exercise. For example, the current version of this work uses previously published expert assessment of collision risk for each species. However, GPS tracking data from birds can provide empirical information on migration routes and foraging activity. Such data from key species of colonial breeding birds during the 2023-2024 breeding seasons highlighted additional areas that could be at risk by illustrating marine area use patterns for sensitive species.

In conclusion, this relativistic risk assessment framework, grounded in quantitative assessment targets and species-specific susceptibility to risks, provides a decision-making tool for future wind farm planning to minimise ecological impacts on Denmark's seabird populations. Recommendations emphasise continued data collection and refinement of species-specific input parameters to enhance reliability of the algorithm, ultimately supporting a balanced approach to wind energy expansion and seabird conservation in Danish waters.

Sammenfatning

Med henblik på at identificere de mest egnede områder til fremtidige udbygning af havvind i Danmark igangsatte Energistyrelsen i 2022 et projekt for at understøtte langsigtet planlægning af fremtidige havvindmølleparker i Danmark. Nærværende rapport vurderer de relative risici for havfugle i forbindelse med udvikling af havvindenergi i danske farvande, med fokus på ændringer i levesteder, fortrængning og kollisionsrisici.

Ved hjælp af en rumlig risikorangeringsalgoritme sigter denne rapport mod at identificere områder med den højeste og laveste følsomhed baseret på havfuglenes udbredelse og antal, indsamlet fra optællinger af fugle fra fly og udført mellem 1999 og 2024. Algoritmen kombinerer disse artsfordelingesestimater med artspecifikke bedømmelsesmål og sårbarhed overfor risikofaktorer (habitatændring, kollision og fortrængning), og producerer kort, der identificerer zoner, hvor fremtidig havvindudvikling kan have relativ stor indvirkning på fugle. Data om fuglenes udbredelse og antal blev indsamlet ved hjælp af Distance Sampling linjetransektmetoden, bestående af 243 optællinger af fugle fra fly udført over 203 forskellige dage og dækkende mere end 150.000 km transekter og mere end 230.000 fugleobservationer. Disse optællinger fokuserede på at afdække fuglenes udbredelse udenfor yngletiden. Et overblik over data kan findes i Appendix 4.

Kystnære og lavvandede områder udviste de højeste følsomheder overfor potentielle ændringer af levesteder og risici for fortrængning i forbindelse med fremtidig havvindudvikling. Disse områder havde høje koncentrationer af lappedykkere, skalleslugere og havdykænder og omfattede kerneområder, som eventuelle vindmølleanlæg og tilknyttede aktiviteter ville kunne påvirke. Havfugle med høj følsomhed over for fortrængning, såsom lommer og visse arter af havdykænder, var særligt udsatte, da disse arter havde tendens til at undgå områder i og omkring vindmølleparker. Disse resultater understreger vigtigheden af at beskytte kystnære og lavvandede områder med høj havfugletæthed, især de områder, der er udpeget som særlige beskyttelsesområder (Fuglebeskyttelsesområder).

Desuden blev offshore-områder identificeret som havende højere relativ kollisionsrisici, især for arter som rider og andre mågefugle, der har større tendens til at flyve i samme højder som turbinebladene. Kortlægningen identificerede særlige offshore-regioner som højrisikozoner for disse arter.

Vurderingerne af kollisionsrisici er baseret på tidligere offentliggjorte ekspertvurderinger af kollisionsrisiko for hver art. GPS-sporingsdata fra fugle, som giver empirisk information om individuelle migrationsruter og fourageringsaktiviteter, er tilvejebragt, og kan forbedre algoritmen i en kommende version. Sådanne data for kolonirugende arter, sporet i 2023 og 2024, bidrog til følsomhedskortlægningen baseret på deres brug af marine områder. Yderligere data kan tilføre ekstra information til risikokortlægningsøvelsen. For eksempel anvender den nuværende version af dette arbejde tidligere offentliggjorte ekspertvurderinger af kollisionsrisiko for hver art, men GPS-sporingsdata fra fugle kan give empirisk information om migrationsruter og fourageringsaktiviteter. Sådanne data fra centrale arter af kolonirugende fugle fra ynglesæsonerne 2023-2024 kan yderligere forbedre de rumlige kort ved at kortlægge følsomme arters anvendelse af det marine miljø i sommerperioden.

Afslutningsvis giver denne relative risikovurderingstilgang, baseret på risikorelaterede beskyttelsesniveauer, kvantitative screeningsmål og sårbarhedsfaktorer for hver havfugleart, et beslutningsværktøj til fremtidig planlægning af placering af havvindmølleparker med henblik på at minimere økologiske påvirkninger på Danmarks havfuglebestande. Anbefalingerne understreger behovet for fortsat dataindsamling af artspecifikke inputparametre for at forbedre algoritmens pålidelighed, hvilket i sidste ende understøtter en afbalanceret tilgang til udvidelse af vindenergi og bevaring af havfugle i danske farvande.

1 Methods

1.1 Spatial risk-ranking algorithm

1.1.1 Assessment objective

This analysis set out to identify areas that minimize risk to seabird species from potential future offshore wind developments. The objective was to provide a spatial representation of relative risk, with each grid value representing the risk of impact to those seabird species addressed in the assessment, relative to all other grid locations on the map. To incorporate multiple seabird species with different conservation status, risks were expressed relative to species-specific assessment targets, which quantified the desired level of protection for each population and associated habitat in the study area. The multi-species assessment also required the inclusion of species-specific susceptibility to hazards associated with offshore wind development. Three hazards were considered, each with different pathways of impact: alteration of core habitat through presence of wind farm structures and associated vessels, displacement through behavioural avoidance of wind farms and associated maintenance traffic, and injury or death through collision with wind turbines. Relative risk maps were generated for each of the three hazards, informed by the species-specific assessment targets, input parameters related to species susceptibility to hazards, and the species abundance and distribution in the study area estimated from aerial line transect surveys (Figure 1.1). Barrier effects with respect to commuting and migration pathways were not included in the maps quantitatively, however, we present relevant colony and tracking data for colonial breeding birds and discuss areas that may be at greater risk due to these effects in the Discussion.

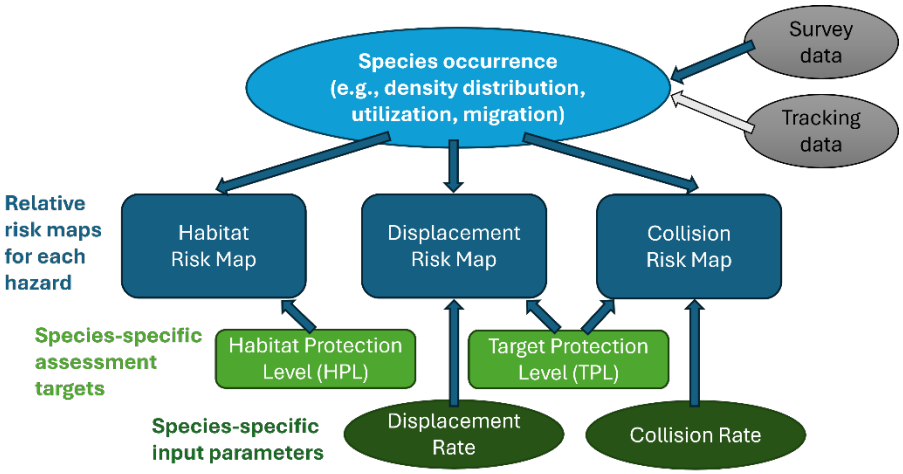

Figure 1.1. Conceptual overview of the approach to map relative risks. The spatial distribution of risks from the three hazards (shown in dark blue) was informed by the spatial occurrence of species (light blue). Data sources are shown in grey: aerial survey data were used to inform the implemented algorithm (dark blue arrows). Tracking data were analysed to inform species space utilization, but this data source did not inform the implemented algorithm at this stage. Species-specific input parameters (dark green) were used to calculate expected risks for each species and hazard. To bring species risks to the same scale relative to assessment targets, target protection levels were specified for each species (TPL) and their habitat (HPL).

1.1.2 Assessment targets

We define risk with respect to two assessment targets: Target Protection Level (TPL) and habitat protection level (HPL). Assessment targets were specified for each species or species group that were analysed together as a species unit in the spatial risk-ranking algorithm. The modelled species units could include one or multiple ecologically similar species identifiable from aerial surveys. The individual species included within each species unit are listed in Table 1.1 and explained in further detail in the section 1.2.1.

The TPL describes the desired level of complete protection for each species unit in Danish national waters, given current population status, trends, and resilience to existing threats. Specifically, the TPL was defined as the proportion of the current population size in the national waters that should be protected from any additional habitat loss, mortality, and impaired reproduction, to maintain or achieve favourable conservation status. For example, in case of an endangered population, where the aim is to avoid any additional impact, the TPL would be set at 100%. The aim of the TPL is to reflect the capacity of the population to cope with additional threats, independent of the type of threat or hazard. In the present work, we express TPL as proportion of the estimated population abundance for each species unit in the Danish EEZ marine region covered by aerial line transect surveys. However, the same principle could be applied to other definitions of populations or sub-populations should they be included in the assessment.

In addition to TPL, we considered the proportion of each species' range that should be protected from any additional habitat alteration, the Habitat Protection Level (HPL). The aim of the HPL was to reflect the dependence of each species on spatially limited resources and was used to ringfence core areas from further wind energy development for each species. In the present work, we defined a single HPL for each species unit, averaging across different seasons that the species unit was expected to be present in the Danish national waters (see section 1.2.1). Seasonally varying species distributions and associated variation in HPL would be possible to implement in future versions of the algorithm.

To account for existing levels of protection for each species, the TPL was adjusted to reflect estimated species abundance outside any Special Protection Areas (SPAs) designated for each species. This assumed that SPA designation had 100% effectiveness in achieving the TPL for the proportion of the population within the protected areas. For example, if the TPL for a species unit was set at 0.8, but half of the total estimated abundance fell within SPAs designated for one or more species in the unit, the TPL was adjusted to 0.4 outside the designated areas.

1.1.3 Quantifying relative species risk

Relative risk of each hazard (habitat alteration, displacement, collision) for each modelled species unit i and spatial location x was expressed as a risk ratio. In clinical trials, risk ratios are often used to express incidence rates of effects, or outcomes, between treatment and control conditions. Similarly, here, risk ratios were calculated between the expected outcomes at each spatial location should a hypothetical future wind farm be placed there (treatment/numerator) and "allowable" outcomes based on the assessment targets for each species unit (control/denominator). The expected outcomes were calculated for three metrics, one for each hazard: the degree of overlap between

core habitat and the hypothetical wind farm, the expected number of birds at risk of displacement, and the expected number of birds at risk of collision. Risk ratio values of > 1 could therefore be interpreted as the expected outcome exceeding allowable levels by this factor value. Conversely, risk ratios < 1 would indicate that the allowable thresholds have not been exceeded. Species-unit-specific values for HPL and TPL were used to calculate the denominator for each hazard, enabling comparisons of relative risk between the modelled species units with different assessment targets (hereafter referred to as "relative species risk").

The relative species risk of exceeding the HPL threshold (h_i^*) for each species unit i and grid location x was calculated as the risk ratio

$$R_{h[i,x]} = \frac{q_{i,x}}{(1 - h_i^*)}$$

where $q_{i,x}$ is the habitat overlap metric, representing the degree of habitat overlap with species unit i in a hypothetical future scenario where a wind farm footprint would cover the 1x1 km grid cell area at the location x. More specifically, $q_{i,x}$ was quantified as the fraction of the species range with a lower density than the estimated density in the grid cell $n_{i,x}$. Species range was defined as the area predicted to contain 0.95 (i.e., 95%) of the species unit's abundance in the study area. Thus, $q_{i,x}$ represents the species' usage of the grid location relative to its range. $R_{h[i,x]}$ was set to its maximum value within any designated SPAs and a surrounding buffer zone, defined by the expected spatial extent of displacement for the species (β_i). In other words, each species unit was ringfenced a core area based on its distribution and HPL, and any additional areas under SPA designations.

The relative species risk of collision and displacement were expressed as the ratio between the expected number of affected individuals as the assessment metric for each grid cell, and the proportion of the population outside any designated SPAs that was allowable to impose the risk (1-TPL_a). Similar to the habitat overlap metric, the expected number of birds at risk of collision at any grid location x was calculated for a hypothetical future scenario where a wind farm footprint would cover the 1x1 km grid cell area at the location x. By contrast, the expected number of displaced birds was calculated for a point source of disturbance at location x, which could displace birds both at the grid location x and its neighbouring cells, depending on the expected spatial extent of displacement for the species unit. With the main objective being spatial risk-ranking, we did not consider different scenarios for wind farm characteristics such as turbine size, spacing or footprint areas.

For collision and displacement, the species risk ratios were calculated respectively as

$$R_{c[i,x]} = \frac{\lambda_i \cdot n_{i,x}}{(N_i - \Delta N_i) \cdot (1 - p_i^*)}$$

and

$$R_{d[i,x]} = \frac{\sum_m^M n_{i,m} \cdot \alpha_i}{(N_i - \Delta N_i) \cdot (1 - p_i^*)}$$

Where for each species unit i, p_i^* is the adjusted target protection level outside SPAs (TPL_a), N_i is the estimated abundance in the study area, and ΔN_i is the abundance of the species unit within any SPAs designated for the unit species. The numerator in each equation aimed to reflect the number of birds potentially at risk from a hypothetical future wind farm placed at a grid location x. For collision risk, this was calculated as the product of proxy collision rate (λ_i) and the estimated density for each species unit in each grid cell $n_{i,x}$. In other words, the number of birds at risk of collision was specified to increase linearly with bird density at any given location. For displacement, the number of susceptible individuals was calculated as the product of displacement rate (α_i) and the estimated species unit density summed over M grid cells in the neighbourhood of each grid location x. The neighbourhood was specified as a circle with a radius equal to the spatial extent of displacement of each species unit, β_i. In other words, the number of birds susceptible to displacement was calculated as proportional to bird density in the neighbourhood of each grid cell, where the neighbourhood size depended on the expected spatial extent of displacement for each species unit.

1.1.4 Input parameters

For each modelled species unit, we set values for TPL (p_i^*), HPL (h_i^*), proxy collision rate (λ_i), proxy displacement rate (α_i), and the expected spatial extent of displacement (β_i). To allow comparisons of the developed spatial risk-ranking algorithm with previously published sensitivity mapping approaches, we aligned, where possible, the input parameters with previously published values (Furness et al., 2013; Certain et al., 2015; Fauchald et al., 2024).

The parameterization and use of the TPL in the algorithm was analogous to previous sensitivity mapping approaches that weight species maps by the level of concern for each population. Similarly, here we derived TPL from the European Red List of Birds (BirdLife International, 2021) (Table 1.1, Table 1.2). Because all the modelled species are expected to range outside Denmark, we based the TPL on a conservation listing at the European level, rather than at the national level. For example, common eider, classified as endangered, was set a TPL of 0.85. In other words, the algorithm aimed to protect 0.85 (i.e., 85%) of the eider population size from any exposure to displacement and collision. Conversely, the non-protected proportion (1-0.85 = 0.15) of the eider population was permitted a level of exposure to these hazards. Modelled species units that included any species classified as vulnerable (grebes, fulmar, velvet scoter, kittiwake) and near-threatened (merganser) were set TPL values of 0.8 and 0.7. The remaining species units were categorised as "least concern" and set a TPL of 0.65 (Table 1.2).

Table 1.1. Species included in the analysis. EURING = EURING species code, ITIS = Integrated Taxonomic Information System, Species unit = an abbreviated label indicating the species or species groups that were analysed together as an ecologically similar species unit in the spatial risk-ranking algorithm, IUCN = European vulnerability status under the IUCN classification (Birdlife International, 2021). LC = least concern, NT = near threatened, VU = vulnerable, EN = endangered

EURING	ITIS	Name (Danish)	Name (English)	Scientific name	Family	Species unit	IUCN
59		Lom sp.	Diver sp.	*Gavia sp.*	Gaviidae	Diver	
20	174474	Rødstrubet lom	Red-throated diver	*Gavia stellata*	Gaviidae	Diver	LC
30	174471	Sortstrubet lom	Black-throated diver	*Gavia arctica*	Gaviidae	Diver	LC
100	174479	Gråstrubet lappedykker	Red-necked grebe	*Podiceps grisegena*	Podicipedidae	Grebe	VU
90	174491	Toppet lappedykker	Great crested grebe	*Podiceps cristatus*	Podicipedidae	Grebe	LC
129		Lappedykker sp.	Grebe sp.	*Podicipedidae sp.*	Podicipedidae	Grebe	
220	174536	Mallemuk	Northern fulmar	*Fulmarus glacialis*	Procellariidae	Fulmar	VU
710	174712	Sule	Northern gannet	*Morus bassanus*	Sulidae	Gannet	LC
2180	175141	Hvinand	Goldeneye	*Bucephala clangula*	Anatidae	Goldeneye	LC
2120	175147	Havlit	Long-tailed duck	*Clangula hyemalis*	Anatidae	Longtailed	LC
2060	175155	Ederfugl	Common eider	*Somateria mollissima*	Anatidae	Eider	EN
2130	175171	Sortand	Common scoter	*Melanitta nigra*	Anatidae	Scoter	LC
2150	175163	Fløjlsand	Velvet scoter	*Melanitta fusca*	Anatidae	Velvetscoter	VU
2210	175187	Toppet skallesluger	Red-breasted merganser	*Mergus serrator*	Anatidae	Merganser	NT
5900	176832	Stormmåge	Common gull	*Larus canus*	Laridae	Gull	LC
5920	176824	Sølvmåge	Herring gull	*Larus argentatus agg.*	Laridae	Gull	LC
5910	176821	Sildemåge	Lesser black-backed gull	*Larus fuscus*	Laridae	LBBG	LC
6000	176815	Svartbag	Great black-backed gull	*Larus marinus*	Laridae	GBBG	LC
5780	824065	Dværgmåge	Little gull	*Hydrocoloeus minutus*	Laridae	Littlegull	LC
6020	176875	Ride	Black-legged kittiwake	*Rissa tridactyla*	Laridae	Kittiwake	VU
6150	176888	Fjordterne	Common tern	*Sterna hirundo*	Laridae	Tern	LC
6160	176890	Havterne	Arctic tern	*Sterna paradisaea*	Laridae	Tern	LC
6159		Hav/fjordterne	Arctic/Common tern		Laridae	Tern	
6110	176932	Splitterne	Sandwich tern	*Thalasseus sandvicensis*	Laridae	Tern	LC
6259		Terne sp.	Tern sp.	*Sterninae sp.*	Laridae	Tern	
6360	176971	Alk	Razorbill	*Alca torda*	Alcidae	Alcid	LC
6345		Alk/lomvie	Razorbill/Guillemot		Alcidae	Alcid	
6340	176974	Lomvie	Common guillemot	*Uria aalge*	Alcidae	Alcid	LC
6380	176985	Tejst	Black guillemot	*Cepphus grylle*	Alcidae	Alcid	LC

Table 1.2. Input parameters to the spatial risk-ranking algorithm, specific to each modelled species unit, alongside published vulnerability factors (Fauchald et al., 2024). Species unit = an abbreviated label indicating the species or species group that were analysed together as a unit in the risk-ranking algorithm (Table 1.1). Input parameters to the algorithm included target protection level (TPL), habitat protection level (HPL), displacement rate (α_i), spatial extent of displacement (β_i), and proxy collision risk ($\boldsymbol{\lambda_i}$). Previously published vulnerability factors (Fauchald et al., 2024) included vulnerability to collision (VC), avoidance score (h), habitat flexiblity score (k), and vulnerability to disturbance (VD), each provided on an ordinal scale 1-5. The input parameters HPL, α_i, and λ_i were informed by the published values for k, h, and VC, respectively, for the relevant species within each modelled species unit. When multiple values were reported for multiple species within the modelled species unit (e.g., divers), the average of reported values was used.

Input parameters							Fauchald et al. 2024				
Species unit	Status	TPL ($\boldsymbol{p_i^*}$)	HPL ($\boldsymbol{h_i^*}$)	$\boldsymbol{\alpha_i}$	$\boldsymbol{\beta_i}$	$\boldsymbol{\lambda_i}$	Relevant species	VC	h	k	VD
Diver	LC	0.65	0.40	0.50	10	0.38	*Gavia arctica, Gavia stellata*	1.9	5.0	4.0	4.5
Grebe	VU	0.80	0.30	0.50	10	0.34	*Podiceps grisegena*	1.7	5.0	3.0	4.0
Fulmar	VU	0.80	0.10	0.30	6	0.46	*Fulmarus glacialis*	2.3	3.0	1.0	2.0
Gannet	LC	0.65	0.10	0.50	10	0.70	*Morus bassanus*	3.5	5.0	1.0	2.0
Goldeneye	LC	0.65	0.40	0.40	8	0.50	*Bucephala clangula*	2.5	4.0	4.0	4.0
Longtailed	LC	0.65	0.40	0.30	6	0.64	*Clangula hyemalis*	3.2	3.0	4.0	3.5
Eider	EN	0.85	0.40	0.30	6	0.44	*Somateria mollissima*	2.2	3.0	4.0	3.5
Scoter	LC	0.65	0.40	0.50	10	0.30	*Melanitta nigra*	1.5	5.0	4.0	4.5
Velvet-scoter	VU	0.80	0.30	0.50	10	0.30	*Melanitta fusca*	1.5	5.0	3.0	4.0
Merganser	NT	0.75	0.40	0.40	8	0.44	*Mergus serrator*	2.2	4.0	4.0	4.0
Gull	LC	0.65	0.20	0.10	2	0.84	*Larus canus*	4.2	1.0	2.0	1.5
LBBG	LC	0.65	0.10	0.10	2	0.84	*Larus fuscus*	4.2	1.0	1.0	1.0
GBBG	LC	0.65	0.20	0.10	2	0.84	*Larus marinus*	4.2	1.0	2.0	1.5
Littlegull	LC	0.65	0.10	0.10	2	0.84	Not available in published literature, parameter values taken from *Larus fuscus*				
Kittiwake	VU	0.80	0.30	0.10	2	0.74	*Rissa tridactyla*	3.7	1.0	3.0	2.0
Tern	LC	0.65	0.30	0.10	2	0.74	*Sterna hirundo, Sterna paradisaea*	3.7	1.0	3.0	2.0
Alcid	LC	0.65	0.33	0.30	6	0.35	*Alca torda, Cepphus grylle, Uria aalge*	1.7	3.0	3.3	3.2

HPL values for each species unit were set based on "habitat flexibility" scores by Fauchald et al., 2024 (Table 1.2). Species that were considered the most dependent on the spatial distribution of their resources (divers, goldeneye, longtailed duck, common eider, common scoter, merganser) were set a HPL of 0.4. Thus, for each of these species, the top 0.4 of their home range area was ringfenced as not available to future development. Species that were considered most flexible in terms of the spatial distribution of their resources (northern fulmar, northern gannet, lesser black-backed gull and little gull) were set a HPL of 0.1. This translated to a larger proportion of their home range (1-0.1=0.9) being considered available to future development. Species with intermediate habitat flexibility were obtained HPL values by linear scaling of the vulnerability scores between the least and most flexible species (Table 1.2).

The rate and spatial extent of displacement were set directly proportional to the "vulnerability to disturbance" scores presented in Fauchald et al. (2024) (Table 1.2). The scaling was informed by previously published values and literature

reviews on the magnitude and spatial extent of species density reduction attributed to the proximity of operational wind farms (Dierschke et al., 2016; Welcker & Nehls, 2016; Avian Displacement Guidance Committee, 2024; Lamb et al., 2024). A recent quantitative meta-analysis by Lamb et al. (2024) supported previously published, more qualitative reviews (e.g., Dierschke et al., 2016) that suggested systematic displacement by divers, grebes, sea ducks, alcids, and gannets. A more mixed response, including both avoidance and attraction at different spatial scales, has been reported for several gull species (e.g., Vanermen et al., 2020; Lamb et al., 2024). As well as taxon, reported magnitude and spatial extent of displacement vary with season and study design, such as study area footprint and distance to reference area (Lamb et al., 2024). Studies with large survey area buffers (>10 km) have reported displacement and avoidance responses at these ranges (10-20 km) (Avian Displacement Guidance Committee, 2024). Similarly, reported magnitude of displacement vary between studies. In the German North Sea, diver abundance was estimated to decrease by 94% within windfarm footprint and 1 km zone, and by 52% within the footprint and 10 km zone (Garthe et al., 2023). In their review of displacement studies, Dierschke et al. (2016) grouped species with a change in abundance of >50% as strong, and ~50% as weak avoidance or attraction. We therefore specified the spatial extent and magnitude of displacement at 10 km and 50%, respectively, for the species that were scored to have the highest avoidance rates (divers, grebes, gannet, common and velvet scoter) by Fauchald et al. (2024). Species that were scored the lowest avoidance rates (gulls, kittiwake, and terns) by the same study were set to displace at 2 km neighbourhoods of each grid cell at a rate of 10%. Intermediate values were obtained by scaling the avoidance scores between these two extremes (Table 1.2).

As an interim approach, the collision parameter was set by linear scaling of the "vulnerability to collision" index in Fauchald et al. (2024) (Table 1.2). While the parameter values did not aim to reflect the absolute rate of birds at risk, the values for this parameter were assumed to be proportional to the actual collision rate, and that the number of birds at risk of collision for each species would increase linearly with the estimated density for each species unit at any given location.

1.1.5 Spatial risk-ranking algorithm and uncertainty

Relative risk maps were generated in four main steps (Figure 1.2). First, risk ratios were calculated in each grid cell of the study area based on the predicted density distributions for each of the 17 modelled species units. This created 17 risk ratio maps for each of the three hazards (habitat overlap, displacement, and collision). Next, a combined map of risk ratios was generated for each hazard by taking the maximum value for each grid cell across the species units. Maximum values were taken to ensure that a low relative risk for one species unit would not compensate for a high relative risk for another at any one location. This second step created three risk ratio maps, each representing maximum species risk at each grid location relative to the assessment targets. In a third step, the maximum risk ratio values were then translated to relative values in space. This was achieved by taking the quantiles of the risk ratio values across the prediction grid. The resulting values between 0-1 represent the ranking of each grid cell by their risk ratio value. For example, a quantile value of 0.95 at a grid location would indicate that 95% of the study area had lower risk ratio values than the value at the grid location. This translation to spatially relative risk was done to allow ranking of areas; the magnitudes of relative risk values were not interpreted due to the paucity of empirical data

available to inform some of the input parameters. Finally, in a fourth step, the spatially relative risk maps for each of the three hazards were combined. Maximum values were taken across the three maps, in order to present the highest-ranking areas across the three hazards with equal weight.

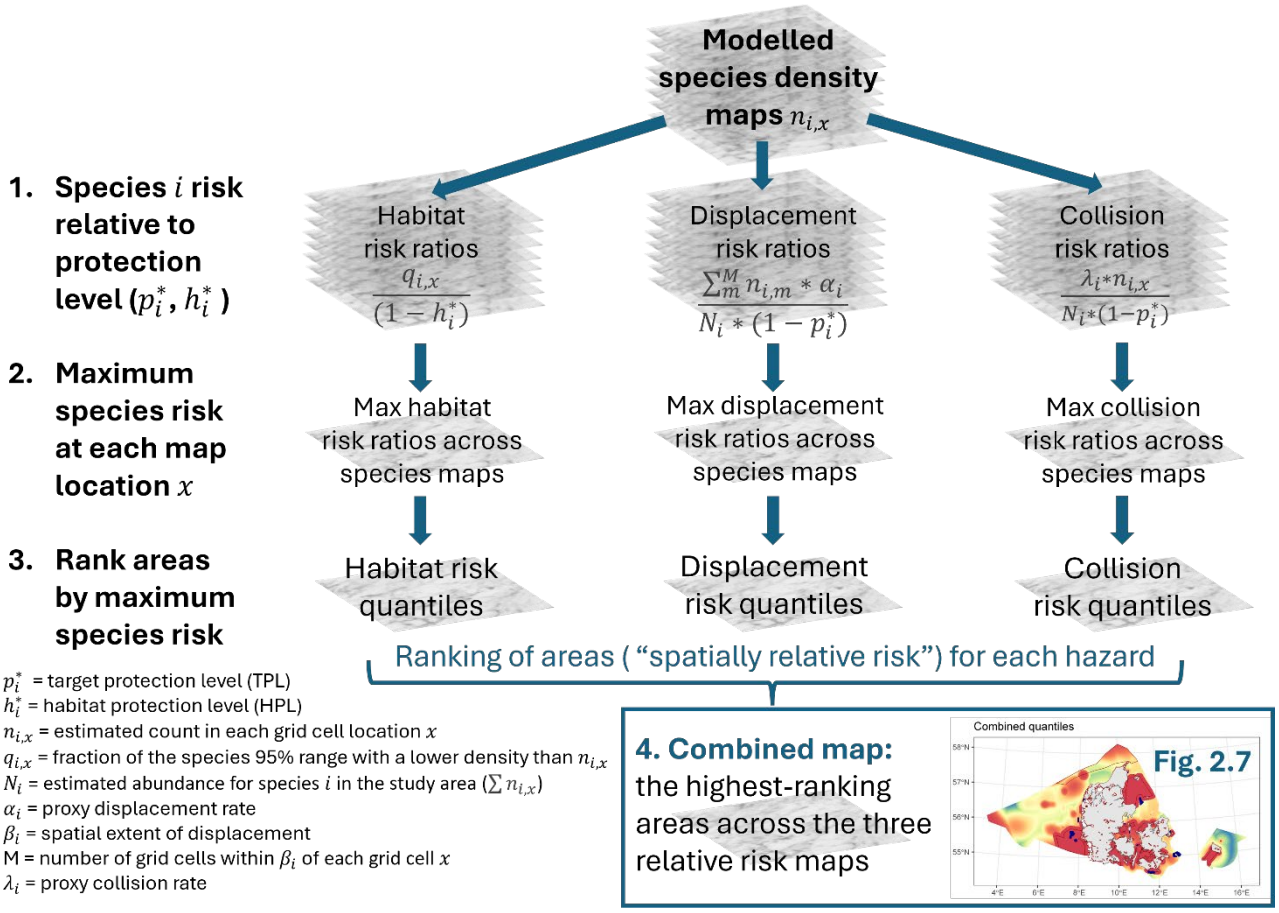

Figure 1.2. Overview of the spatial risk-ranking algorithm and key input parameters. The algorithm was applied to 17 species units (subscript *i*), some of which combined ecologically similar species identifiable from aerial surveys (see Table 1.1).

To propagate uncertainty from the spatial analysis, the above four steps were repeated 500 times, each time using a different bootstrap prediction for species unit densities. To represent uncertainty, the ratio of standard deviation to mean (i.e., coefficient of variation) was calculated over the resulting 500 combined hazard maps. Uncertainty on input parameters (TPL, HPL, displacement and collision rates for each species unit) was not included.

1.2 Aerial survey data analysis

1.2.1 Modelled species and seasons

Spatial density distribution maps were estimated separately for 17 seabird species units, representing either individual species or species groups (Table 1.1). Ecologically similar bird species that are challenging to identify to species level from aircraft were grouped together. The groups included red- and black-throated divers (hereafter, divers), red-necked and great crested grebe (hereafter, grebes), common- and herring gull (hereafter, grey gulls), common-, arctic-, and sandwich terns (hereafter, terns), and razorbills and common guillemots (hereafter, alcids). For brevity, the 17 species and species groups (Table 1.1) are referred to as the modelled species units. These species units represented the majority of species detections in the dataset (Table 1.3).

Table 1.3. All species records with over 70 total observations (N_{det}) in the analysed dataset. The first part of the table shows the species that were included in the spatial risk-ranking algorithm and the label of the associated species unit, which combined some ecologically similar, field-identified species groups together. The second part of the table shows species or species groups that were excluded from the implemented risk-ranking algorithm or GPS analyses.

English name	Implemented in algorithm	GPS analysis	AU_code	EURING	Danish name	Scientific name	Species unit	N_{det}
Common scoter	TRUE	FALSE	98	2130	Sortand	*Melanitta nigra*	Scoter	57849
Common eider	TRUE	FALSE	95	2060	Ederfugl	*Somateria mollissima*	Eider	37806
Herring gull	TRUE	FALSE	256	5920	Sølvmåge	*Larus argentatus agg.*	Gull (Grey gulls)	35599
Razorbill/ guillemot	TRUE	TRUE	287	6345	Alk/lomvie		Alcid	14228
Long-tailed Duck	TRUE	FALSE	93	2120	Havlit	*Clangula hyemalis*	Longtailed	8880
Northern gannet	TRUE	FALSE	34	710	Sule	*Morus bassanus*	Gannet	6151
Velvet scoter	TRUE	FALSE	99	2150	Fløjlsand	*Melanitta fusca*	Velvetscoter	5392
Red-breasted Merganser	TRUE	FALSE	106	2210	Toppet skallesluger	*Mergus serrator*	Merganser	5171
Diver sp.	TRUE	FALSE	1	59	Lom sp.	*Gavia sp.*	Diver	4849
Black-legged kittiwake	TRUE	FALSE	268	6020	Ride	*Rissa tridactyla*	Kittiwake	4670
Black-backed gull	TRUE	FALSE	258	6000	Svartbag	*Larus marinus*	GBBG	4383
Red-throated diver	TRUE	FALSE	2	20	Rødstrubet lom	*Gavia stellata*	Diver	4085
Goldeneye	TRUE	FALSE	90	2180	Hvinand	*Bucephala clangula*	Goldeneye	2296
Common guillemot	TRUE	TRUE	288	6340	Lomvie	*Uria aalge*	Alcid	2254
Common gull	TRUE	FALSE	255	5900	Stormmåge	*Larus canus*	Gull (Grey gulls)	1932
Little gull	TRUE	FALSE	266	5780	Dværgmåge	*Hydrocoloeus minutus*	Littlegull	1769
Arctic/Common tern	TRUE	FALSE	277	6159	Hav/fjordterne		Tern	1721
Northern fulmar	TRUE	FALSE	16	220	Mallemuk	*Fulmarus glacialis*	Fulmar	1653
Sandwich tern	TRUE	TRUE	282	6110	Splitterne	*Thalasseus sandvicensis*	Tern	803
Red-necked grebe	TRUE	FALSE	7	100	Gråstrubet lappedykker	*Podiceps grisegena*	Grebe	666

English name	Imple-mented in algorithm	GPS analysis	AU_code	EURING	Danish name	Scientific name	Species unit	N_{det}
Razorbill	TRUE	FALSE	286	6360	Alk	*Alca torda*	Alcid	623
Arctic tern	TRUE	TRUE	276	6160	Havterne	*Sterna paradisaea*	Tern	574
Crested Grebe	TRUE	FALSE	8	90	Toppet lappedyk-ker	*Podiceps cristatus*	Grebe	508
Tern sp.	TRUE	FALSE	283	6259	Terne sp.	*Sterninae sp.*	Tern	450
Lesser black-backed gull	TRUE	TRUE	257	5910	Sildemåge	*Larus fuscus*	LBBG	421
Grebe sp.	TRUE	FALSE	9	129	Lappedykker sp.	*Podicipedidae sp.*	Grebe	177
Black-throated diver	TRUE	FALSE	3	30	Sortstrubet lom	*Gavia arctica*	Diver	87
Black guillemot	TRUE	FALSE	289	6380	Tejst	*Cepphus grylle*	Alcid	25
Common tern	TRUE	FALSE	275	6150	Fjordterne	*Sterna hirundo*	Tern	7
Great cormorant	FALSE	FALSE	35	720	Skarv	Phalacrocorax carbo		5109
Mute swan	FALSE	FALSE	53	1520	Knopsvane	Cygnus olor		5097
Black-headed gull	FALSE	FALSE	263	5820	Hættemåge	Chroicocephalus ridibundus		1685
Gull sp.	FALSE	FALSE	269	6009	Måge sp.	Laridae sp.		1534
Mallard duck	FALSE	FALSE	72	1860	Gråand	Anas platyrhynchos		1146
Brent goose	FALSE	FALSE	66	1680	Knortegås	Branta bernicla		697
Greylag goose	FALSE	FALSE	59	1610	Grågås	Anser anser		504
Eurasian wigeon	FALSE	FALSE	80	1790	Pibeand	Mareca penelope		439
Goosander	FALSE	FALSE	105	2230	Stor skallesluger	Mergus merganser		379
Shelduck	FALSE	FALSE	71	1730	Gravand	Tadorna tadorna		365
Eurasian oyster-catcher	FALSE	FALSE	182	4500	Strandskade	Haematopus ostrale-gus		164
Eurasian coot	FALSE	FALSE	177	4290	Blishøne	Fulica atra		96
Canada goose	FALSE	FALSE	68	1660	Canadagås	Branta canadensis		95
Whooper swan	FALSE	FALSE	55	1540	Sangsvane	Cygnus cygnus		84
Barnacle goose	FALSE	FALSE	67	1670	Bramgås	Branta leucopsis		81
Eurasian curlew	FALSE	FALSE	202	5410	Stor regnspove	Numenius arquata		78
Eurasian teal	FALSE	FALSE	75	1840	Krikand	Anas crecca		73

For each modelled species unit, we estimated a single density surface, averaging across all survey years and seasons in Danish waters. However, for species whose presence in Danish waters is strongly seasonal, due to their migration schedule, the spatial analysis excluded survey data from seasons that the species unit was considered absent *a-priori* (Table 1.4). This avoided introducing uncertainty to the static density distribution maps that was solely due to seasonal variation in presence-absence. For example, divers were considered absent during summer, and therefore only surveys from autumn, winter, and spring were included in the spatial analysis for this species unit.

Table 1.4. Definition of seasons and exclusion of survey data. For strongly migratory species or species groups, survey data were excluded from seasons that the modelled species unit were a-priori considered as absent in Danish waters.

Season	Start date	Absent species units
Spring	1 March	
Summer	15 June	Divers, long-tailed duck, little gull
Autumn	15 September	Long-tailed duck, terns
Winter	15 November	LBBG, terns

1.2.2 Survey data sample size and coverage

Visual aerial surveys were used to collect data on seabirds using line transect distance sampling methods (Buckland et al., 2001). The dataset consisted of 243 aerial surveys from 203 different days between 1999-2024. The surveys covered 151,551 km of transect line, with each segment approximately 500 m long and up to 1000 m wide. Of the total 232,496 species detections, 213,832 were of the species selected for modelling in this project, and 207,175 of which were retained in analysis after a data validation exercise to account for any left-right bias indicating undue influence by sighting conditions, such as sun glare (Appendix 2).

The surveys provided an extensive spatial coverage over Danish marine waters, though with lower effort in the offshore regions of the North Sea (Figure 1.2.). Most of the surveys were carried out over the winter and spring period (Figure 1.3) the start date for each seasonal period (spring, summer, autumn and winter) is given in Table 1.4. The largest number of observations came from common scoter, common eider and the grey gull species units (N > 15,000) while the fewest observations were of lesser black-backed gull, little gull, and the grebe species unit (N < 1000) (Table 1.1, Table 1.3).

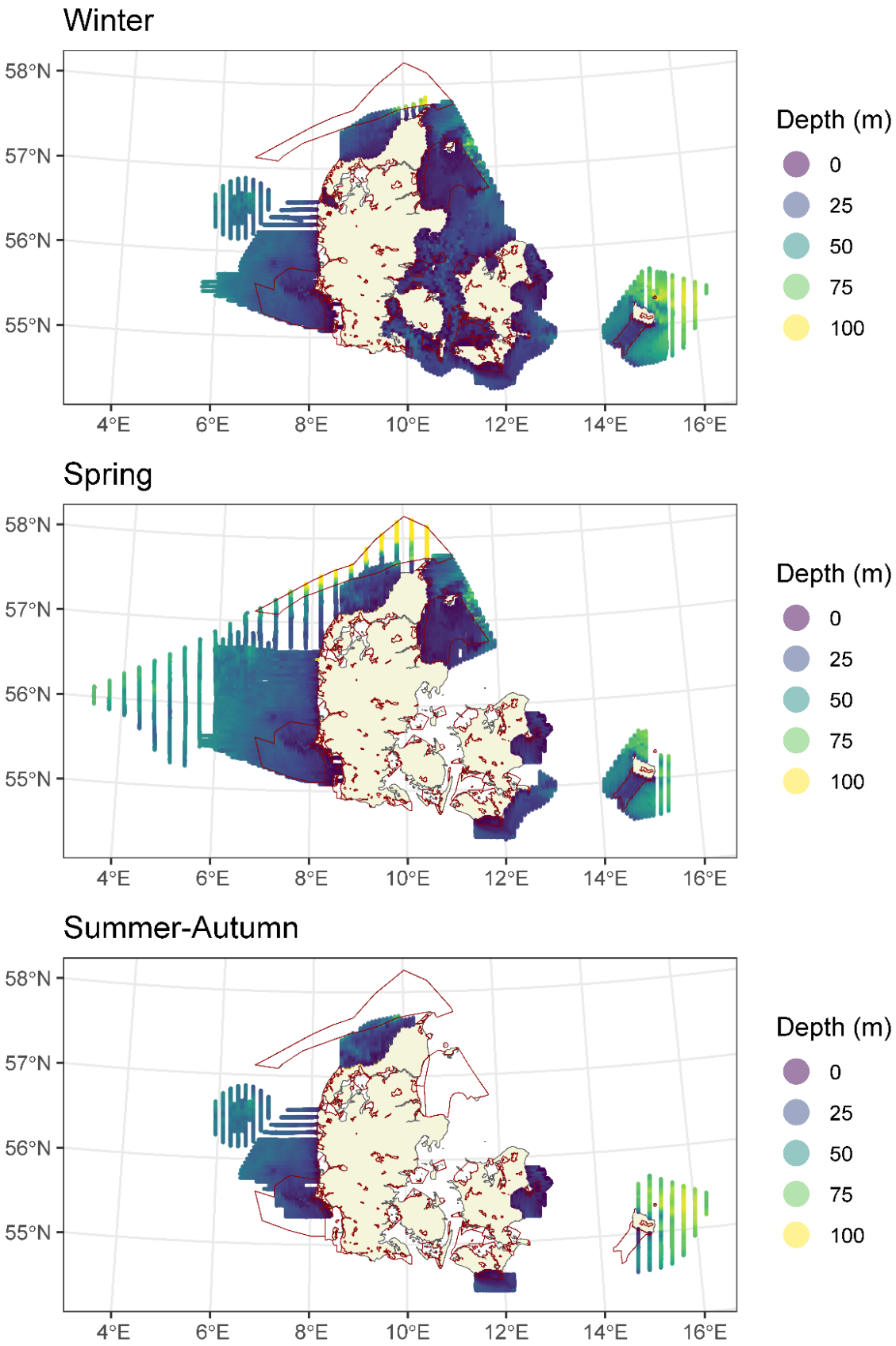

Figure 1.3. Spatial coverage of surveys by season. Each segment is coloured by the associated water depth. Seasons are defined in Table 1.4. Red polygons delineate SPAs, irrespective of species designation.

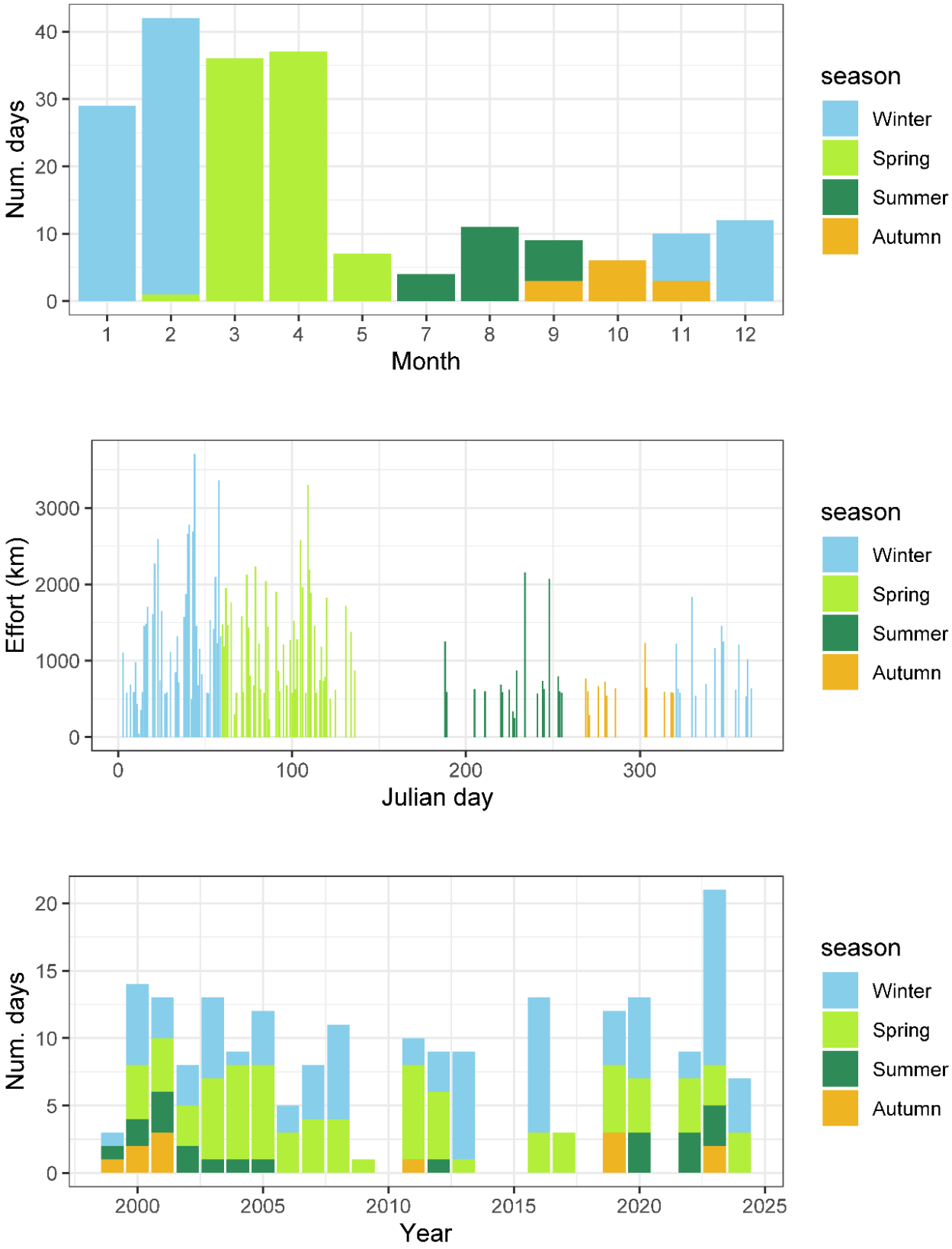

Figure 1.4. Temporal coverage of surveys by season and year. Seasons are defined in Table 1.4.

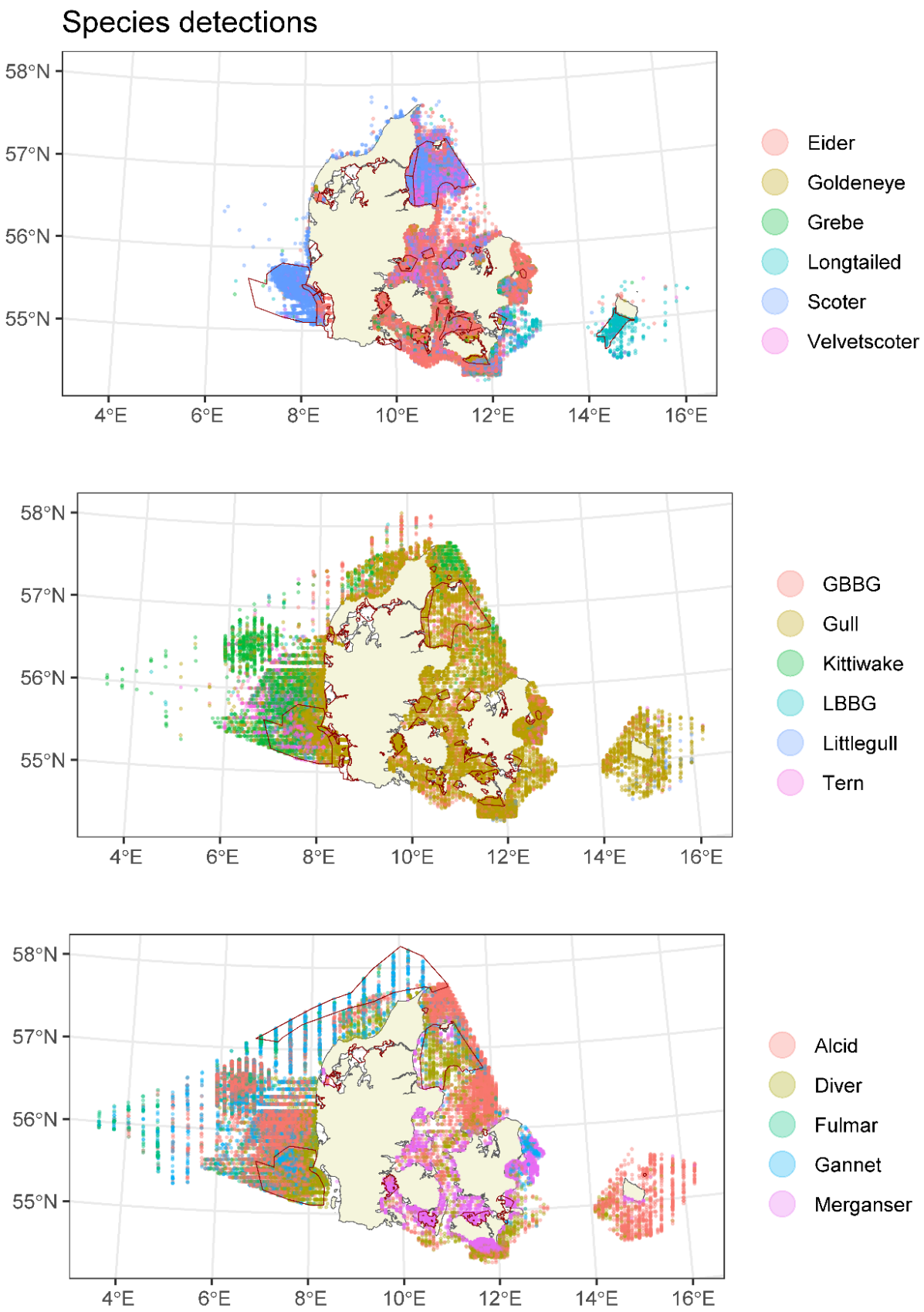

Figure 1.5. Spatial distribution of species detections, pooling surveys across all seasons and years. Species labels in the legend refer to modelled species units listed in Table 1.1. Most recent data are shown on top; though presented in transparent colour, species units with fewer detections may be behind species with greater number of detections. Red polygons delineate SPAs designated for one or more species within each species unit in each panel.

1.2.3 Distance sampling analysis

Distance sampling analyses were conducted for each species unit by pooling data across all surveys. When fitting detection functions, the effects of covariates, other than perpendicular distance, are incorporated into the detection function model directly (Multiple Covariate Distance Sampling, MCDS) (Buckland et al., 2001; Marques & Buckland, 2004; Marques et al., 2007). Half normal and hazard rate functional forms were trialled for the relationship of detectability with distance and the candidate variables that might affect this relationship were bird group size, behaviour (sitting vs flying), observer, and sea state (Table 1.5). BIC was used to choose between competing models (functional form and variables). Further details on the distance sampling methodology are provided in Appendix 2.

Table 1.5. Candidate covariates for detection functions.

Name	Covariate type	# Parameters	Description
Group size	Continuous	1	Bird group size
Behaviour	Categorical	1	S (sitting or diving) and F (flying or flushing)
Observer	Categorical	>1	Observer initials. Observers were merged to "Other" category when they had <30 observations in total, or no observations in any one distance band
Sea state	Categorical	8	0, 0.5, 1, 1.5, 2, 2.5, 3, 3.5 (calm to rough)
Sea state (4)	Categorical	4	0, 1, 2, 3 (calm to rough)

1.2.4 Spatial model fitting and selection

The outputs from the detection function analysis give a detectability-corrected count in a small area (segment). The spatial modelling process was undertaken using a generalised additive model framework with an error family suitable for count per unit area response data, the Tweedie distribution. Segment area was therefore included as a log-scale offset term in the model.

Candidate variables included a set of one-dimensional terms, water depth and distance to coast, that were permitted to change linearly or non-linearly with the response, and a two-dimensional term using geographic coordinates to account for surface patterns, which could be result from unmodelled environmental variability. The flexibility of any smooth functions (1D or 2D) was determined using BIC, whilst the more computationally intensive 5-fold cross-validation was used to choose between competing models (inclusion or exclusion of variables).

The response data were collected along survey lines in sequence, and so consecutive observations were likely to be correlated in space and time. With a spatial term included, any resulting temporal autocorrelation in model residuals was accounted for by using robust standard errors as part of the modelling framework. These essentially inflate the standard errors in relation to the positive correlation observed within pre-specified blocks (here, transects) of residuals.

All models were fitted using the MRSea R package (Scott-Hayward et al., 2023; R Core Team, 2024). and subjected to various diagnostic checks (e.g. assessment of the assumed mean-variance relationship, a key assumption check). Further methodological details on model specification, fitting, and diagnostics are available in Appendix 2.

1.2.5 Model predictions

Using the best selected model for each species unit, predictions of counts were made to a grid of points (each point representing a 1km^2 grid cell) across the study area. The uncertainty in the detection function was estimated using a parametric bootstrap (n=500) of the fitted distance sampling model. This generated new estimated counts for each segment. The best selected spatial model was then re-fitted to each of the new datasets to obtain a new set of parameter estimates for the model. The final output of this process was a parametric bootstrap procedure using the robust variance-covariance matrix from each parametric bootstrap model. These were used to calculate 500 sets of model predictions for every grid cell in the study area. To obtain 95% percentile-based confidence intervals and a coefficient of variation for each grid cell, the 2.5% and 97.5% quantiles of the 500 bootstrap predictions were taken along with the standard deviation. The distribution maps and sets of bootstrap predictions were used as inputs to the risk-ranking algorithm, as detailed in the section 1.1.5.

1.3 Breeding colonial bird species utilization of marine areas

In this section we analyse GPS and colony count data to explore space utilisation of four seabird species to assess how these types of output may be included as inputs to the spatial risk-ranking algorithm. Whilst this has not been included at this stage, we discuss this possibility in the discussion. Under this part of the project, we used results from 95 GPS tagged birds of four species from six breeding colonies in Denmark from 2023 and 2024 combined with breeding bird colony census data from 2010 to 2023 to describe, model and evaluate their utilization of Danish marine areas.

1.3.1 Study species

Four species of differing abundance, distribution and foraging behaviour typical of Danish breeding seabird species were selected:

- Lesser black-backed gull (*Larus fuscus*). An opportunist species, foraging on various prey items on land and at sea, breeding in relatively few colonies throughout the country. The breeding population has been increasing and is currently approx. 4,500 pairs (Danish Database on Colonial Coastal Birds, Dept. of Ecoscience, Aarhus University, unpublished data). The lesser black-backed gull is a long-distance migrant, most wintering along coastlines of Southwest Europe and Northwest Africa.
- Sandwich tern (*Thalasseus sandvicensis*). A specialist plunge-diving, surface feeding fish-eating tern, primarily dependent on sandeels (*Ammodytidae*), breeding at a few, widely dispersed colonies. The breeding population has been fluctuating and is currently approx. 3,000 pairs. The Sandwich tern is a long-distance migrant, wintering along the western coast of Africa.
- Arctic tern (*Sterna paradisaea*). A generalist tern, feeding on small fish and crustaceans caught at the sea surface. In Denmark, it breeds mostly in relatively small colonies, numbering 2,300 breeding pairs. The Arctic tern is a long-distance migrant, wintering in the Southern Ocean.
- Common guillemot (*Uria aalge*). A specialist deep-diving auk, feeding mostly on clupeid fish, mainly confined to one Danish colony on Græsholmen near Bornholm. The breeding population has been increasing, and the current size is unknown. The common guillemot is resident in the Baltic throughout the year.

1.3.2 Breeding colonies

GPS tags were deployed on colonial breeding birds in spring 2023 and 2024 at six locations in Denmark. The colonies were Sprogø, Als Odde, Krik Sandø, Hirsholm, Græsholmen near Christiansø and Klægbanken (Figure 1.5).

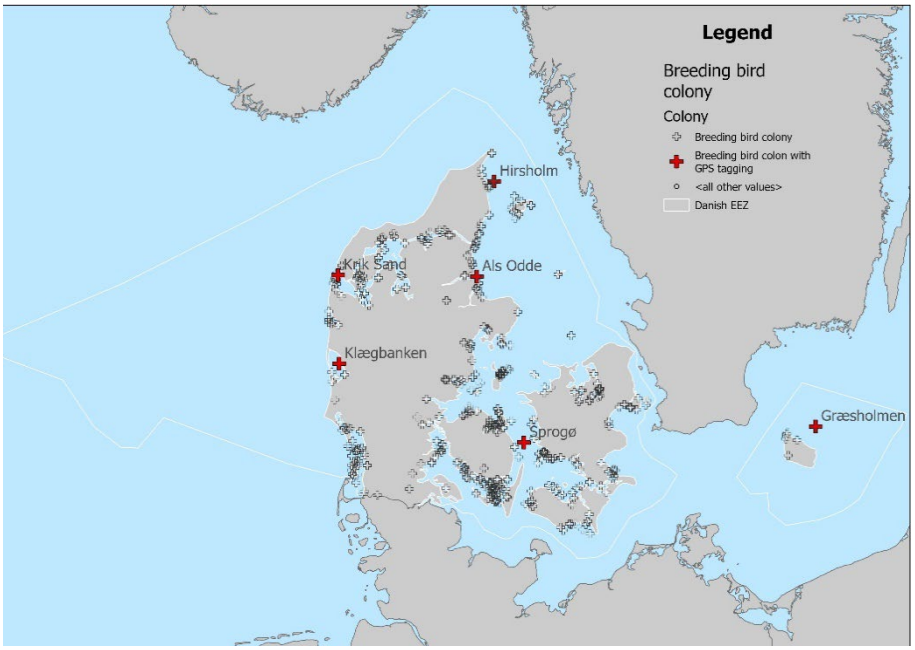

Figure 1.6. The geographical distribution of 450 recorded-breeding colonies in Denmark where at least one of the four species have been recorded breeding between 2010 and 2022 (Danish Database on Colonial Coastal Birds, Dept. of Ecoscience, Aarhus University, unpublished data).

1.3.3 GPS tagging

PathTrack GPS tags were deployed on 95 breeding birds as follows: 26 lesser black-backed gulls at Sprogø, Klægbanken and Hirsholm, 25 Sandwich terns at Krik Sandø, Sprogø and Hirsholm, 25 Arctic terns on Krik Sandø and Als Odde and 19 common guillemots on Græsholm. Most birds were tagged in 2023 (90) and five birds were tagged in 2024 (Table 1.6). Most tagged birds were incubating eggs at the time of tagging, but some common guillemots had recently hatched chicks.

Table 1.6. The number of GPS tagged birds from four species at six coastal bird colonies during the breeding seasons of 2023 and 2024. The number given in bold represents the number of tags fitted to birds, the number in brackets those that provided data for the analysis.

	Lesser black- backed gull		**Sandwich tern**		**Arctic tern**		**Common guillemot**	
	2023	2024	2023	2024	2023	2024	2023	2024
Krik Sandø			9 (9)		**5** (5)			
Græsholmen							14 (12)	5 (4)
Sprogø	8 (7)		**6** (6)					
Klægbanken	8 (8)							
Hirsholm	10 (8)		**10** (10)					
Als Odde					20 (14)			

Birds were tagged with different devices according to species, which affected attachment and download methods (Pathtrack Ltd, West Yorkshire, UK) (Table 1.7).

Table 1.7. PathTrack GPS tag models used for the four avian species in this project. Tag data communication method (Data upload), weight, attachment methods and GPS position collection frequency are given.

Species	Model	Data upload	Weight (max)	Attachment method	Extra sensors	GPS frequency (breeding season)
Common guillemot	nanoFix GEO+RF	Local base station (UHF)	13 g	Taped to back feathers	Depth sensor	10 min
Arctic tern	nanoFix GEO+RF Mini	Local base station (UHF)	2.75 g	Taped to back feathers		15 min
Sandwich tern	nanoFix GEO+RF Mini	Local base station (UHF)	3.25 g	Teflon ribbon harness round legs on back		10 min
Lesser black-backed gull	nanoFix GEO+GSM	GSM network	18 g	Teflon ribbon harness round legs on back		5 or 10 min

1.3.4 GPS data analysis

Data from the GPS-tagged birds were selected from individuals that succeeded in breeding. We analysed the distance of each bird travelled from its colony over time, visualizing this as a time series. For many birds, a consistent maximum distance from the colony was evident, beyond which they did not typically travel. This threshold was similar across individuals of the same species. However, some lesser black-backed gulls exhibited periodic, extended deviations beyond their maximum distance, lasting several days, after which they returned to the colony and resumed typical behaviour. These intermittent deviations suggested a lack of nesting, so we excluded these birds' records entirely from the breeding dataset. For one bird that left the colony permanently—indicated by sustained departures beyond their normal maximum distance—we excluded only the data after they departed, retaining earlier records for analysis. Distribution data was used from the day of tagging until 31 July of each year for all species. Points over land were removed from the analysis using the EEA coastline dataset (European Environment Agency, 2017).

For each bird species, we fitted a generalized additive model (GAM) with a binomial error distribution and a logit link function, estimated using restricted maximum likelihood (REML) using the mgcv (v1.8-34; Wood, 2011) and scam (v 1.2-17, Pya & Wood, 2014; Pya, 2024) packages in R version 4.3.3 (2024) to model the geographical utilization of the marine area, based on the GPS tag data.

For this modelling approach we needed to create pseudo-absence points. Across the extent of the presence points for each species, defined by creating a raster dataset with a resolution of 0.01 degrees and extent of the records for a species, points were created in random locations using the R package dismo (Hijmans et al. 2023). More points than were needed were created, then pseudo-absence points within 10m of any individual bird track location were removed to reduce the possibility of the pseudo-absence points confounding the models' ability to differentiate conditions associated with presence and absence. Finally, a random selection of the remaining points was selected to equal the number of presence points.

The model used the spline-smoothed distance to coast, the distance to the colony as well as bathymetry (water depth) as covariates. For sandwich tern,

"distance to coast" was smoothed monotonically decreasing. For lesser black-backed gull "distance to coast" and "distance to colony" both were smoothed monotonically decreasing and "bathymetric depth" monotonically increasing. For the common guillemot, breeding almost solely in one Danish colony, including distance to coast would have predicted bird presence around coastlines across Denmark, and therefore only unsmoothed "distance to colony" was used in the model. For common guillemot a two-dimensional smooth of the geographical coordinates was also included. This was possible because the Christiansø area is the only breeding area for the species in Denmark, and therefore it was not necessary to model the utilization of sea areas away from the common guillemot breeding colony. Based on the results from these models, the aim was to model the potential spatial distribution and utilization of these lesser-black backed gull, sandwich terns and arctic terns throughout the Danish waters from all their other colonies and for common guillemot around their one colony. This was carried out using the existing database of the size (i.e. number of breeding pairs) and distribution of all known breeding colonies throughout Denmark gathered in most recent years (see below). The GAM model was then used to predict the extent and distribution of their use of marine areas out from all the Danish nesting colonies, weighing each colony according to the number of breeding pairs at the site.

For sandwich tern, the most recent data on colony-specific breeding abundance from 2023 was used, that for arctic tern was from 2022. The latest lesser black-backed gull data used originated from 2019, because the 2023 data was incomplete, and 2022 data lacked data for lesser black-backed gull from two of the three colonies in which the birds were tagged. For common guillemot, Græsholmen is the only colony in Denmark (hence no weighing was required).

2 Results

2.1 Aerial survey data analysis

Observer and group size were the most frequently selected covariates to explain detection probability (Table 2.1) for each species or species group that were modelled together as a species unit (Table 2.1). The northern gannet, common scoter and lesser black-backed gull were estimated with the highest probabilities of detection ($p > 0.3$) while grebes were estimated the lowest probabilities ($p < 0.21$). Unsurprisingly, given the large number of detections, after adjusting for detectability, the common eider and common scoter were estimated to be the most abundant species units in the area covered by the surveys (Table 2.1).

Spatial analysis results for each species unit are summarized in Table 2.2. Spatial estimates of counts, associated uncertainty, and model diagnostics are provided for each species unit in Appendix 3.

Table 2.1. Summary of distance analysis results. Num par. = number of parameters, P(d) = average detection probability, SE = standard error, GOF $\chi 2$= Chi-square goodness-of-fit test statistic, Ndet = sample size of species detections. Species unit = label indicating species or species groups that were analysed together as a unit (Table 1.1).

Species unit	Key	Covariates	Num. par	P(d)	SE x 100	GOF χ^2	N_{det}
Alcid	hr	~ Behaviour + Group size + Sea state (4)	7	0.215	0.17	0.16	14855
Diver	hr	~ Observer + Behaviour + Group size	10	0.219	0.39	0.44	4265
Eider	hr	~ Observer + Group size	17	0.257	0.17	8.47	37049
Fulmar	hr	~ Group size	3	0.277	0.93	0.08	1521
Gannet	hr	~ Observer + Group size	10	0.341	0.57	72.95	6111
GBBG	hr		2	0.238	0.62	0.00	2523
Goldeneye	hr	~ Group size + Observer	10	0.243	1.18	0.16	975
Grebe	hn	~ Observer	3	0.209	0.57	9.40	892
Gull	hr	~ Group size	3	0.253	0.26	0.03	15341
Kittiwake	hr	~ Group size	3	0.250	0.50	0.00	3207
LBBG	hn		1	0.302	1.42	2.74	272
Littlegull	hr		2	0.201	1.29	0.00	304
Longtailed	hr	~ Observer + Group size + Behaviour	11	0.225	0.24	0.31	8760
Merganser	hr	~ Observer + Group size + Behaviour	9	0.244	0.61	6.27	3220
Scoter	hn	~ Observer	21	0.326	0.12	426.47	54570
Tern	hr		2	0.228	0.83	0.00	1143
Velvetscoter	hr	~ Observer + Group size	9	0.262	0.40	0.17	5345

Table 2.2. Summary of spatial modelling results. Num. par = number of parameters, Dispersion par. = dispersion parameter, CV score = cross-validation score. Candidate models included 1-dimensional terms (water depth or distance to coast) both with and without 2-dimensionsal surface estimate (1D2D and 2D Only models, respectively).

Species unit	Best model	1D terms	Num. par	Dispersion par.	CV score	Abun-dance	Lower 2.5%	Upper 97.5%
Alcid	Best 1D2D	Water depth	16	36.1	36.3	95755	85812	114641
Diver	Best 1D2D	Water depth	19	28.9	3.4	16764	15487	20186
Eider	Best 1D2D	Dist. to coast	15	305.4	1814.5	510816	492783	585157
Fulmar	Best 1D2D	Dist. to coast	18	48.2	6.3	43772	72695	113345
GBBG	Best 1D2D	Dist. to coast	13	130.2	18.5	15649	10604	30635
Gannet	2D Only		16	42.1	1.5	15890	12017	24032
Goldeneye	1D Only	Water depth	2	260.1	22.0	12746	12185	17957
Grebe	2D Only		14	159.1	6.9	5806	4833	8187
Gull	Best 1D2D	Dist. to coast	25	205.3	239.1	98280	122159	177780
Kittiwake	2D Only		12	37.3	1.9	9514	9503	12335
LBBG	2D Only		16	59.5	0.3	706	545	1385
Littlegull	Best 1D2D	Dist. to coast	14	101.8	0.6	1450	1111	2418
Longtailed	Best 1D2D	Dist. to coast	4	171.9	92.9	39944	34303	48936
Merganser	2D Only		10	64.1	15.0	19980	18410	23538
Scoter	2D Only		8	5555.6	127899.2	740599	657798	905214
Tern	Best 1D2D	Water depth	15	91.3	3.4	4198	3461	6351
Velvetscoter	Best 1D2D	Water depth	12	91.7	15.6	41962	37092	50483

2.2 Relative risk-mapping

The spatial risk-ranking algorithm was executed in a step-wise fashion for each of the three hazards: habitat overlap, displacement risk, and collision risk (Figure 1.2). Because the outputs of each step builds upon the previous step, understanding each step and associated assumptions is important for the interpretation of the final output. We have therefore structured the results to follow this step-wise workflow. We discuss the results of each hazard first (Figures 2.2, 2.4-5), and the influence of the modelled species distributions and key input parameters on these outputs. These include the spatial range and heterogeneity in each species distibution (Figure 2.1), the inclusion of SPA designations in the algorithm (Figure 2.2), and the spatial extent of displacement parameter (Figure 2.6). We then describe the final output showing the highest-ranking areas across the three hazards (Figure 2.7, top panel), and associated uncertainty (Figure 2.7 and Figure 2.8). To facilitate discussion of relative risks for each species, we summarize species-specific values within the highest and lowest-ranking areas of the combined map (Figure 2.7, top panel). For illustration purposes, we chose the top and bottom quartiles (25% and 75%) for this summary (Figure 2.4 and Figure 2.5).

Habitat overlap: The spatially relative species risk for habitat overlap was the highest for species units with geographically narrow distribution ranges in inshore areas, with multiple SPAs designated for the modelled species (Figure 2.1., Figure 2.2., Table 1.2). The highest-ranking areas for habitat risk were maintained when SPA designations were excluded from the algorithm (Figure 2.3.), indicating that the designated areas successfully captured the high-use areas for these species. The highest-risk areas overlapped most with the core areas of divers and common scoters, with 0.41 and 0.26 of the species ranges exceeding the HPL, respectively (Figure 2.4.). Areas identified as the

lowest relative risk overall still overlapped with the core areas of great black-backed gulls, grey gulls, and alcids, though to a lesser extent than in the highest-risk areas (Figure 2.5). For alcids, the reduction in habitat overlap from the highest to lowest risk areas was 77%.

Displacement risk: The highest relative risk areas for displacement were similarly found inshore (Figure 2.2). The species units identified as highest risk from displacement included the grebes, velvet scoter, common scoter, and the divers (Figure 2.4). Though divers maintained a risk ratio higher than other species in the lowest-risk areas, the average displacement risk ratio for divers was reduced by almost 80% compared to the highest risk areas (Figure 2.5).

The relative risk surface for displacement was less heterogenous, i.e., smoother, than the relative risk surfaces for habitat overlap and displacement (Figure 2.2). This is because the expected number of displaced birds at each spatial location not only accounted for the density of birds in the 1 km^2 grid cell, but also its neighbourhood, depending on the spatial extent of displacement parameter specified for each species unit (Table 1.2). To demonstrate the influence of the input parameter on the mapping of displacement, we re-re-calculated the number of displaced birds under three alternative values for the spatial extent of displacement (β_i, km), with alcids as an example (Figure 2.6). The figure illustrates that specifying a larger spatial extent of displacement increases both the magnitude of the displacement metric and creates smoother patterns in space than when specifying a more localized effect of displacement.

Collision risk: The collision map identified several potential hotspots of relative risk further offshore (Figure 2.2). The species units identified as having the highest relative risk from collision included the kittiwake and other gull species (Figure 2.4). Compared to the highest-risk areas, areas identified as the lowest risk reduced the average relative collision, as well as displacement and species risk values for all species units except for alcids (Figure 2.4, Figure 2.5). For alcids, the only relative risk reduction related to habitat overlap. However, the collision risk ratios for grey gulls, little gulls and the longtailed duck remained high compared to other species in the areas identified as lowest combined risk (Figure 2.5).

Combined map: The final output of the spatial risk-ranking algorithm (Figure 2.7, top panel) combined the highest-ranking areas across the three hazards (i.e., the three panels in Figure 2.2). Despite combining the three spatially relative risk maps by their maximum value, the combined map identified areas that ranked relatively low across all three hazards, compared to other marine areas in Denmark. These included two offshore areas in the North Sea, an area in Skagerrak northeast of Jutland, and an area east of Bornholm in the Baltic Sea (Figure 2.5 and Figure 2.7, top panels). However, uncertainty in the species distribution modelling led to uncertainty in the ranking of large parts of the area east of Bornholm (Figure 2.8, middle panel). The area northeast of Jutland had a higher risk of exceeding the specified HPLs compared the two offshore areas in the North Sea (Figure 2.8 middle panel and Figure 2.9 top panel). Despite the uncertainty in the species distributions, the algorithm was able to consistently identify the majority of Danish marine waters as either higher or lower risk than other areas in 95% of the bootstraps (Figure 2.9 middle and bottom panels).

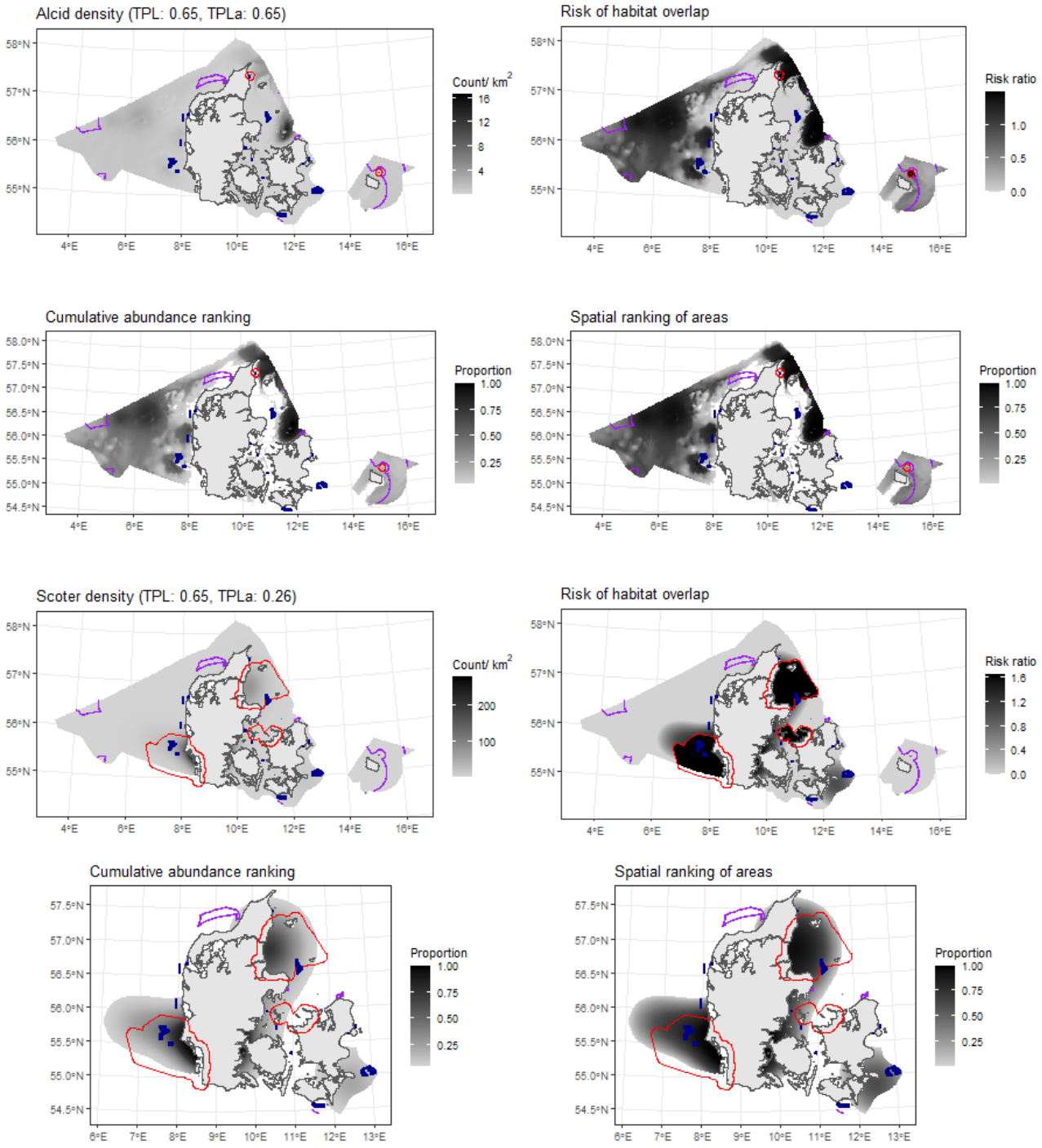

Figure 2.1. A comparison of relative habitat risk for two species units (Alcids top four and Scoters bottom four) with the same target protection level (TPL) but with different distribution and range (sliding grey scale) and SPA designations (red). For each species unit, the panels also illustrate the calculation of the habitat risk ratio, which represents the relative species risk and final output for this hazard in Step 1 of the algorithm (Figure 1.2). The top left panel shows the estimated density distribution, and top right the habitat risk ratio. Bottom left panels show the species unit abundances as cumulative percentiles (up to 0.95, defining species range), while the bottom right panel shows top use areas as cumulative percentiles of the species range (i.e., the numerator of the habitat risk ratio $q_{i,x}$) (Figure 1.2). Top four panels: Razorbill/common guillemot (species unit Alcid), with spatially extensive species range with little overlap between core and designated areas. Bottom four panels: Common scoter, with more limited species range and core areas covered by SPAs. Purple contours indicate, for reference, areas identified as relatively low combined risk to all species units in Figure 2.5. Blue symbols show existing wind turbines. Red polygons delineate SPAs that are designated for one or more species included in each species unit. Equivalent maps for all species units are available in Appendix 3. Species units are individual species or species groups modelled together, and are listed in Table 1.1

Figure 2.2. The spatially relative risk for habitat overlap, displacement, and collision, expressed as quantiles of values across each surface. These maps represent the ranking of areas by the maximum relative species risks for each hazard in Step 3 of the algorithm (Figure 1.2). The maximum relative species risks were obtained as the maximum risk ratios for each grid cell in Step 2 of the algorithm (Figure 1.2) across all modelled species units (individual species or species groups modelled together, Table 1.1). Blue symbols show existing wind turbines. Red polygons delineate SPAs, irrespective of species designation.

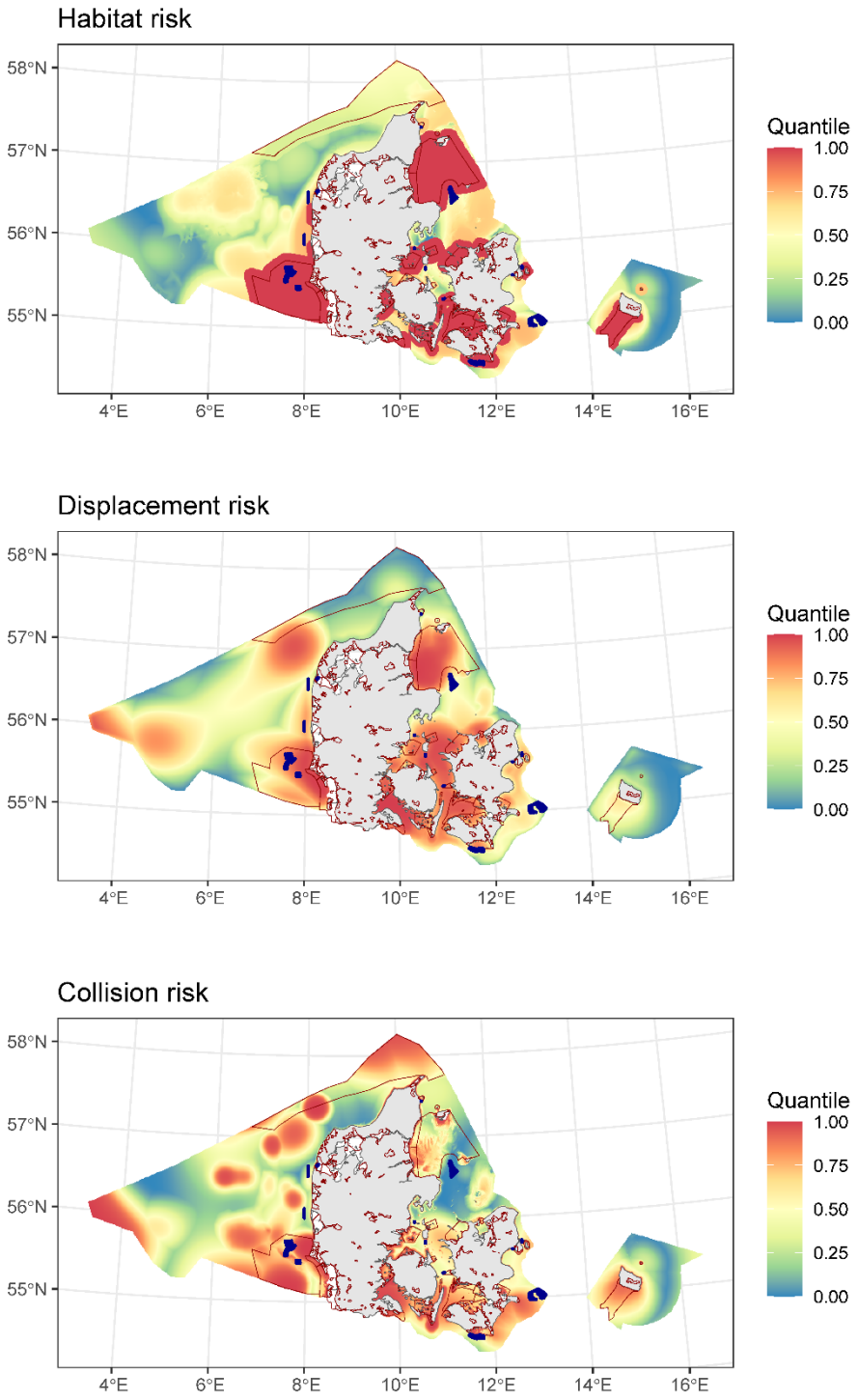

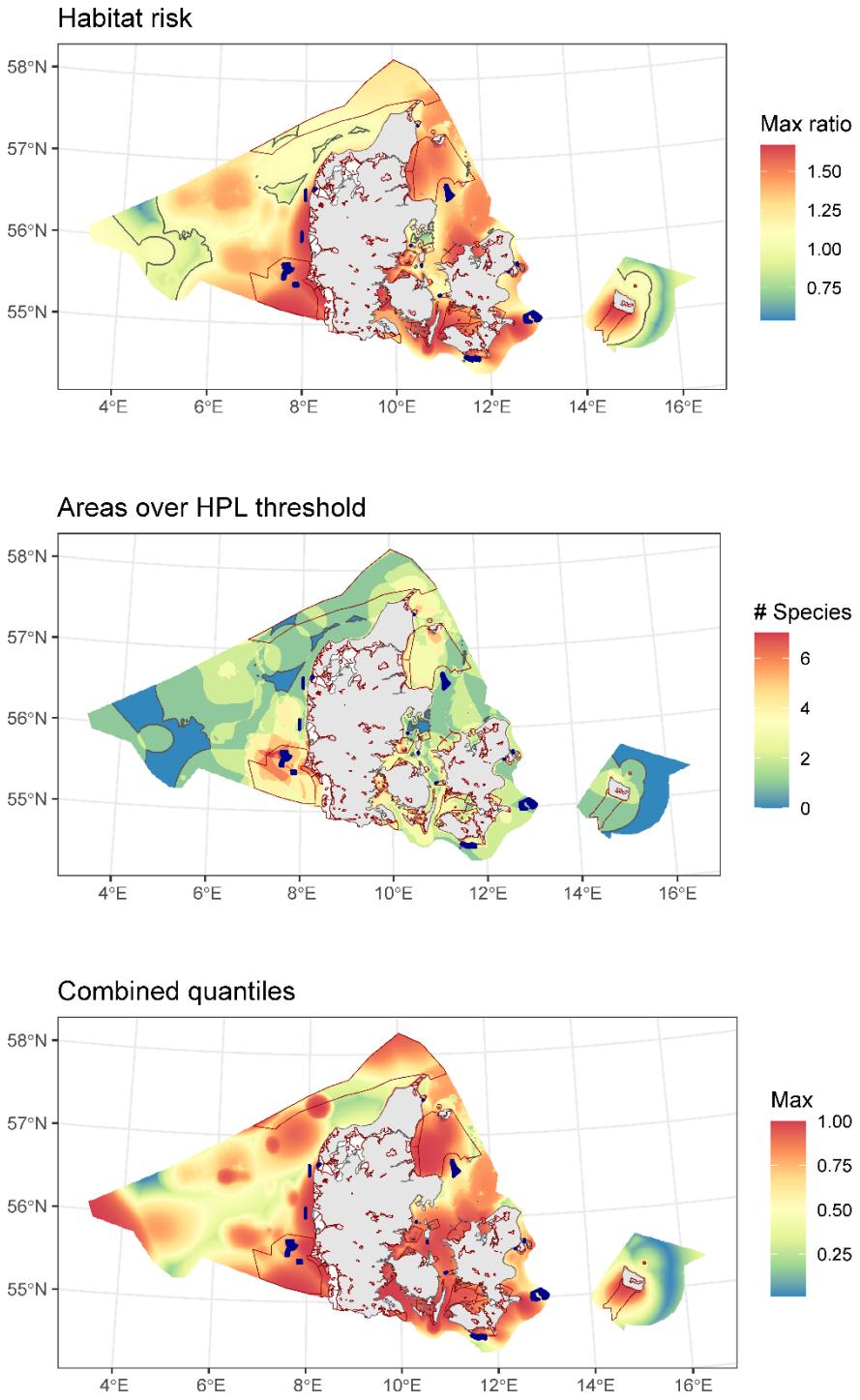

Figure 2.3. The risk of habitat overlap (top and middle panels) and combined spatially relative risk across all three hazards (bottom panel), when excluding SPA designations from the risk-ranking algorithm. Red polygons delineate SPAs, irrespective of species designation. Top panel: the maximum habitat risk ratio across species, representing the output of Step 2 of the algorithm for this hazard (Figure 1.2). Middle panel: the number of species units (individual species or species groups modelled together, Table 1.1) that exceeded the HPL threshold. For example, blue means that one species unit exceeds the threshold in the area, while green means no species unit exceed the threshold. Bottom panel: the combined spatially relative risk map, showing the highest-ranking areas across the three hazard maps (habitat overlap, displacement, collision) when SPA designations were excluded from the algorithm to produce each panel. The combined map represents the final output of the algorithm (Figure 1.2). Blue symbols show existing wind turbines.

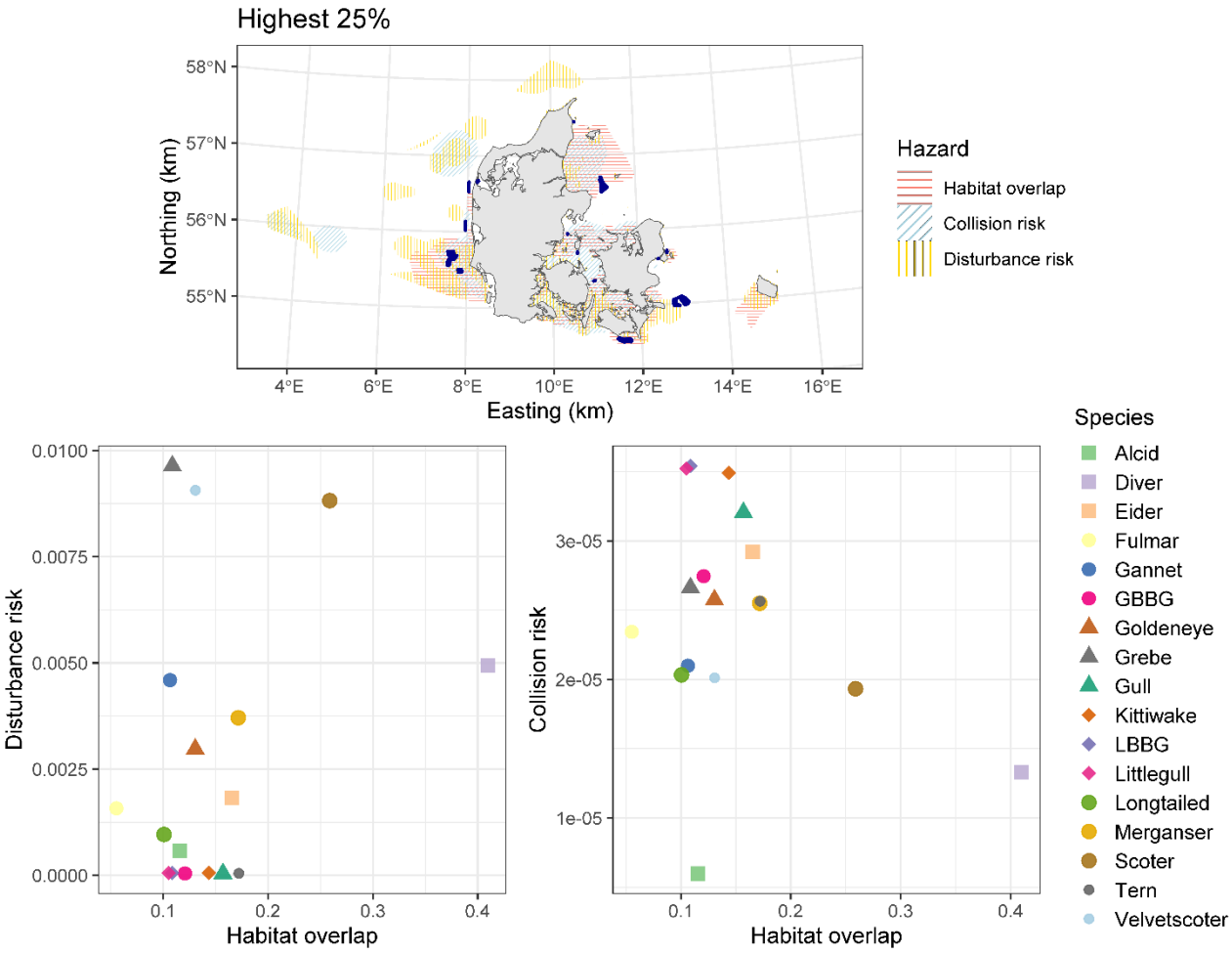

Figure 2.4. Areas identified as the highest spatially relative risk to species for each of the three hazards (top panel) and associated risk ratio values for each species unit (bottom panel). Average disturbance and collision risk ratio values are shown for areas in the combined hazard map that exceed the third quartile (75% quantile), i.e., the intersection of the areas shown in the top panel. Habitat overlap (the proportion of the area where relative habitat risk > 0) for each species unit in the bottom panels are shown without adjustment to SPAs. Species labels in the legend represent modelled species units (individual species or species groups modelled together) listed in Table 1.1

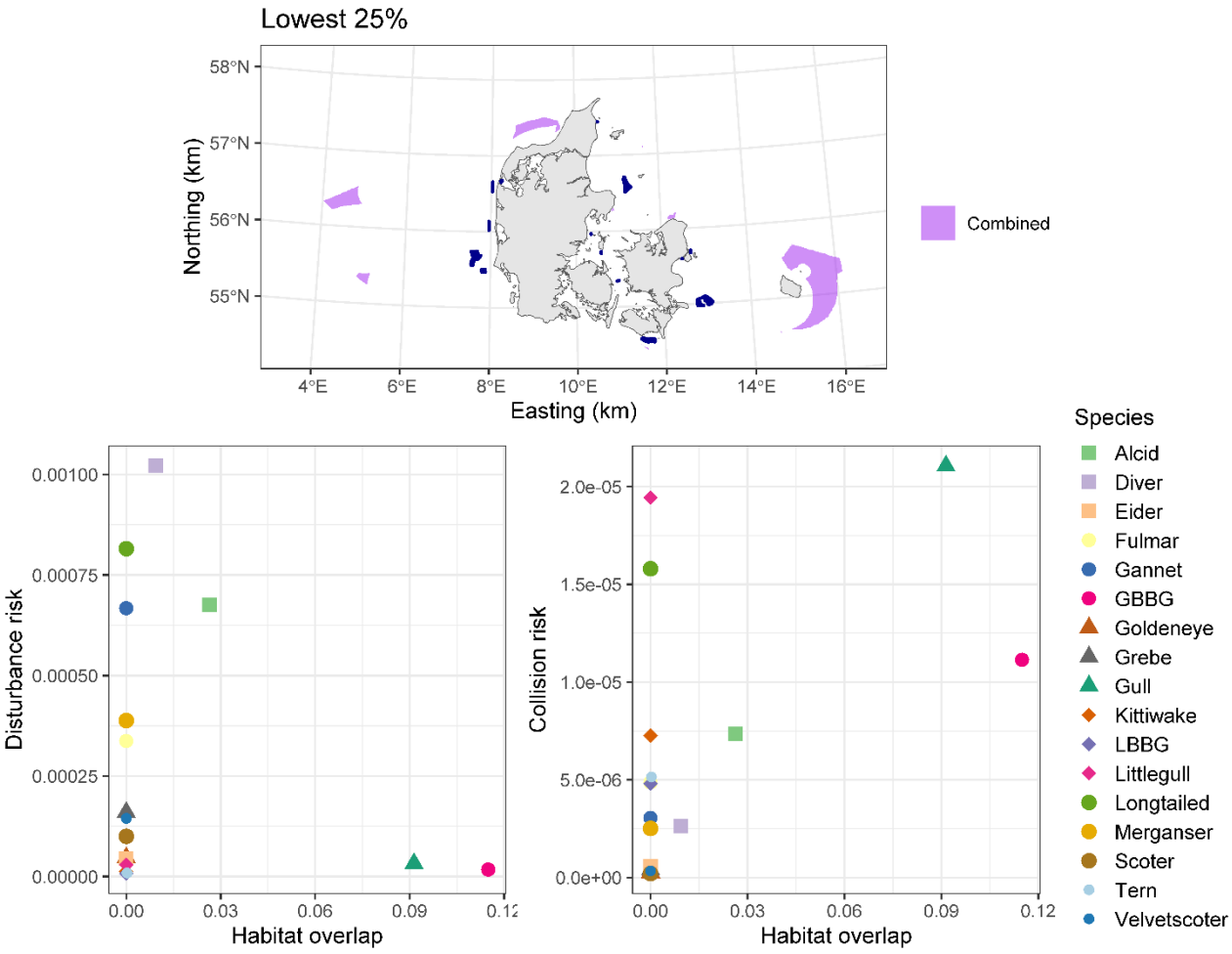

Figure 2.5. Areas identified as the lowest spatially relative risk to species across all three hazards (top panel, purple areas) and associated risk ratio values for each species unit (bottom panel). Average disturbance and collision risk ratio values are shown for areas in the combined map that do not exceed the first quartile (25% quantile). Habitat overlap (the proportion of the area where relative habitat risk > 0) for each species unit in the bottom panels are shown without adjustment to SPAs. Species labels in the legend represent modelled species units (individual species or species groups modelled together) listed in Table 1.1.

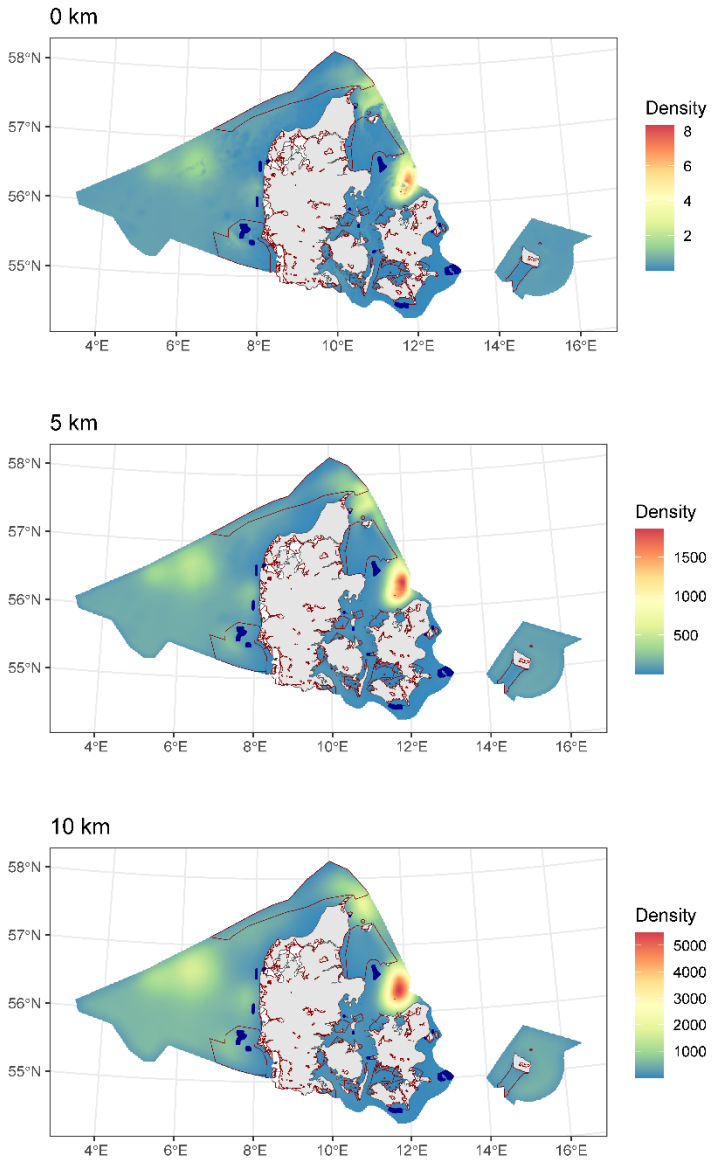

Figure 2.6. An illustration of how the spatial extent of displacement parameter (β_i, km) influences the expected number of displaced birds at each grid cell location. Example based on razorbill/common guillemot (species unit: Alcid). Blue symbols show existing wind turbines. Red polygons delineate SPAs, irrespective of species designation.

Treating each of three hazards with equal weight, the combined map identified two main areas that were lower in relative species risk than other marine areas in Denmark, namely west of Nordjylland and north and east of Bornholm, near the Ertholmene SPA designated for breeding common guillemot and razorbill (Figure 2.5, Figure 2.7). The area north and east of Bornholm was associated with higher uncertainty in species distribution estimates (Figure 2.7, Figure 2.8). Across bootstrap estimates, areas west of Nordjylland did not cross the HPL threshold for any species >90% of time (Figure 2.8). The area was also selected as the lower 50% risk area for collision and disturbance in the majority of bootstrap redraws of the two hazard maps (Figure 2.8).

Figure 2.7. The main output of the spatial risk-ranking algorithm with associated uncertainty (top and middle panels) and average number of species units that exceeded HPL thresholds (bottom panel). Top: the combined spatially relative risk map, showing the highest-ranking areas across the three hazard maps (habitat overlap, displacement, collision). The combined map represents the final output of the algorithm (Figure 1-2). Middle panel: coefficient of variation (CV) across 500 re-draws of the combined map based on bootstrapped count estimates. Bottom panel: the average number of species units that exceeded the HPL threshold over 500 bootstraps. Blue symbols show existing wind turbines. Red polygons delineate SPAs, irrespective of species designation.

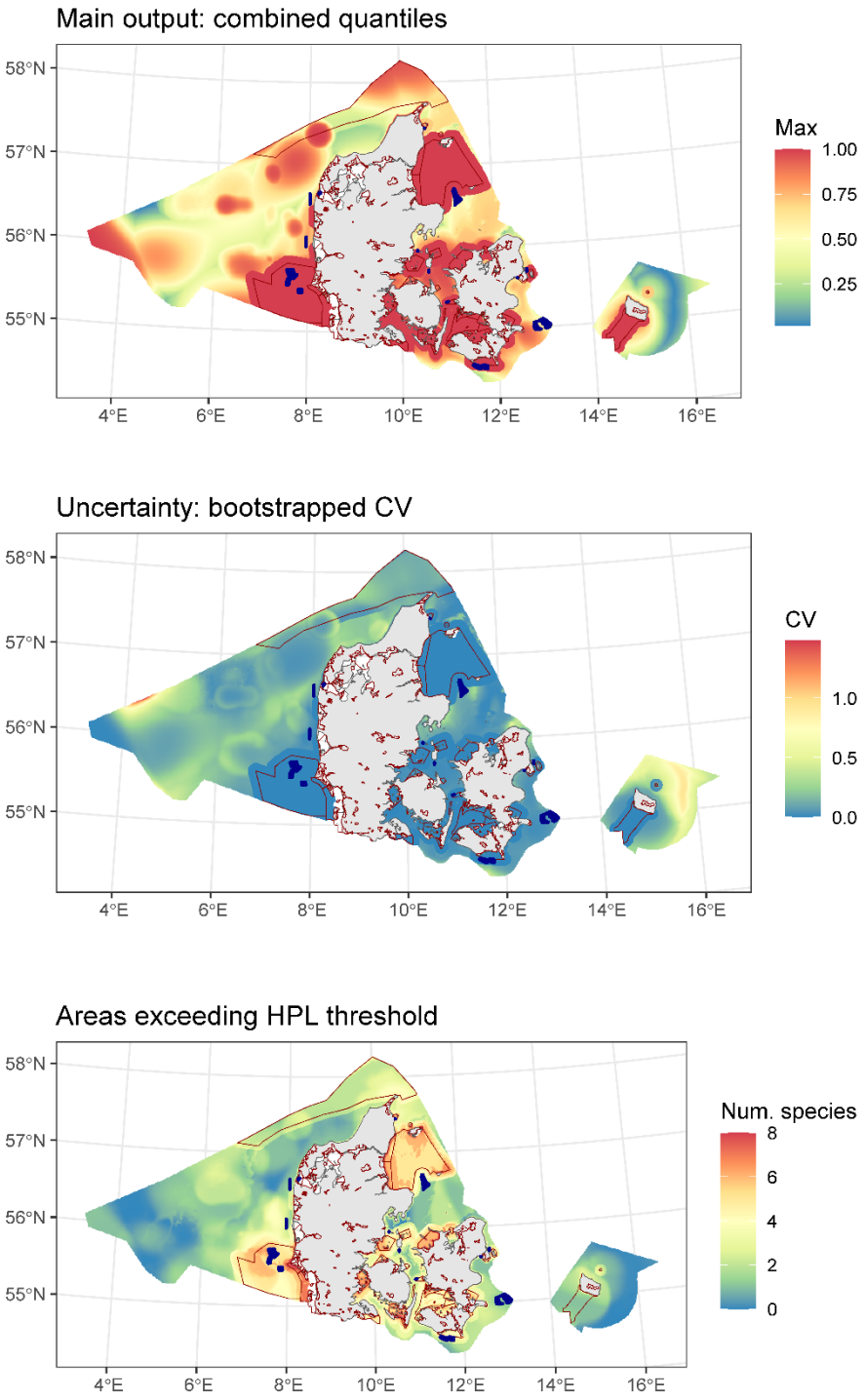

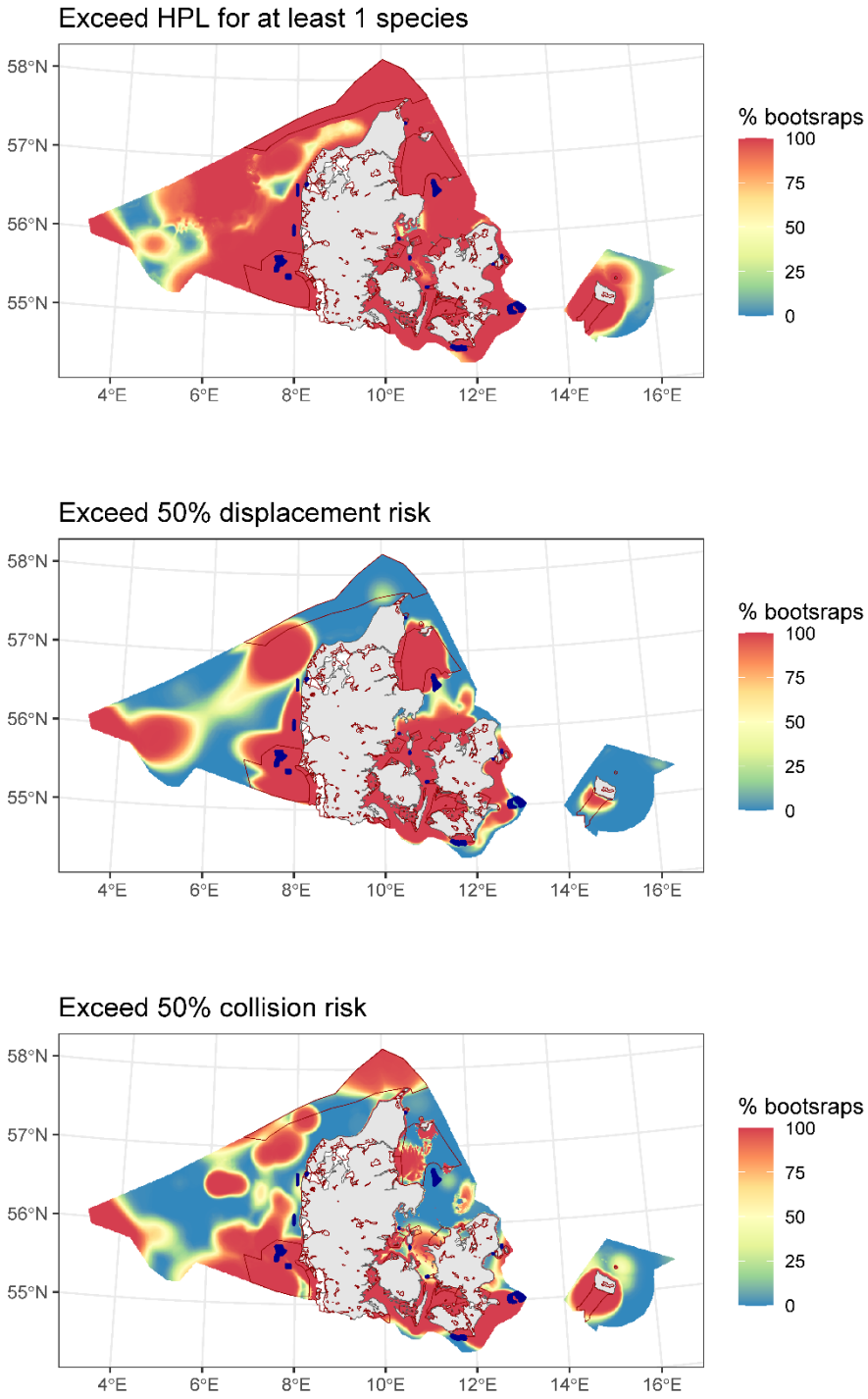

Figure 2.8. Percentage of bootstrapped risk maps that exceeded HPL threshold for at least one species unit (top panel) or 50% quantiles for displacement or collision (middle and bottom panels). The top panel can be interpreted as the risk of not achieving the assessment target for habitat overlap (HPL) for at least one species in each 1x1 km^2 grid cell, should it overlap with a wind farm footprint in the future. The red areas in the middle and bottom panels can be interpreted as high confidence in the ranking of marine areas as higher risk than other areas in terms of displacement and collision, respectively. Blue symbols show existing wind turbines. Red polygons delineate SPAs, irrespective of species designation.

2.3 Breeding colonial birds

The data from the GPS tagged birds showed that the tern species generally utilize marine areas close to land, with the exception of the lesser black-backed gull which used more offshore areas than the terns and furthermore also foraged far inland. Common guillemots utilized marine water at medium distances from land, compared to the other three species. The analyses presented here are based on data from the time of tagging up until 31 July of each year. Thus, the utilization of the marine area is not necessarily confirmed to the near area of the colonies, as many birds will have left the breeding colony before that time.

2.3.1 Sandwich tern

GPS tags were deployed on a total of 25 sandwich terns, producing a total of 116,077 positions. Of these, 112,487 positions were obtained before 1 August 2023 (Figure 2.9.).

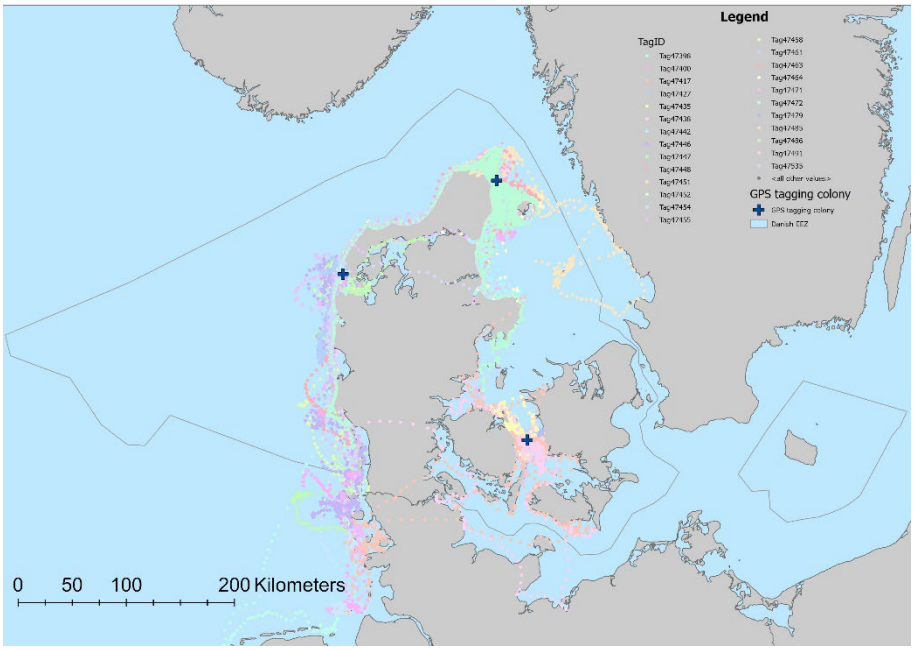

Figure 2.9. Tracking data from 25 Sandwich Terns during summer 2023.

Based on GPS-positions from 25 sandwich terns from the three colonies, Sprogø, Hirsholm and Krik Sandø, the marine utilization by sandwich terns up until 31 July was modelled. The results showed that the birds were mostly found in coastal waters. Highest utilization was the west coast of Jutland and particularly the southeastern parts of Danish North Sea (Figure 2.10.).

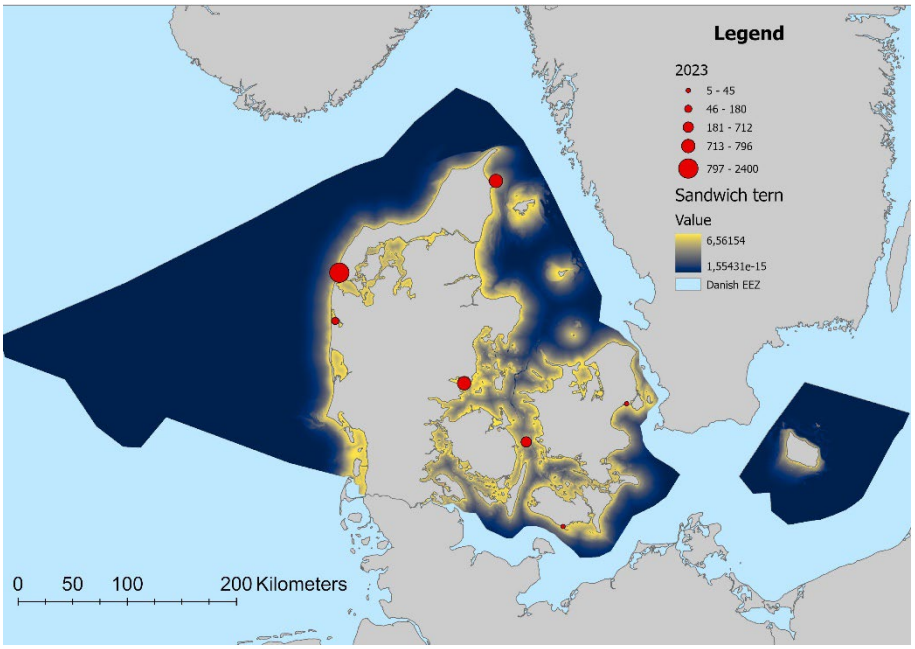

Figure 2.10. The estimated sandwich tern average presence in the marine area during the breeding season, up until 31 July. The colonies of 2023 used for the model are shown, indicating the number of breeding pairs in the colonies that year. Average presence was not weighted by colony size.

2.3.2 Arctic tern

GPS tags were deployed on 25 arctic terns in the Als Odde and the Krik Sandø colonies. Of those, 19 tags produced positions for the birds, providing a total of 2,785 positions. Most of these tags regretably felt off the birds after a very

short time. Only six birds produced more than 100 positions. Tags were deployed on 22 and 24 May 2023, and the longest period for data delivery by a bird was up until 4 June. The arctic terns utilised areas close to the colony more than was the case for sandwich tern (Figure 2.11.). This may be because the time window for the tagging was rather short and did not include the post-breeding period. Thus, these birds were more confined to waters close to the colonies than was the case for later summer situations for sandwich tern.

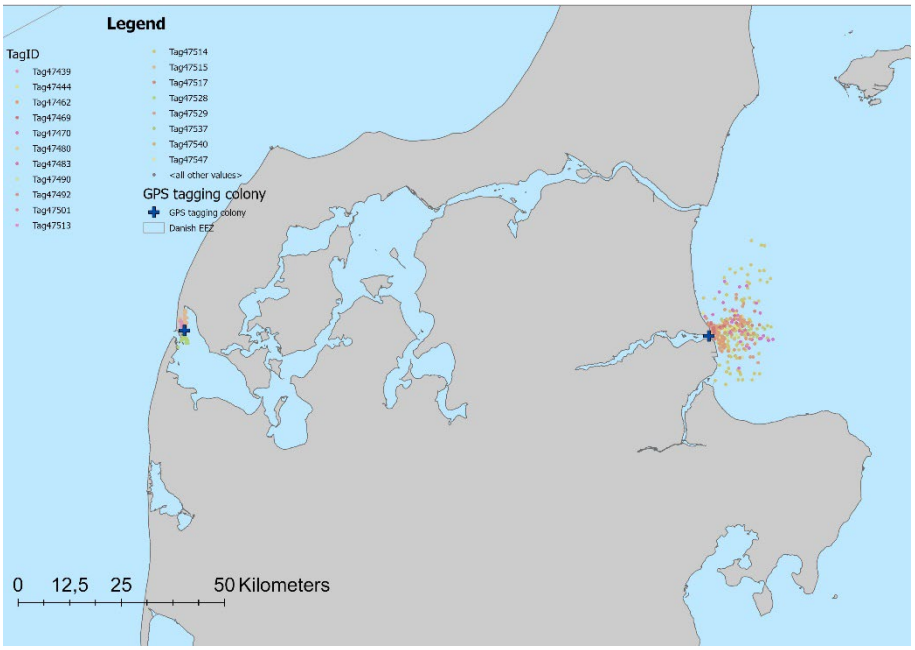

Figure 2.11. Tracking data from 19 Arctic Terns during summer 2023.

Using the distribution pattern from those two colonies and information on breeding colonies and sizes from 2022 the arctic tern utilization of the marine areas was modelled, indicating that the species used coastal or shallow waters (Figure 2.12.).

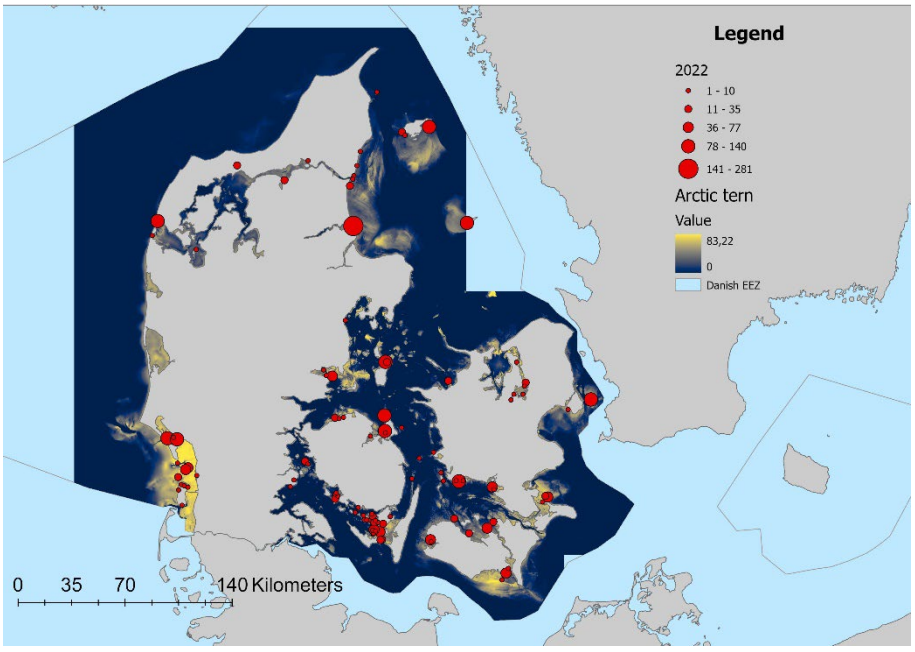

Figure 2.12. The estimated arctic tern average presence in the marine area during the breeding season, up until 4 June. The colonies of 2022 used for the model are shown, indicating the number of breeding pairs in the colonies that year. Average presence was not weighted by colony size.

2.3.3 Lesser black-backed gull

GPS tags were deployed on 26 lesser black-backed gulls at the Sprogø, Klægbanken and Hirsholm colonies. Of those, 23 tags produced positions from 24 birds (one tag, Tag 19331, was re-used on a different bird after falling off the first bird), providing a total of 335,287 positions. Lesser black-backed gulls utilized both marine and terrestrial areas over the summer, and in the marine areas moved much further offshore than was the case for the tern species (Figure 2.13.).

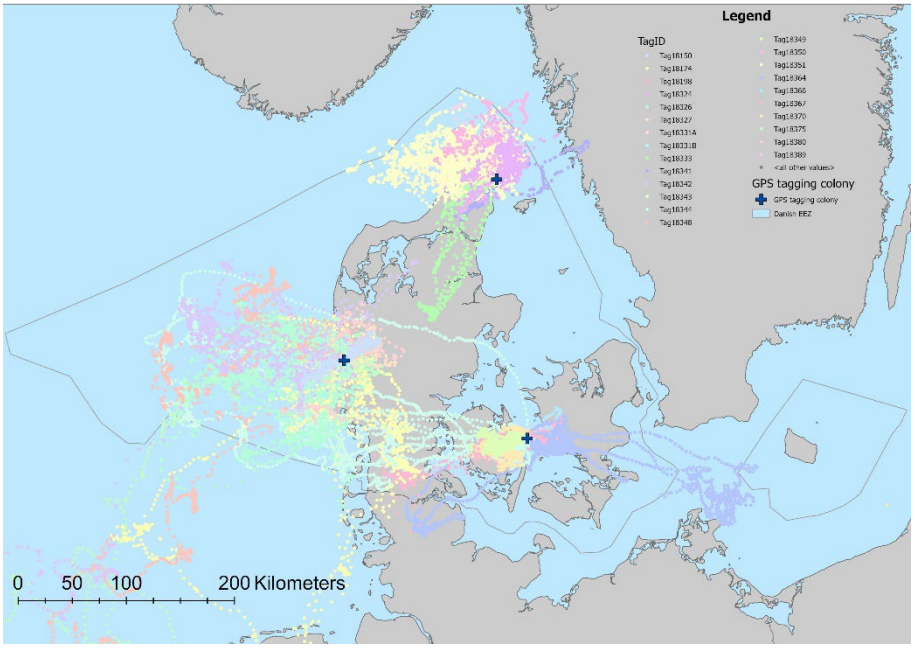

Figure 2.13. Tracking data from 24 lesser black-backed gulls during summer 2023.

Lesser black-backed gulls utilized both coastal and more offshore areas over the breeding season and the summer, though the coastal areas are most important for them. They utilized the western parts of the Danish North Sea less than the inner Danish waters and the eastern Danish North Sea (Figure 2.14.).

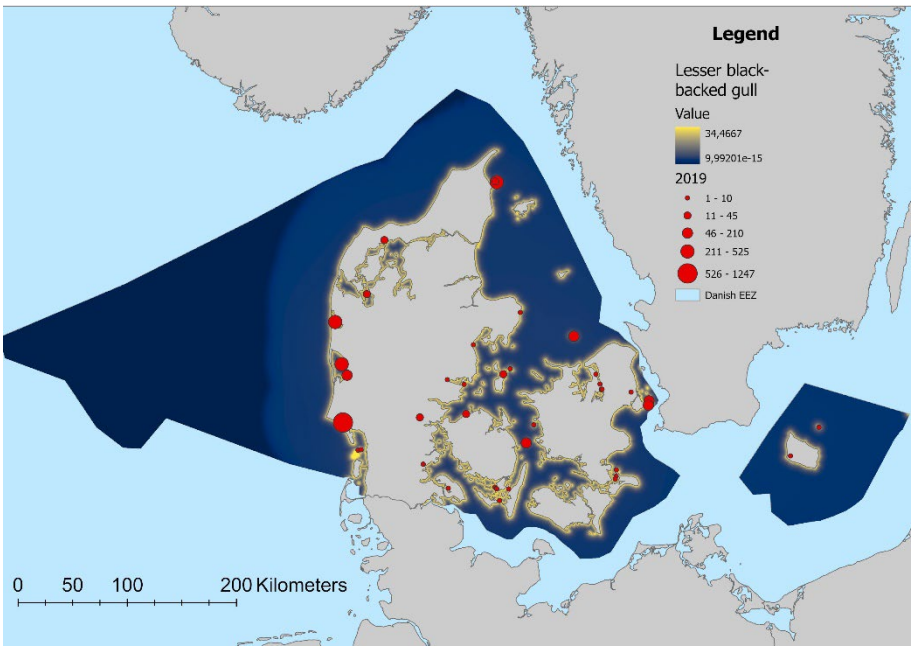

Figure 2.14. The estimated lesser black-backed gull average presence in the marine area during the breeding season, up until 31 July. The colonies of 2019 used for the model are shown, indicating the number of breeding pairs in the colonies that year. Average presence was not weighted by colony size.

2.3.4 Common guillemot

GPS tags were deployed on 19 common guillemots on Græsholmen near Christiansø, 15 in June 2023 and four in June 2024. Of those, 16 tags produced positions, providing a total of 9,077 positions.

Common guillemots feed primarily on small fish. They utilized the sea in all directions around Christiansø (Figure 2.15.).

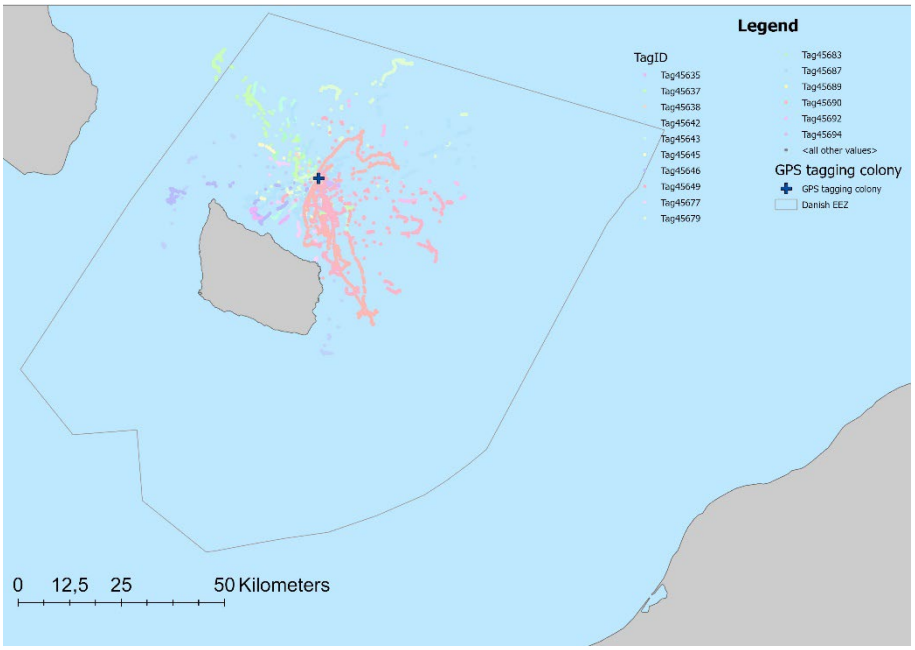

Figure 2.15. Tracking data from 16 common guillemots during summers of 2023 and 2024.

The area northeast of Bornholm was used most intensively by common guillemots over the breeding season (Figure 2.16.). The tags fell off the birds after a relatively short period of time, producing data from between two and 17 days. Since Græsholmen is the largest breeding colony of common guillemot in Denmark, with the only other small colony at nearby Hammeren, the modelled utilization of the marine areas is based on the data from Græsholmen directly, with no procedure to estimate utilization of the sea from other colonies.

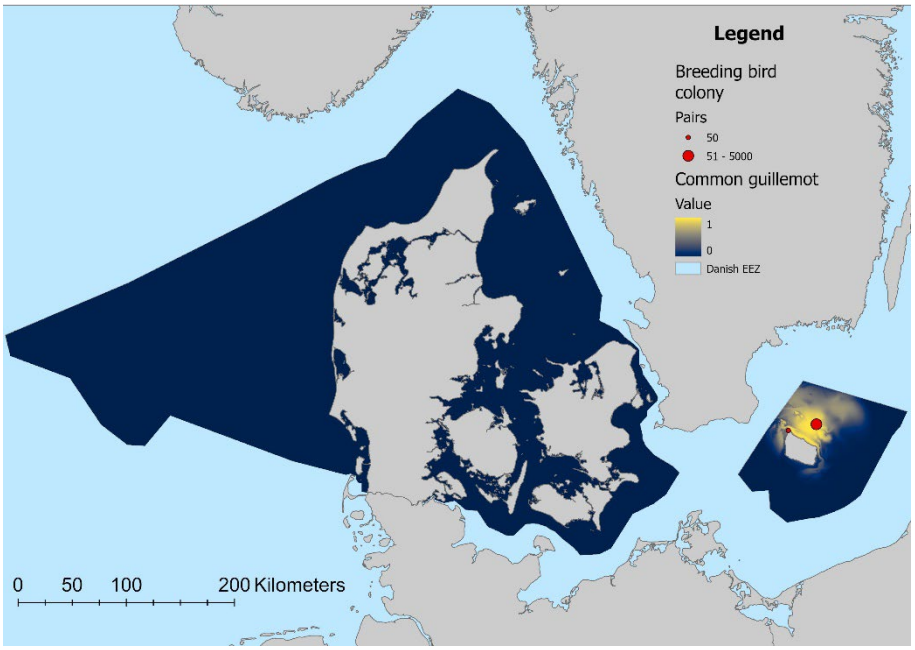

Figure 2.16. The estimated common guillemot average presence in the marine area during the breeding season, up until 21 June. The colonies are shown, indicating the approximate number of breeding pairs. Average presence was not weighted by colony size.

3 Discussion

We have developed and presented an approach to map relative risk to seabirds from future offshore wind energy developments throughout Danish marine waters. Risks for each hazard (habitat alteration, displacement, collision) were quantified relative to explicit assessment targets and according to their respective pathways of impact (Figure 1.1, Figure 1.2). The proposed spatial risk-ranking algorithm uses quantitative input parameters that can be informed by results from empirical displacement studies, collision risk modelling, and population modelling. Another advantage of the fully quantitative algorithm is that uncertainty can be propagated through the entire process. While we consider the results preliminary and outline several important caveats for their use below, the developed framework provides a foundation to refine the algorithm and accumulate upon additional empirical evidence to reduce assessment uncertainty. We also discuss results from the tracking data analyses that shed light on areas and hazards that have not yet been implemented in the spatial risk-ranking algorithm.

3.1 Risk-mapping: use notes and caveats

The results in this report can be used to identify potential development areas that minimize the risk of habitat alteration, displacement and collision to the modelled seabirds within the study area of Danish marine waters. The maps should not be used to extrapolate risks for non-modelled species, life history contexts, or hazard types not currently implemented in the algorithm, such as effects during the breeding season, barrier effects during daily commuting between colonies and at-sea foraging areas, or collision risk during migration. Importantly, the spatial risk-ranking was based on species density distributions estimated from aerial survey efforts focused on the winter and spring seasons, and to a smaller degree on summer and autumn distributions (Figure 1.3). During primary wind feather moult in late summer, many waterbirds are flightless for a three-week period, a time in which they are very sensitive to human disturbances. Data from this period of year is limited in this present analysis. This should be born in mind when interpreting the relative risk maps.

The input parameters describing the susceptibility of each species to collision and displacement were derived from published literature. The parameter values for each species were selected to average over reported effects from different studies, which could vary e.g., in offshore wind farm design and location (Section 1.1.4). The presented relative risk maps are therefore based upon current knowledge of impacts, pooled across different exposure contexts. The assessment did not consider different development scenarios or future changes in offshore wind farm design, such as wider spacing of larger turbines. It is possible that such changes, or other time-dependent processes such as habituation, will influence the susceptibility of different species to hazards differently, and consequently the distribution of relative species risks in space.

An important difference to previous sensitivity mapping approaches is that the maps presented here combine multiple species by maximum values, rather than sums or weighted averages, at any given location. This means that a high relative risk for one species cannot be compensated for by multiple low-risk species at the same location. This ensures a precautionary approach where the maps can be used to minimize risk for all species given their assessment targets, rather than the majority of species of concern.

The maps represent ranking of areas by relative species risk, which cannot be used to evidence negligible impact on seabird populations. Spatially relative risk means that values in each grid location are ranked with respect to all other grid locations in the study area. Relative species risk means that the risk posed by the three hazards (habitat overlap, displacement, and collision) are expressed relative to the user-specified assessment targets, target protection level (TPL) and habitat protection level (HPL). Furthermore, the combined map treats each of the three hazards as equal concern for populations. In reality, the same number of birds impacted by habitat alteration, displacement, or collision are likely to have three different levels of population impact. It is also important to note that the current approach to quantifying relative habitat risk considers all habitat alteration as unwanted, which does not account for potential positive effects, e.g., through reef effects or habitat enhancement. However, it would be possible to include such effects in the algorithm when more knowledge becomes available about possible positive effects of offshore wind farm structures for some species.

We present results for species units, some of which combined more than one ecologically similar species (Table 1.1). This approach was considered a pragmatic first approach to the multi-species assessment, as not all species are fully identifiable from aerial surveys. Because abundance estimates were made for each species unit, and maximum values were used to combine relative risks across multiple species, this choice did not influence the weighting of individual species on the multi-species hazard maps for habitat overlap, displacement and collision. In other words, the combined relative risk maps based on species units would be the same as maps based on individual species, as long as the input parameters for each species within each species unit were specified to be the same. However, it is worth noting that the maps presenting number of species exceeding HPL thresholds (Figure 2.3. middle panel, Figure 2.7. bottom panel) summarize the number of species units, rather than individual species.

The presented spatially relative risks were informed by cross-sectional surveys, rather than individual-based monitoring data, and as such, assume that spatially relative risks are proportional to species density. In other words, the approach does not account for any heterogeneity in space use or susceptibility to hazards within each population. Actual risks to populations emerge from the risks accumulated to their constituent individuals, which can vary within and between individuals over time and space. Cross-sectional metrics of impact can be expected to proxy actual impacts in well-mixed populations with space use resembling the ideal free distribution. However, the approach may under- or over-estimate risks when the population is not well-mixed, such as due to individual site fidelity, or differential exploitation of resources between age- and sex-classes.

The density distribution estimates underpinning the risk surfaces were generated by pooling aerial surveys across different seasons and multiple years

(1999-2024). To model species whose presence in Danish marine waters is strongly seasonal, data were *a-priori* excluded from seasons when they were considered absent (Table 1.4). The spatial patterns of risk therefore represent a long-term average of when the species are expected to be seasonally present in Denmark, and do not account for any changes in species abundance or density during the 25-year survey period.

The density distribution maps were estimated without correcting for availability bias (Dunn et al., 2024). This means that the presented estimated abundances can somewhat under-estimate the underlying, true abundance of birds present in Danish waters, particularly for diving species such as auks and divers.

3.2 Breeding and migratory birds

Spatial usage of the marine areas by colonially breeding birds over the summertime was estimated based upon GPS tagging data, but not yet implemented in the risk-ranking algorithm (see section 2.3). Future versions of the algorithm could be informed by these data. For example, GPS tagging data from migratory bird species could help to describe migration corridors and, in some cases, also flight altitude for the assessment of collision risk.

Since the present version of the algorithm is primarily based on the spatial distribution of birds over the non-breeding period of their life cycle, the addition of abundance and behaviour of breeding and migratory birds is likely to improve the use of the tool. For instance, the marine area east of Bornholm was identified as having a low risk for birds about offshore wind farms (Figure 2.5.). The GPS data from breeding birds showed that part of that area was utilized by breeding common guillemots (Figure 2.16.) and can potentially alter the result of the risk assessment. The inclusion of empirical data on the distributions of breeding and migratory birds will be addressed in upcoming versions of the risk-ranking algorithm.

3.3 Next steps and future developments

An essential next step is to carry out a statistical sensitivity analysis to address how uncertainty in the input parameters affect the outputs of the algorithm, both in terms of the three hazard maps and the combined risk map. The robustness of the algorithm should also be considered in terms of its assumptions and structure. A comparison of the risk maps both including and excluding species SPA designations indicated that, for the present study area and modelled species units, the outputs were not unduly influenced by the assumption of complete protection by species in designated SPAs.

All species units were modelled using the same general framework, but it is possible that the distribution maps of some species could be improved by tailoring the code. Additionally, all distance measures used in the spatial maps are Euclidean (as the crow flies) and some species may benefit from using Geodesic (as the fish swims) distances, under which distances are measured around obstacles, such as land, rather than across such obstacles. Inclusion of survey data from Swedish Kattegat could improve the framework especially for razorbills/common guillemots.

We envision several improvements and extensions to the spatial risk-ranking framework for seabird species (Figure 3.1). For example, breeding bird utilization could be included in the existing impact pathways. Movement

corridors could be considered by allowing a migration intensity map to inform an additional impact pathway for barrier effects. Future iterations of the algorithm could also consider individual species currently combined to species units (Table 1.1), provided that reliable estimates can be made of the composition of individual species in the combined unit abundance. This approach would likely still require assuming the same relative distribution of species within each unit but would be able to account for any differences in their total abundance, assessment targets and susceptibility to hazards (Table 1.1, Table 1.2). In a similar approach, to incorporate additional species currently excluded from the algorithm due to low sample size (Table 1.3), it may be possible to include ecologically similar species as a proxy. While it is not possible to estimate spatial distribution for some species with few detections, an estimate of detectability and abundance may still be possible through the distance sampling framework. Multi-species distance-sampling analyses, and joint species distribution modelling may also offer feasible avenues to borrow statistical power and make most of the available data.

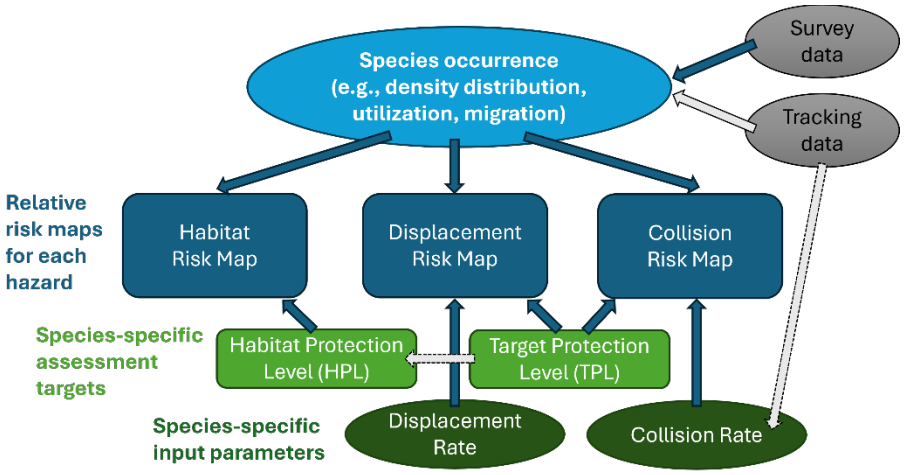

Figure 3.1. Future directions for the spatial risk-ranking approach. Future versions of the algorithm (grey arrows) could incorporate tracking data to inform species occurrence that is then input to each impact pathway (dark blue arrows). The tracking data could also be used to inform flight parameters to inform collision rates. We also envision that the target protection levels of each species should also inform the target protection levels of their habitat.

At this stage of development, we have focused on the interpretation of spatially relative risk, i.e., ranking of areas according to relative species risk. We do not attempt to interpret the magnitude of relative risk ratio values for each species unit due to the paucity of empirical data currently available to inform the associated input parameters e.g., on collision rates. However, there is scope to reduce uncertainty in the input parameters by informing these with further empirical results and collision risk modelling (Figure 3.1), as well as cross-validating relative species risks with population-level impact assessments for well-known species. This would allow a greater interpretative power and applicability of this approach to future strategic and cumulative risk assessments.

The spatial risk-ranking algorithm could be implemented as an interactive assessment tool, such as a ShinyApp. An interactive tool would allow users to modify input parameters for different use-cases and to generate and compare different scenarios, e.g., between different seasons, or under different assumptions about species-level impacts.

We foresee substantial scope to adapt and apply the assessment approach to different receptor groups than seabirds. Though the specific impact pathways vary, the developed algorithm and basic principles, such as target protection levels, could be applied to a broad range of species and phases of wind farm life cycle, thus providing consistency in assessment approach. For example, for marine mammals with seasonal variation in distribution, the algorithm could be used to generate seasonal maps to compare potential risks from pile driving between summer versus winter. Similar to the multiple hazard maps presented here for seabirds, multiple impact pathways could be considered for noise impacts on marine mammals, such as auditory injury and avoidance or other behaviour response. Indeed, the impact pathways could be user-specified as part of a comprehensive, interactive assessment tool.

4 Acknowledgments

This project was funded by Energistyrelsen. Via a contract between Energistyrelsen and NIRAS, Aarhus University/DCE and University of St. Andrews were subcontracted to conduct this risk assessment for birds. We are thankful to Energinet and NIRAS for the support provided.

A number of pilots and ornithological observers have contributed in the collection of data. We are very thankful to air companies, pilots and observers for their flexibility and support in this work.

5 References

Anthony Cox, L. 2008. "What's wrong with risk matrices?". *Risk Analysis* 28: 497–512.

Avian Displacement Guidance Committee. 2024. "Guidance for Pre- and Post-Construction Monitoring to Detect Changes in Marine Bird Distributions and Habitat Use Related to Offshore Wind Development".

Best, B. D., and P. N. Halpin. 2019. "Minimizing wildlife impacts for offshore wind energy development: Winning tradeoffs for seabirds in space and cetaceans in time". *PLoS ONE* 14: 1–26.

BirdLife International. 2021. "European Red List of Birds". *2021*.

Bradbury, G., M. Trinder, B. Furness, A. N. Banks, R. W. G. Caldow, and D. Hume. 2014. "Mapping Seabird Sensitivity to offshore wind farms". *PLoS ONE* 9.

Buckland, S. T., D. R. Anderson, K. P. Burnham, J. L. Laake, D. L. Borchers, and L. Thomas. 2001. "Introduction to Distance Sampling: Estimating Abundance of Biological Populations". Oxford University Press, United Kingdom.

Certain, G., L. L. Jørgensen, I. Christel, B. Planque, and V. Bretagnolle. 2015. "Mapping the vulnerability of animal community to pressure in marine systems: disentangling pressure types and integrating their impact from the individual to the community level". *ICES Journal of Marine Science* 72: 1470–1482.

Cox, L. A., D. Babayev, and W. Huber. 2005. "Some limitations of qualitative risk rating systems". *Risk Analysis* 25: 651–662.

Dierschke, V., R. W. Furness, and S. Garthe. 2016. "Seabirds and offshore wind farms in European waters: Avoidance and attraction". *Biological Conservation* 202: 59–68.

Dunn, R. E., J. Duckworth, S. O. Brien, R. W. Furness, L. Buckingham, M. Bogdanova, and J. A. Green. 2024. "Temporal and spatial variability in availability bias has consequences for marine bird abundance estimates during the non-breeding season". *bioRxiv*: 1–25.

European Environment Agency. 2017. "EEA coastline for analysis". https://sdi.eea.europa.eu/catalogue/srv/api/records/af40333f-9e94-4926-a4f0-0a787f1d2b8f.

Fauchald, P., V. M. S. Ollus, M. Ballesteros, A. Breistøl, S. Christensen-Dalsgaard, S. Molværsmyr, A. Tarroux, G. H. Systad, and B. Moe. 2024. "Mapping seabird vulnerability to offshore wind farms in Norwegian waters". *Frontiers in Marine Science* 11: 1–15.

Furness, R. W., H. M. Wade, and E. A. Masden. 2013. "Assessing vulnerability of marine bird populations to offshore wind farms". *Journal of Environmental Management* 119: 56–66.

Garthe, S., and O. Hüppop. 2004. "Scaling possible adverse effects of marine wind farms on seabirds: Developing and applying a vulnerability index". *Journal of Applied Ecology* 41: 724–734.

Garthe, S., H. Schwemmer, V. Peschko, N. Markones, S. Müller, P. Schwemmer, and M. Mercker. 2023. "Large-scale effects of offshore wind farms on seabirds of high conservation concern". *Scientific Reports* 13: 1–13.

Gibbs, M. T., and H. I. Browman. 2015. "Introduction: Risk assessment and risk management: A primer for marine scientists". *ICES Journal of Marine Science* 72: 992–996.

Hill, M. O. 1973. "Diversity and Evenness: A Unifying Notation and Its Consequences". *Ecology* 54: 427–432.

Kelsey, E. C., J. J. Felis, M. Czapanskiy, D. M. Pereksta, and J. Adams. 2018. "Collision and displacement vulnerability to offshore wind energy infrastructure among marine birds of the Pacific Outer Continental Shelf". *Journal of Environmental Management* 227: 229–247.

Lamb, J., J. Gulka, E. Adams, A. Cook, and K. A. Williams. 2024. "A synthetic analysis of post-construction displacement and attraction of marine birds at offshore wind energy installations". *Environmental Impact Assessment Review* 108: 107611.

Leys, C., C. Ley, O. Klein, P. Bernard, and L. Licata. 2013. "Detecting outliers: Do not use standard deviation around the mean, use absolute deviation around the median". *Journal of Experimental Social Psychology* 49: 764–766.

Linkov, I., D. Loney, S. Cormier, F. K. Satterstrom, and T. Bridges. 2009. "Weight-of-evidence evaluation in environmental assessment: Review of qualitative and quantitative approaches". *Science of the Total Environment* 407: 5199–5205.

Marques, F. F. C., and S. T. Buckland. 2004. "Covariate models for the detection function". Pages pp31--47 *in* S. T. Buckland, D. R. Anderson, K. P. Burnham, J. L. Laake, D. L. Borchers, and L. Thomas, editors. *Advanced Distance Sampling*. Oxford University Press, United Kingdom.

Marques, T. A., L. Thomas, S. G. Fancy, and S. T. Buckland. 2007. "Improving estimates of bird density using multiple-covariate distance sampling". *Auk* 124: 1229–1243.

Pya, N. 2024. "scam: Shape Constrained Additive Models. R package version 1.2-17". https://cran.r-project.org/package=scam.

Pya, N., and S. N. Wood. 2014. "Shape constrained additive models". *Statistics and Computing* 25: 543–559.

R Core Team. 2024. "R: A Language and Environment for Statistical Computing". R Foundation for Statistical Computing.

Scott-Hayward, L. A. S., M. L. Mackenzie, C. R. Donovan, C. G. Walker, and E. Ashe. 2014. "Complex Region Spatial Smoother (CReSS)". *Journal of Computational and Graphical Statistics* 23: 340–360.

Scott-Hayward, L. A. S., M. L. Mackenzie, C. G. Walker, G. Shatumbu, W. Kilian, and P. du Preez. 2023. "Automated surface feature selection using SALSA2D: Assessing distribution of Elephant carcasses in Etosha National Park".

Stelzenmüller, V., M. Coll, R. Cormier, A. D. Mazaris, M. Pascual, C. Loiseau, J. Claudet, S. Katsanevakis, E. Gissi, A. Evagelopoulos, B. Rumes, S. Degraer, H. Ojaveer, T. Moller, J. Giménez, C. Piroddi, V. Markantonatou, and C. Dimitriadis. 2020. "Operationalizing risk-based cumulative effect assessments in the marine environment". *Science of the Total Environment* 724.

Tamis, J. E., P. de Vries, R. H. Jongbloed, S. Lagerveld, R. G. Jak, C. C. Karman, J. T. Van der Wal, D. M. Slijkerman, and C. Klok. 2016. "Toward a harmonized approach for environmental assessment of human activities in the marine environment". *Integrated environmental assessment and management* 12: 632–642.

Tyack, P. L., L. Thomas, D. P. Costa, A. J. Hall, C. M. Harris, J. Harwood, S. D. Kraus, P. J. O. Miller, M. Moore, T. Photopoulou, E. Pirotta, R. M. Rolland, L. H. Schwacke, S. E. Simmons, and B. L. Southall. 2022. "Managing the effects of multiple stressors on wildlife populations in their ecosystems: developing a cumulative risk approach". *Proceedings of the Royal Society B: Biological Sciences* 289: 20222058.

USEPA. 2016. "Generic Ecological Assessment Endpoints (GEAEs) For Ecological Risk Assessment: Second Edition With Generic Ecosystem Services Endpoints Added". *Usepa*.

Vanermen, N., W. Courtens, R. Daelemans, L. Lens, W. Müller, M. Van De Walle, H. Verstraete, and E. W. M. Stienen. 2020. "Attracted to the outside: A meso-scale response pattern of lesser black-backed gulls at an offshore wind farm revealed by GPS telemetry". *ICES Journal of Marine Science* 77: 701–710.

Verling, E., R. Miralles Ricós, M. Bou-Cabo, G. Lara, M. Garagouni, J. M. Brignon, and T. O'Higgins. 2021. "Application of a risk-based approach to continuous underwater noise at local and subregional scales for the Marine Strategy Framework Directive". *Marine Policy* 134.

Walker, C. G., M. L. Mackenzie, C. R. Donovan, and M. J. O'Sullivan. 2011. "SALSA - a spatially adaptive local smoothing algorithm". *Journal of Statistical Computation and Simulation* 81: 179–191.

Welcker, J., and G. Nehls. 2016. "Displacement of seabirds by an offshore wind farm in the North Sea". *Marine Ecology Progress Series* 554: 173–182.

Wood, S. N. 2011. "Fast stable restricted maximum likelihood and marginal likelihood estimation of semiparametric generalized linear models". *Journal of the Royal Statistical Society. Series B: Statistical Methodology* 73: 3–36.

6 Appendix 1: Glossary

Table 6.1. Glossary of terms

Term	Definition
Assessment metric	An explicit expression of the environmental value to be assessed. Analogous to assessment end-point: "An explicit expression of the environmental value to be protected, operationally defined as an ecological entity and its attributes" (USEPA, 2016). Here, we use three assessment metrics: the degree of overlap with core habitat, the expected number of seabirds at risk of displacement, and the expected number of birds at risk of collision.
Assessment outcome	The outcome value of assessment metrics following environmental (risk) assessment
Assessment target	The desired, or acceptable, value for each assessment metric, which can be used to benchmark the performance of assessment outcomes in achieving targets. Such benchmarking also enables the comparison of assessment outcomes of receptors with different targets. We considered the following assessment targets: Habitat protection level (HPL, h_i^*): the proportion of each species' range that should be protected from any additional habitat alteration, reflecting the dependence of each species on spatially limited resources. HPL was used to benchmark the degree of overlap with core habitat metric. Target protection level (TPL, p_i^*): the desired level of complete protection for each species unit in Danish national waters, given current population status, trends, and resilience to existing threats. Specifically, the TPL was defined as the proportion of the current population size in the national waters that should be protected from any additional habitat loss, mortality, and impaired reproduction, to maintain or achieve favourable conservation status. TPL was to benchmark both the displacement and collision metrics.
Hazard	The source of risk. "Element which alone or in combination has the intrinsic potential to give rise to risk" (ISO 31000). Here, we considered three hazards: habitat overlap, displacement, and collision due to wind farm presence.
Risk	In the broadest sense, defined as "The effect of uncertainty on objectives" (ISO 31000). Typically used to describe both the likelihood and consequence of unwanted or adverse effects, such as in ecological risk assessment (ERA) (Gibbs & Browman, 2015). When the objective of the ERA is to protect individuals or populations of animals, risk can be defined as "The probability of harmful effects to the health of individuals or to populations integrated over a defined time period" (Tyack et al., 2022).
Risk-ranking	The ordinal ranking of risk from low to high values. Risk-rankings only contain information about the order of values, or the position of an element in an ordered series, not absolute value or magnitude differences in risk level.
Relative risk	Risk expressed relative to a chosen benchmark level of risk. While relative risk does not express the absolute value of risk, relative risk can be ranked, as well as inform about the magnitude differences in risk compared to the benchmark. Here, we quantify relative risk to collision and displacement as the ratio between expected number of affected individuals and the acceptable number of affected individuals (1-TPL). Similarly, to quantify relative risk of habitat overlap, the expected overlap with core habitat was benchmarked by the acceptable level of overlap (1-HPL).
Relative species risk	Species risks expressed relative a species benchmark, such as a minimum viable population size. In this work, we define relative species risk with respect to assessment targets. Relative species risks were calculated for each hazard as relative risk ratios, with the assessment metric as the numerator and assessment target in the denominator.
Spatially relative risk	Risk expressed relative in space. Spatially relative risks may be benchmarked relative to a specific area, or represent a ranking within the whole area. With the assessment objective being a spatially explicit risk-ranking (i.e., a sensitivity map), we chose the ranking approach, and thus the mapped risks are relative to the lowest and highest values in Danish marine waters.
Species unit	Individual species or ecologically similar species groups (Table 1.1) that were analysed together as a unit in the analysis. Individual species within species groups were assumed to have broadly similar distribution and habitat preference, target protection level, displacement rate and collision risk.

7 Appendix 2: Spatial analysis details

7.1 Data collection

Visual aerial surveys were used to collect data on seabirds using line transect distance sampling methods (Buckland et al., 2001). During these surveys, trained observers searched for, and recorded birds into distance bands in addition to environmental conditions at the time (e.g. sea state or sun glare). The detections were recorded in four distance bins (A-D) with categories of: 0m - 119m, 119m-388m, 388m-956m and 956m-1456m perpendicular to the survey track line (Figure 6.1). No band under the plane was recorded. Not all detections could be identified to species level, in which case species were identified to the nearest taxon (Table 1.1).

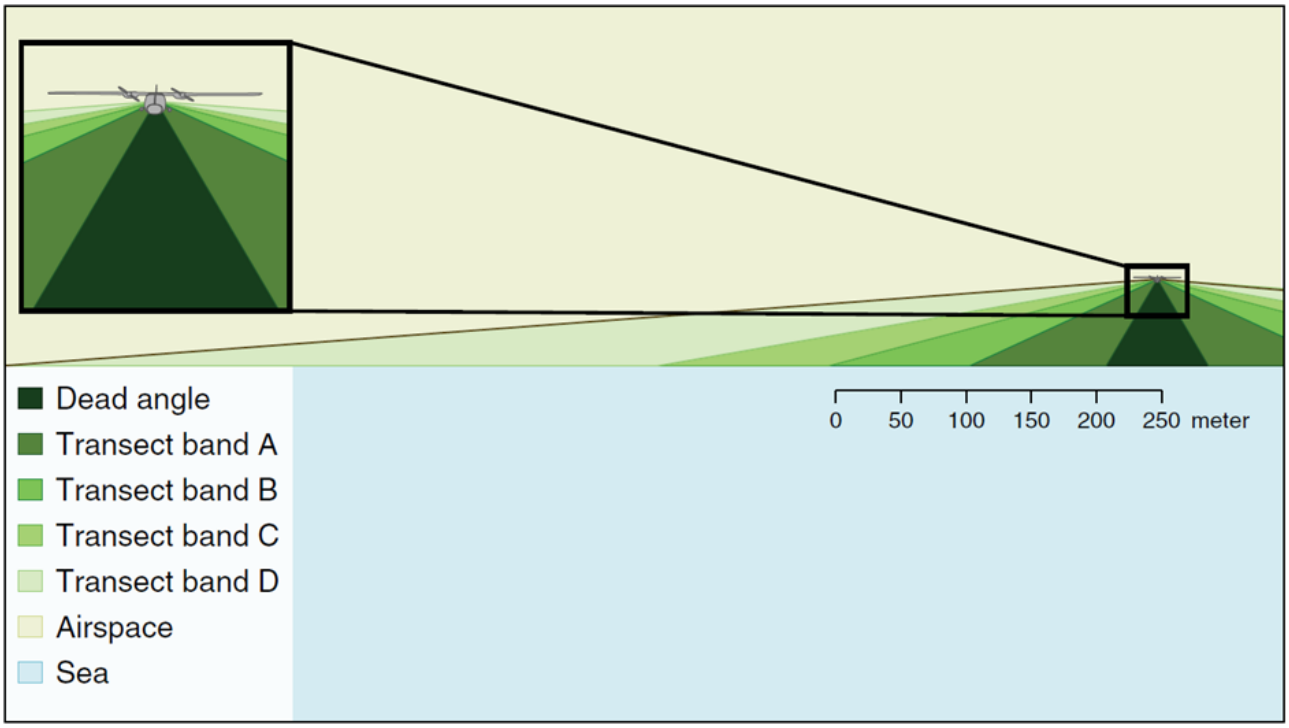

Figure 6.1. The transect band definitions for aerial line transect surveys. From the survey altitude of 76 m, there is a dead angle of 44 m on each side of the survey track that the observers could not cover.

7.2 Data processing

Each surveyed transect from each survey day and aircraft were given a unique identifier Survey transects were divided into 0.5 km segments. Survey effort, environmental variables (e.g., water depth) and any species detections were associated with the time and coordinate information for each segment. All latitude/longitude locations were converted to UTMs using UTM Zone 32N with Datum ETRS.

Detection of seabirds from aerial surveys can be influenced by sighting conditions, such as sun glare and sea state. Data to describe sighting conditions is usually collected in-situ, however in few cases when this is absent, alternative methods are required to identify (and adjust for) heterogeneity in the detection probability. Accounting for such heterogeneity is particularly important when using the distance sampling method, where near-perfect detection at the track line is an often-required assumption.

We used detection information from band A for the left-hand and right-hand sides of the aircraft to identify transect lines with likely poor sighting conditions. For all modelled species units except flying Gannet and Kittiwake (Table 1.1), which are much easier to see even when glare is present, the identified transects had observations from the affected side removed and the coverage reduced to one side (i.e. returning a one-sided transect).

The effects of glare, and any mitigations as a result, was approached using a dedicated analysis. The analysis was designed to quantify the extent that directional sun glare can lead to left/right hand side bias in counts within a single transect line with the same direction of travel. Specifically, we assumed that the proportion of left or right sightings in band A should be 0.5 and follow a Binomial distribution. We compared the proportions for each transect to a critical value calculated as the quantile of the Binomial distribution ($n, p = .5$) at three standard errors greater than the mean and where is equal to the number of observations on the transect. Three standard errors is a common measure in extreme value theory (Leys et al., 2013). Any transects whose values were greater than the critical value had the observations from the smaller side removed and the coverage reduced to a single side.

7.3 Modelled species and seasons

The distance and spatial analyses were carried out separately for 17 seabird species units, representing either individual species or species groups (Table 1.1). Ecologically similar bird species that are challenging to identify to species level from aircraft were grouped together. The groups included red- and black-throated divers (hereafter, divers), red-necked and crested grebe (hereafter, grebes), common- and herring gull (hereafter, grey gulls), common-, arctic-, and sandwich terns (hereafter, terns), and razorbills and common guillemots (hereafter, alcids). Hereafter, for brevity, the 17 species and species groups (Table 1.1) are referred to as the modelled species units.

For each modelled species unit we estimated a single density surface, averaging across all survey years and seasons in Danish waters. However, for species whose presence in Danish waters is strongly seasonal, due to their migration schedule, the spatial analysis excluded survey data from seasons that the species unit was considered absent *a-priori* (Table 1.4). This avoided introducing uncertainty to the static density distribution maps that was solely due seasonal variation in presence-absence. For example, divers were considered absent during summer, and therefore only surveys from autumn, winter, and spring were included in the spatial analysis for this species unit.

7.4 Distance sampling analysis

Distance sampling analyses were conducted for each species unit by pooling the information from each survey. For all species except gannet, band D was removed from analysis owing to little or no observations from that distance bin.

When fitting detection functions, the effects of covariates, other than perpendicular distance, are incorporated into the detection function model directly (Multiple Covariate Distance Sampling, MCDS)(Buckland et al., 2001; Marques & Buckland, 2004; Marques et al., 2007). In these cases, the probability of detection becomes a multivariate function, which represents the probability of detection at perpendicular distance and covariates. In this study, using a half-normal detection function $e^{-(\frac{y^2}{\sigma^2})}$ the covariates were incorporated via the scale term, σ, where for sighting j, σ has the form:

$$\sigma_j = \exp\left(\beta_0 + \sum_{q=1}^{Q}(\beta_q v_{j,q})\right)$$

where β_0, and β_q $(q = 1, \dots, Q)$ are parameters to be estimated (Buckland et al., 2001). Both half-normal and hazard rate detection functions were fitted with BIC used to choose between the two models. The candidate variables trialled were bird group size, behaviour, observer, and sea state (Table 4). Observers that had small sample size (<30 observations in total, or any distance bands with no observations) were combined into "Other" category. Sea state, a classification of wave activity, was recorded in classes of 0.5, and was tested both with and without rounding to the nearest integer. Observations with sea states greater than four were removed.

7.5 Modelling framework

The response variable for the spatial models was bird counts in a small area (segment) corrected for detectability. This response variable was modelled using a Tweedie framework, which includes an estimated dispersion parameter (φ) and Poisson-Gamma mixing parameter (ξ) to return an appropriate mean-variance relationship. The mixing parameter takes values from 1 (equivalent to quasi-Poisson) and 2 (equivalent to Gamma). If the estimated parameter was close to one, the models were considered quasi-Poisson.

Model selection included a set of one-dimensional models with a single candidate covariate each (water depth, distance to coast). Additionally, to account for more realistic (and localised) surface patterns, which could be caused by unmodelled environmental variability, a spatial surface was also fitted to each model. Specifically, a two-dimensional CReSS-based surface using a Gaussian radial basis function was included in the model (Scott-Hayward et al., 2014).

As an illustration, the following equation represents an example of a Tweedie model with log link function, fitted with a one-dimensional smooth term (e.g., bathymetry) alongside a two-dimensional spatial smooth:

$$y_{i,j} \sim Tw(\mu_{i,j}, \varphi, \xi)$$
$$\mu_{i,j} = e^{\beta_0 + s_1(Bathymetry_{i,j}) + s_2(Xpos_{i,j}, Ypos_{i,j})}$$

where $y_{i,j}$ is the estimated count for transect i segment j and s_1 represents either a quadratic -spline or natural cubic spline smooth of depth. Here, s_2 is a two dimensional smooth of space (with coordinates $Xpos_{i,j}$ and $Ypos_{i,j}$ in UTMs). Implicit in this model are also coefficients for the intercept (β_0) and any spline-based coefficients associated with the smooth terms. The effort associated with each observation varied depending on the associated segment

length and width. Segment area was therefore included as a log-scale offset term in the model.

A globally applicable depth or distance to coast term and a more flexible spatial term were trialled for inclusion in each model, to indicate how spatial patterns should be modelled in each case. In other words, this quantifies if any spatial patterns are sufficiently described by the one-dimensional covariates (which applies the same across the surface) or if a more considered approach to spatial patterns was required for each species. For example, if the model selection procedure resulted in the inclusion of depth and the exclusion of a two-dimensional spatial element, then this signals that any spatial patterns are primarily a function of the depth, regardless of the geographical location of this depth in the survey area.

If the two-dimensional spatial term was selected for inclusion in a model, then the spatial density patterns, over and above any environment-related terms, were accommodated using a spatially adaptive term. This permitted different amounts of flexibility across the surface in a targeted, yet parsimonious, way. In other words, relatively complex spatial patterns could be accommodated with very few parameters.

Selection between competing models was undertaken using a 5-fold cross validation metric, whilst preserving any within-transect correlation via the appropriate blocking structures.

7.6 Model specification, selection and fitting

CReSS-SALSA based spatially adaptive generalized additive models, with targeted flexibility, were fitted to data from each survey to allow for non-linear relationships between the one-dimensional and two-dimensional covariates and the response (Walker et al., 2011; Scott-Hayward et al., 2014, 2023).

All covariates were permitted to have a linear or nonlinear relationship with the response, and when a smooth term was included in a model, it was specified to be either a quadratic (degree 2) B-spline (df=3,4,5) or a natural cubic spline (df=2,3,4). In cases where these degrees of freedom boundaries were reached however, a broader range of parameters were trialled instead. The degrees of freedom for these terms determine the flexibility of these smooth relationships - the more degrees of freedom, the more flexible, and the more non-linear, the relationship can be.

The location of this flexibility (along the x-axis) in these terms (e.g., depth) was also determined as part of the model selection process. This permitted the relationship in some areas of the covariate range to be relatively complex (e.g., in shallow waters) and the relationship in other areas (e.g., in deep waters) to be relatively simple. In both smooth types, a maximum of three internal knots was permitted along with the spline-specific number of boundary knots. The number and location of knots was determined by an objective fit criterion.

The spatial patterns in each analysis were based on a two-dimensional spatial term, which varied in complexity. The flexibility of the spatial element constituted part of the model selection procedure and for each survey was determined using a Spatially Adaptive Local Smoothing Algorithm (SALSA). While this model selection element technically occurred between limits (df=[2,100]), in practice, the flexibility chosen in each case was not bounded by those values, since the selection procedure occurred well within the bounds of the specified range.

The MRSea R package, designed to fit both CReSS and SALSA type models, was used for model fitting and a 5-fold cross-validation (CV) procedure was used to govern all model selection elements (Scott-Hayward et al., 2023; R Core Team, 2024). The CV procedure attempts to balance the fit to data unseen by the model while minimising the number of parameters, and was used to both select terms and the extent of their flexibility in each model. Note, this cross validation was predicated on preserving correlated blocks of survey data (transect lines) so that any residual autocorrelation present was not disrupted when choosing folds. This was considered necessary to ensure independent sampling units under the scheme.

The response data were collected along survey lines in sequence, and so consecutive observations were likely to be correlated in space and time. In other words, points closer together in space and/or time were likely to be more similar than points that were distant in time and/or space. The covariates included in the model were unlikely to explain these patterns in full, and so some element of these patterns likely remain in model residuals. Such patterns are a violation of residual independence, which underpin traditional model approaches such as Generalized Additive Models. Therefore, robust standard errors were used as part of the MRSea modelling framework to account for residual autocorrelation.

Uncertainty about model parameter estimates proceeded via robust standard errors due to the nature of the survey procedure. These essentially work by inflating the standard errors in relation to the positive correlation observed within pre-specified blocks of residuals. In cases, where this residual correlation is minimal, the adjustments are small, and when the correlation is more extreme, the inflation is larger.

A transect-based blocking structure was used to reflect potential correlation within blocks while independence (i.e., no correlation) between blocks was assumed. To ensure this assumption was realistic, the decay of any residual correlation to zero (i.e., independence) with the distance between points (within blocks along transects) was assessed visually. Specifically, transects in each survey were used as the blocking structure and an Auto Correlation Function (ACF) plot on this basis was used to check the suitability of this blocking structure, via a 'decay to zero' trend within blocks.

7.7 Model diagnostics

To assess the adequacy of model fit in each case, a range of diagnostic measures were used.

The assumed mean-variance relationship under the model was assessed visually using plots of the fitted values from the model against the variance of

the residuals. In this analysis, Tweedie models were employed which assume a nonlinear mean-variance relationship:

$$Var(y) = V(\mu)\phi = \mu^{\xi}\phi$$

where ϕ is the dispersion parameter. The dispersion parameter was estimated for each model and this estimate was used in the visual assessment of this mean-variance relationship assumed to hold under the model. The power parameter was estimated prior to model fitting using a maximum likelihood profile approach. Based on the nature of the response data, values of were permitted between 1 (Quasi-Poisson) and 2 (Gamma).

QQ plots and residuals against predicted values plots were assessed to ascertain the level of agreement between the data and the model. These plots were created using the DHARMa R package and using simulated residuals. Regarding interpretation, the left panel is a uniform QQ plot, and the right panel shows residuals against predicted values, with outliers highlighted in red. Given these outputs, we would expect that a correctly specified model shows:

a) straight 1-1 line, as well as no compelling evidence against the null hypothesis of a correct overall residual distribution, as indicated by the p-values for the associated tests in the QQ-plot.

b) visual homogeneity of residuals in both the vertical and horizontal directions, in the residuals against predictor plot.

Pearson residuals for each model were also visualised spatially to ensure there were no areas of consistent bias across the survey area. This would be indicated by clusters of negative or positive residuals in spatially similar locations.

Residual independence was not assumed to hold under the model and instead model inference proceeded under robust standard errors. As described, Auto Correlation Function (ACF) plots were instead used to check the suitability of this blocking structure, via a 'decay to zero' trend within blocks.

8 Appendix 3: Spatial outputs, diagnostics and risk-mapping by species unit

8.1 Razorbill/ common guillemot. Species unit “Alcid”

8.1.1 Aerial survey dataset

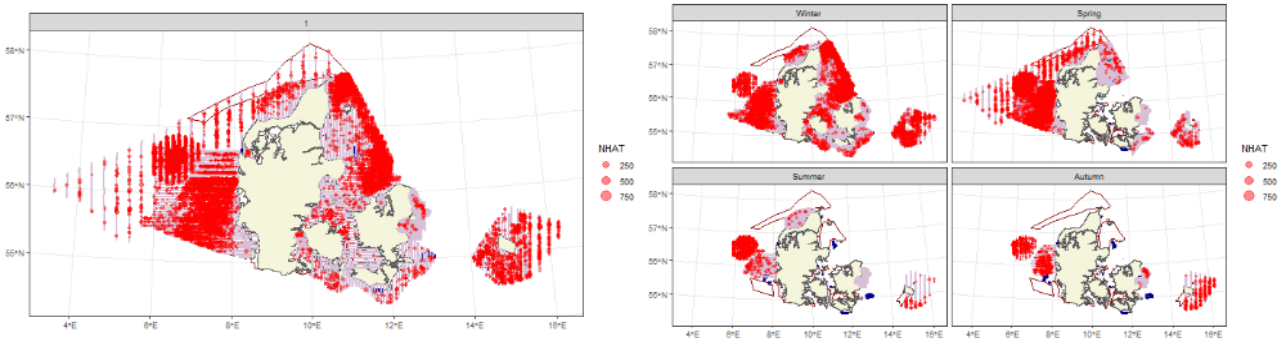

Figure 8.1. Maps showing observed counts (red) and effort segments (pink). Left panel: analyzed dataset for the species unit, pooled across those seasons the species unit was considered present (Table 1.4). Right panel: all data for the species unit, split across the seasons.

8.1.2 Spatial model outputs

Figure 8.2. Maps showing predicted counts (top) and bootstrapped uncertainty (bottom), overlaid with data. Data are shown as average counts in a grid of 20-km-wide hexagons.

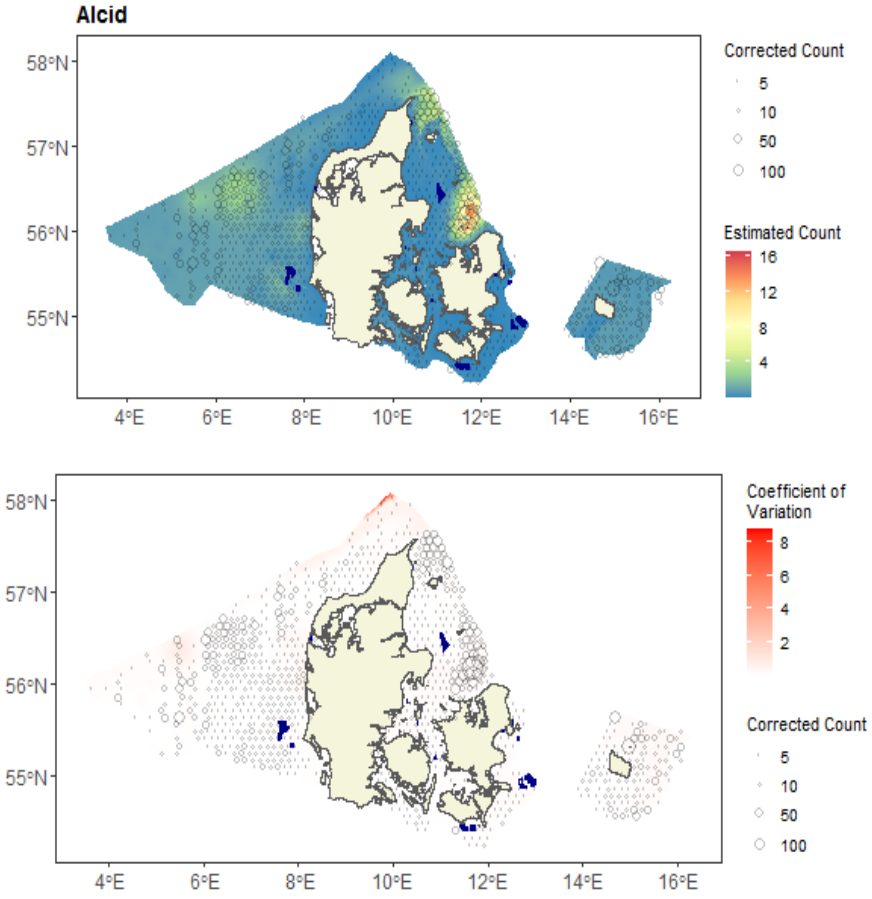

8.1.3 Diagnostics for the spatial model

Var. 1D	Var. 2D	# Pars.	Dispersion par.	CV score
s(depth, df=3)	s(x,y, df=12)	16	36.1	36.3

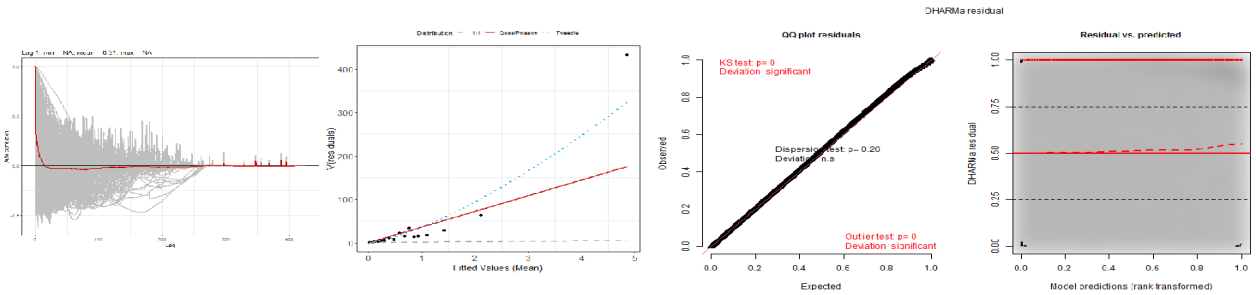

Figure 8.3. Figure showing diagnostics for the selected best spatial model. Left-most panel: within-block autocorrelation function, with the grey lines representing the residual correlation observed in each transect and the red line the average of these values across transects. Second panel: the estimated Tweedie mean-variance relationship (red line) against observed values (black symbols), with grey dashed line showing 1:1 relationship for reference. Third and right-most panel: QQplot and residuals against predicted values. The red stars are outliers and the red line is a smooth spline around the mean of the residuals.

8.1.4 Risk-mapping

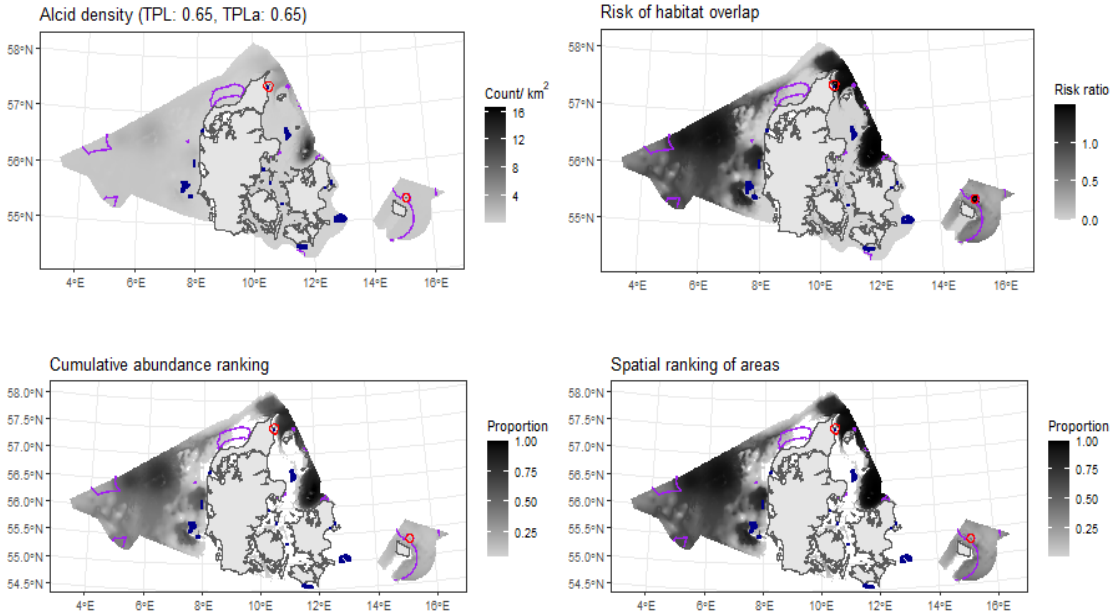

Figure 8.4. Figure showing the rescaling of estimated density distribution to habitat risk for the species unit. Bottom left and right: species unit abundance and top-use areas as cumulative percentiles (up to 0.95 abundance, defining species unit range). Red polygons: SPAs designated for one or more species in the species unit. Purple polygons: low-risk areas identified in Figure 2.5. Blue symbols: existing wind turbines.

8.2 Red-throated diver/ black-throated diver. Species unit "Diver"

8.2.1 Aerial survey dataset

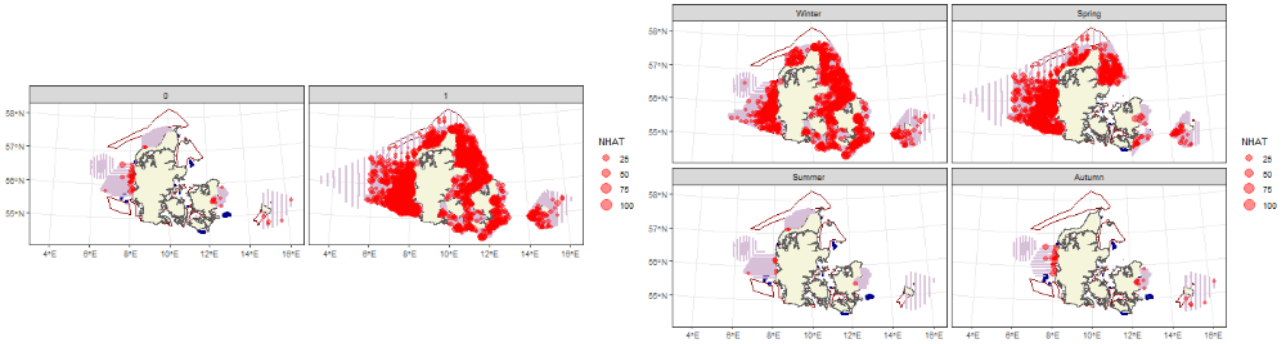

Figure 8.5. Maps showing observed counts (red) and effort segments (pink). Left panel: analyzed dataset for the species unit, pooled across those seasons the species unit was considered present (Table 1.4). Right panel: all data for the species unit, split across the seasons.

8.2.2 Spatial model outputs

Figure 8.6. Maps showing predicted counts (top) and bootstrapped uncertainty (bottom), overlaid with data. Data are shown as average counts in a grid of 20-km-wide hexagons.

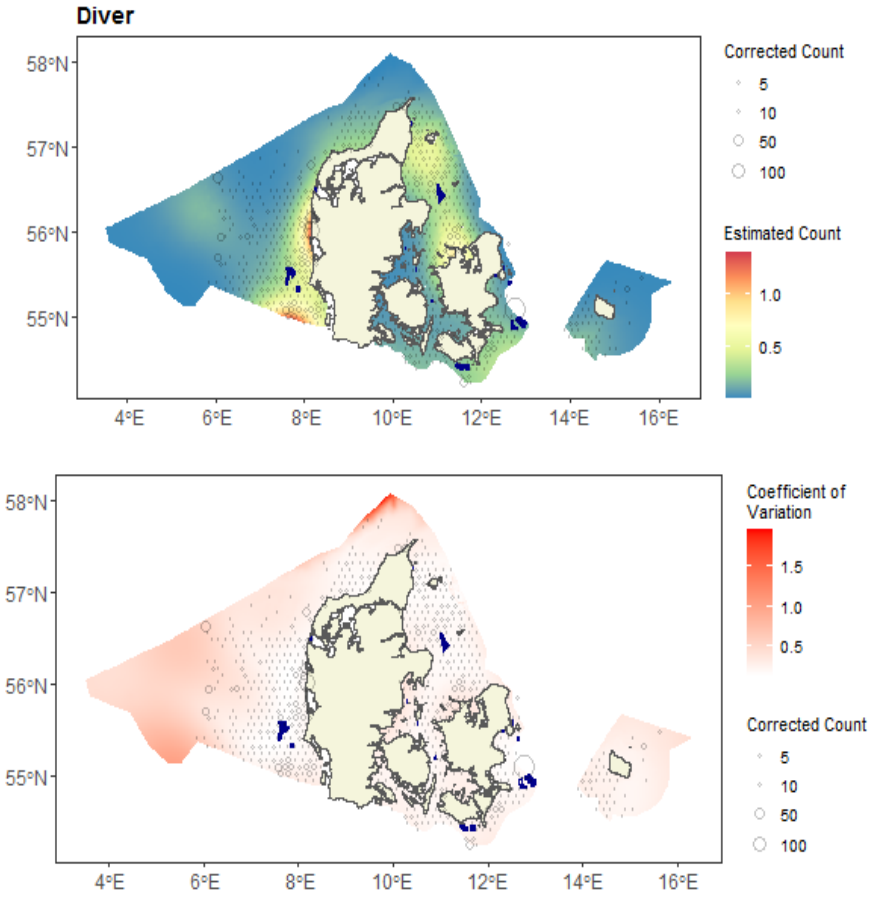

8.2.3 Diagnostics for the spatial model

Var. 1D	Var. 2D	# Pars.	Dispersion par.	CV score
depth, df=1	s(x,y, df=17)	19	28.9	3.4

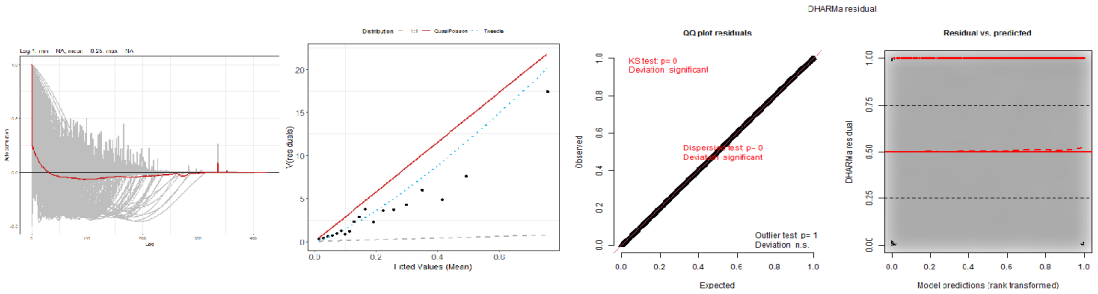

Figure 8.7. Figure showing diagnostics for the selected best spatial model. Left-most panel: within-block autocorrelation function, with the grey lines representing the residual correlation observed in each transect and the red line the average of these values across transects. Second panel: the estimated Tweedie mean-variance relationship (red line) against observed values (black symbols), with grey dashed line showing 1:1 relationship for reference. Third and right-most panel: QQplot and residuals against predicted values. The red stars are outliers and the red line is a smooth spline around the mean of the residuals.

8.2.4 Risk-mapping

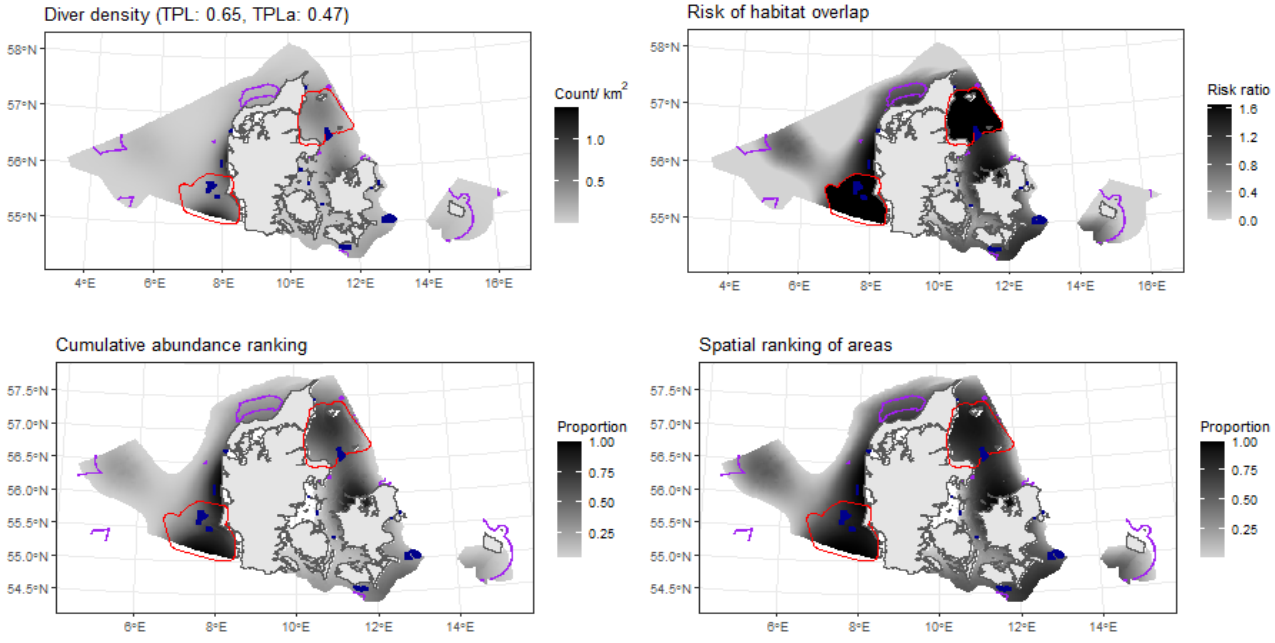

Figure 8.8. Figure showing the rescaling of estimated density distribution to habitat risk for the species unit. Bottom left and right: species unit abundance and top-use areas as cumulative percentiles (up to 0.95 abundance, defining species unit range). Red polygons: SPAs designated for one or more species in the species unit. Purple polygons: low-risk areas identified in Figure 2.5. Blue symbols: existing wind turbines.

8.3 Common eider. Species unit “Eider”

8.3.1 Aerial survey dataset

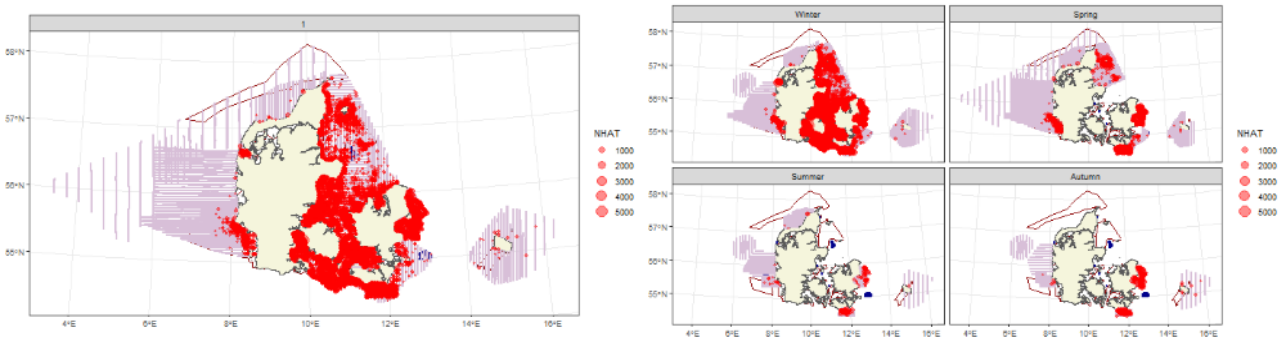

Figure 8.9. Maps showing observed counts (red) and effort segments (pink). Left panel: analyzed dataset for the species unit, pooled across those seasons the species unit was considered present (Table 1.4). Right panel: all data for the species unit, split across the seasons.

8.3.2 Spatial model outputs

Figure 8.10. Maps showing predicted counts (top) and bootstrapped uncertainty (bottom), overlaid with data. Data are shown as average counts in a grid of 20-km-wide hexagons.

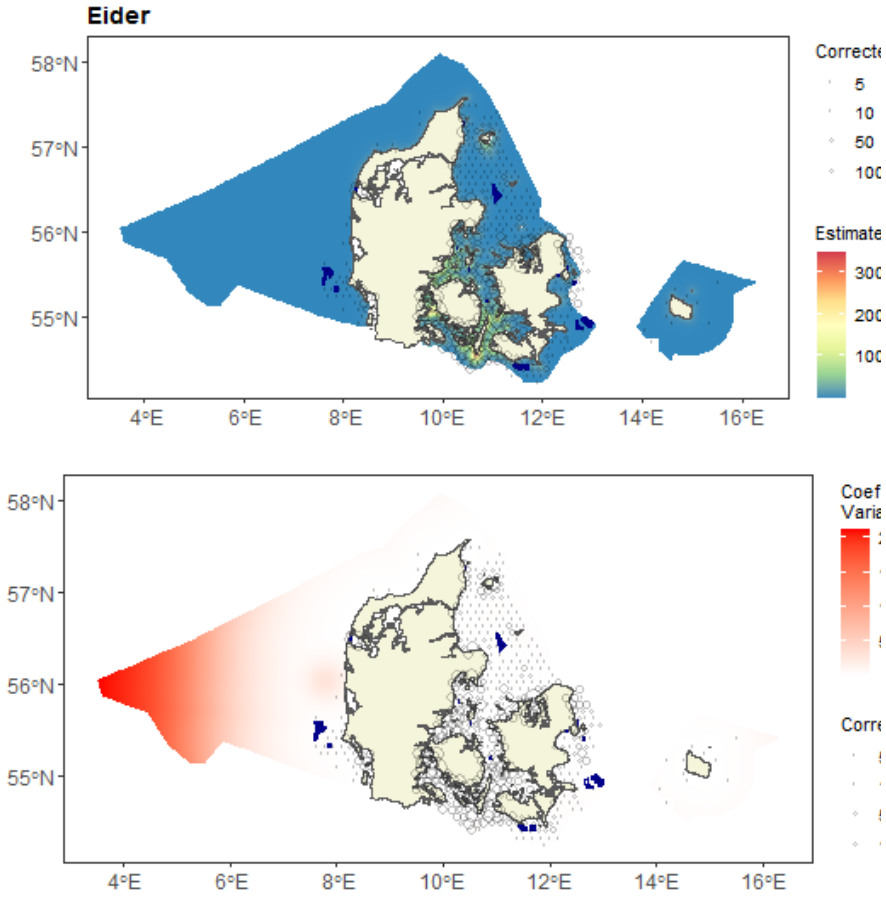

8.3.3 Diagnostics for the spatial model

Var. 1D	Var. 2D	# Pars.	Dispersion par.	CV score
s(distcoast, df=2)	s(x,y, df=12)	15	305.4	1814.5

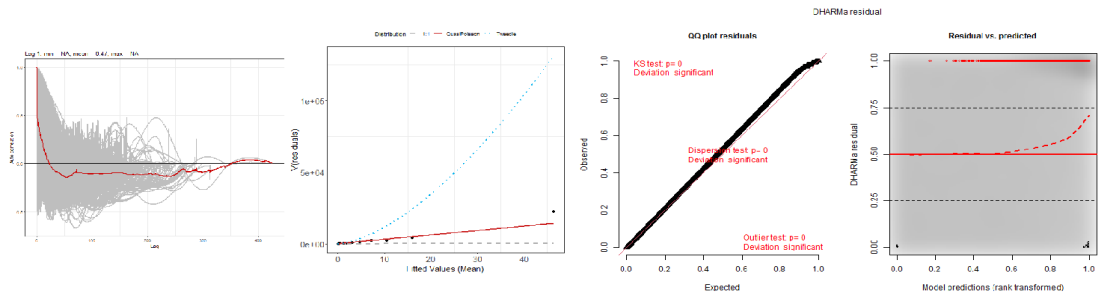

Figure 8.11. Figure showing diagnostics for the selected best spatial model. Left-most panel: within-block autocorrelation function, with the grey lines representing the residual correlation observed in each transect and the red line the average of these values across transects. Second panel: the estimated Tweedie mean-variance relationship (red line) against observed values (black symbols), with grey dashed line showing 1:1 relationship for reference. Third and right-most panel: QQplot and residuals against predicted values. The red stars are outliers and the red line is a smooth spline around the mean of the residuals.

8.3.4 Risk-mapping

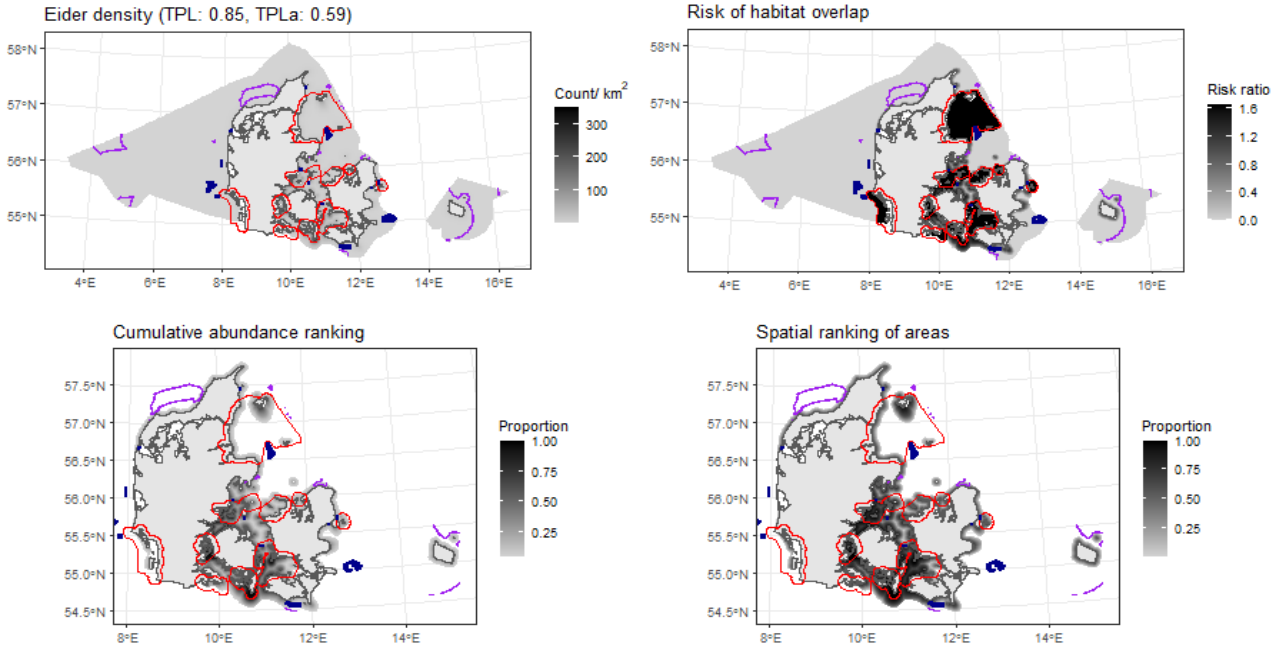

Figure 8.12. Figure showing the rescaling of estimated density distribution to habitat risk for the species unit. Bottom left and right: species unit abundance and top-use areas as cumulative percentiles (up to 0.95 abundance, defining species unit range). Red polygons: SPAs designated for one or more species in the species unit. Purple polygons: low-risk areas identified in Figure 2.5. Blue symbols: existing wind turbines.

8.4 Northern fulmar. Species unit “Fulmar”

8.4.1 Aerial survey dataset

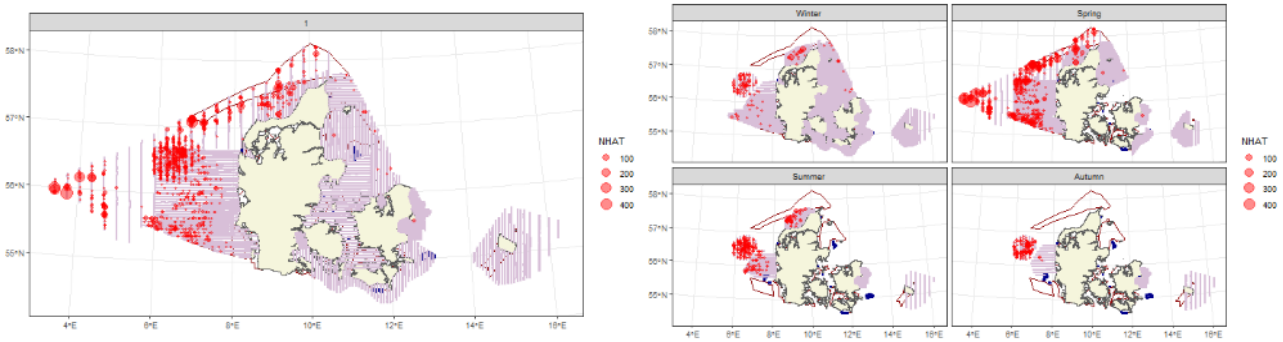

Figure 8.13. Maps showing observed counts (red) and effort segments (pink). Left panel: analyzed dataset for the species unit, pooled across those seasons the species unit was considered present (Table 1.4). Right panel: all data for the species unit, split across the seasons.

8.4.2 Spatial model outputs

Figure 8.14. Maps showing predicted counts (top) and boot-strapped uncertainty (bottom), overlaid with data. Data are shown as average counts in a grid of 20-km-wide hexagons.

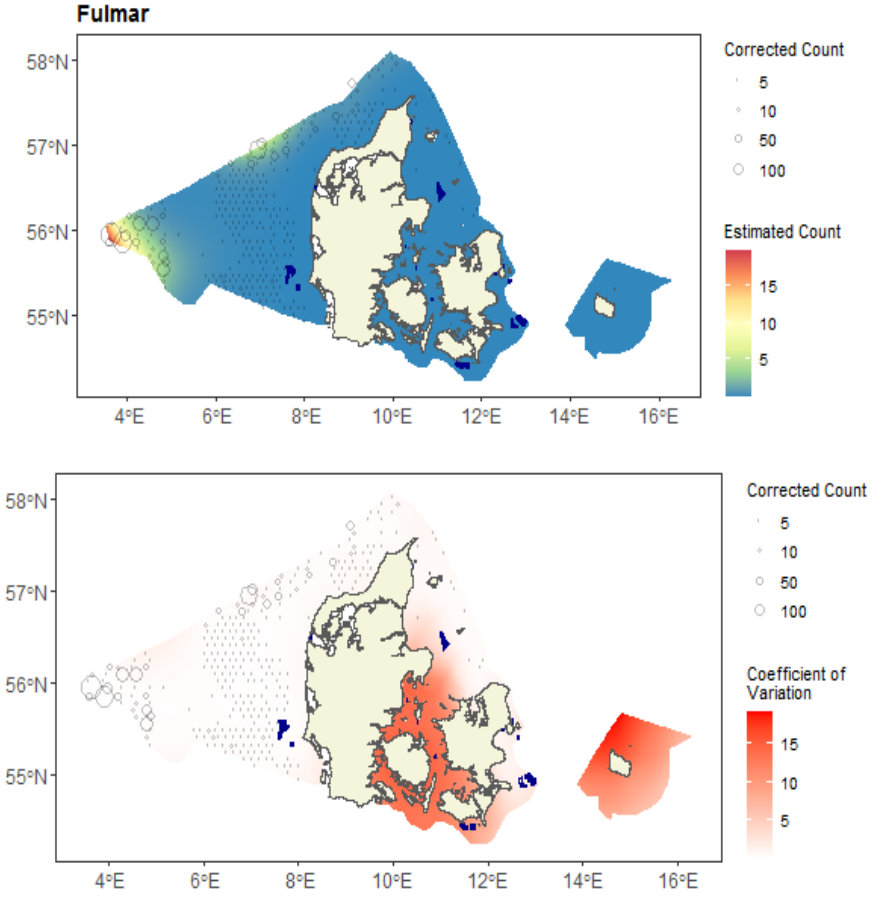

8.4.3 Diagnostics for the spatial model

Var. 1D	Var. 2D	# Pars.	Dispersion par.	CV score
s(distcoast, df=3)	s(x,y, df=14)	18	48.2	6.3

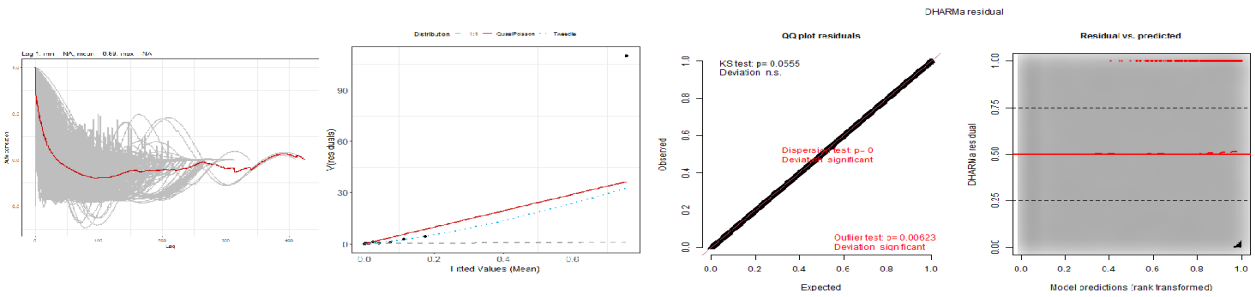

Figure 8.15. Figure showing diagnostics for the selected best spatial model. Left-most panel: within-block autocorrelation function, with the grey lines representing the residual correlation observed in each transect and the red line the average of these values across transects. Second panel: the estimated Tweedie mean-variance relationship (red line) against observed values (black symbols), with grey dashed line showing 1:1 relationship for reference. Third and right-most panel: QQplot and residuals against predicted values. The red stars are outliers and the red line is a smooth spline around the mean of the residuals.

8.4.4 Risk-mapping

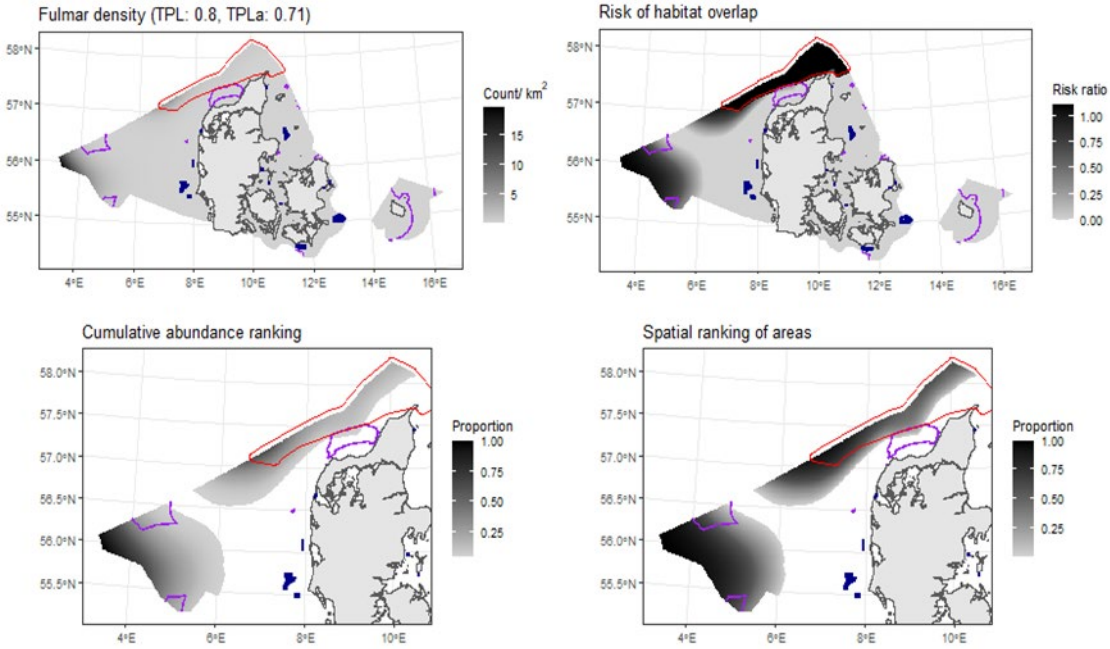

Figure 8.16. Figure showing the rescaling of estimated density distribution to habitat risk for the species unit. Bottom left and right: species unit abundance and top-use areas as cumulative percentiles (up to 0.95 abundance, defining species unit range). Red polygons: SPAs designated for one or more species in the species unit. Purple polygons: low-risk areas identified in Figure 2.5. Blue symbols: existing wind turbines.

8.5 Northern gannet. Species unit “Gannet”

8.5.1 Aerial survey dataset

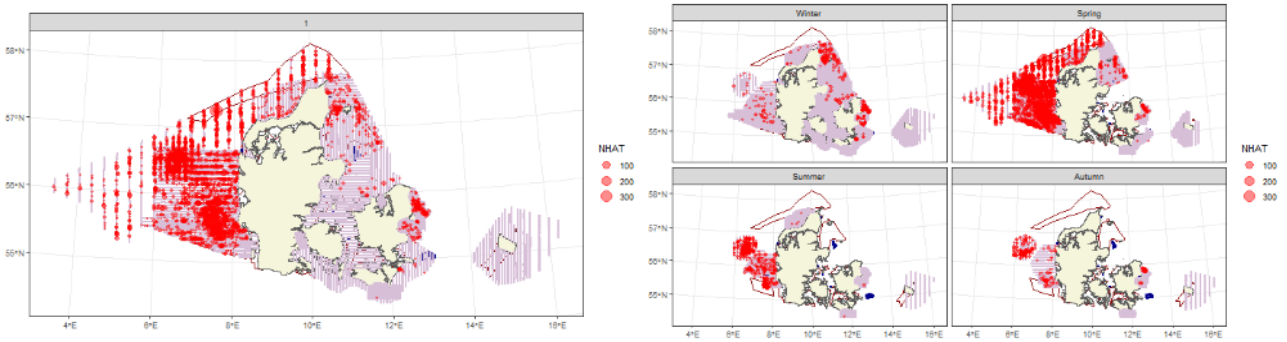

Figure 8.17. Maps showing observed counts (red) and effort segments (pink). Left panel: analyzed dataset for the species unit, pooled across those seasons the species unit was considered present (Table 1.4). Right panel: all data for the species unit, split across the seasons.

8.5.2 Spatial model outputs

Figure 8.18. Maps showing predicted counts (top) and boot-strapped uncertainty (bottom), overlaid with data. Data are shown as average counts in a grid of 20-km-wide hexagons.

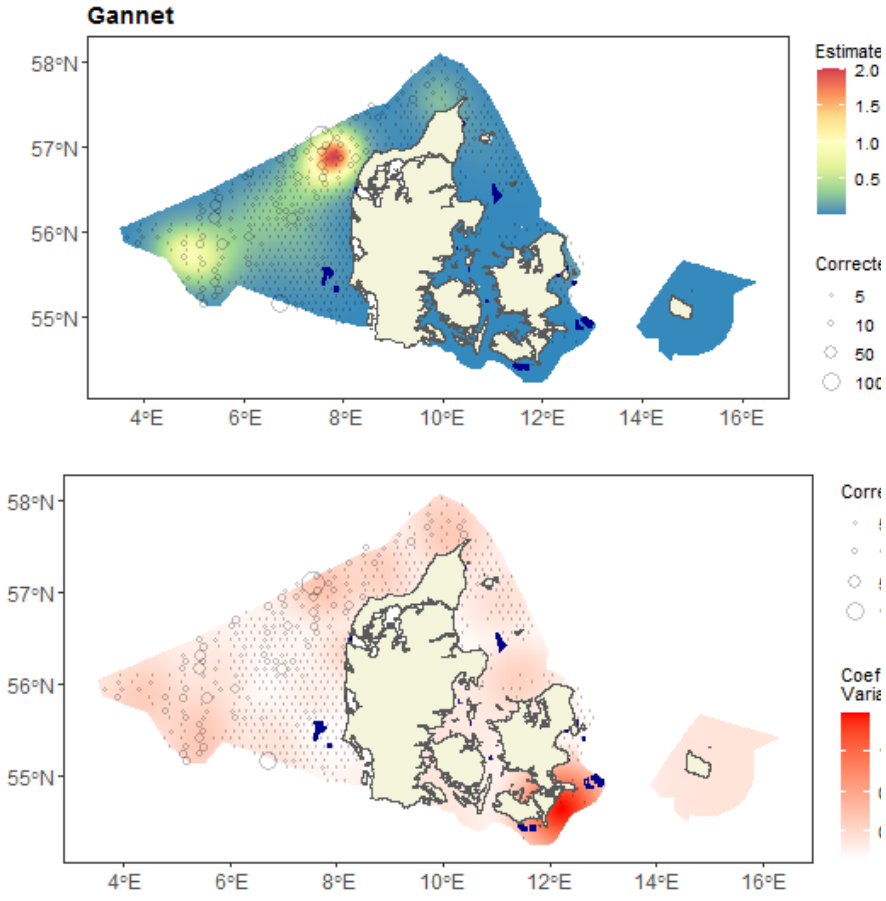

8.5.3 Diagnostics for the spatial model

Var. 1D	Var. 2D	# Pars.	Dispersion par.	CV score
NA	s(x,y, df=15)	16	42.1	1.5

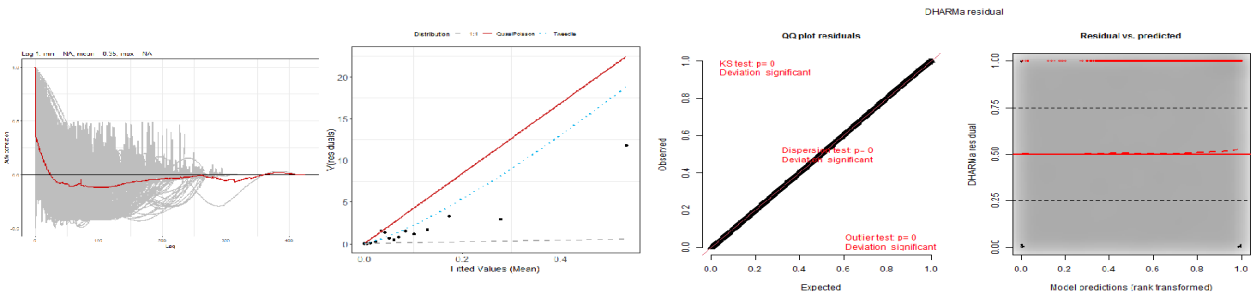

Figure 8.19. Figure showing diagnostics for the selected best spatial model. Left-most panel: within-block autocorrelation function, with the grey lines representing the residual correlation observed in each transect and the red line the average of these values across transects. Second panel: the estimated Tweedie mean-variance relationship (red line) against observed values (black symbols), with grey dashed line showing 1:1 relationship for reference. Third and right-most panel: QQplot and residuals against predicted values. The red stars are outliers and the red line is a smooth spline around the mean of the residuals.

8.5.4 Risk-mapping

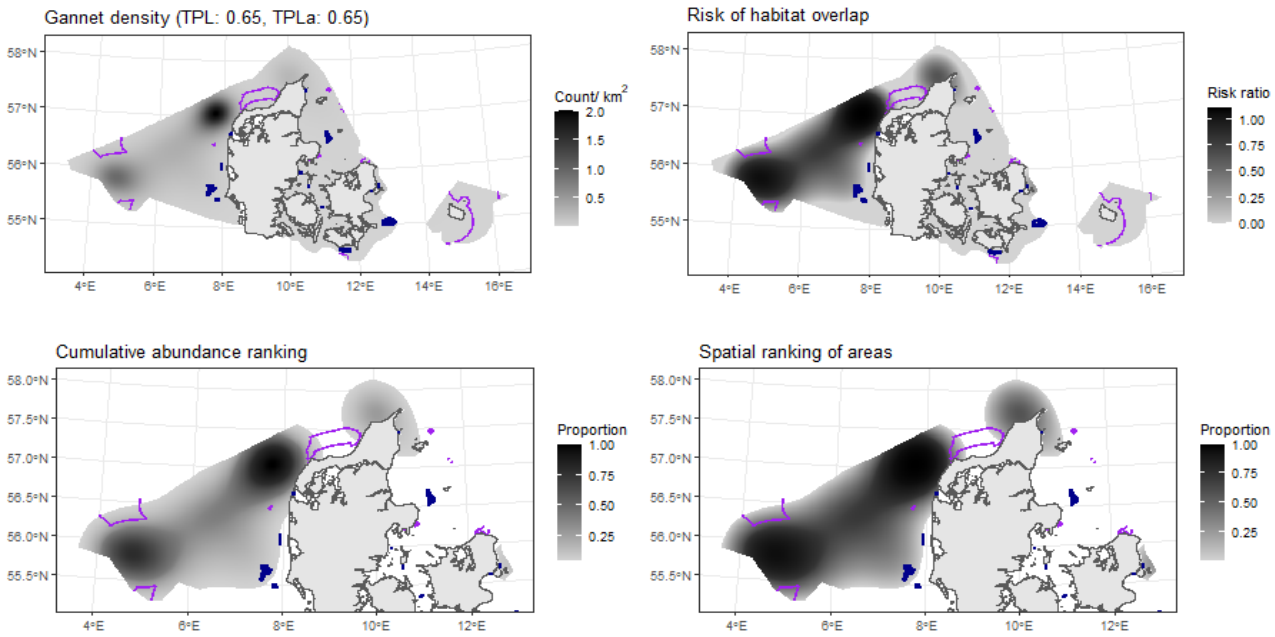

Figure 8.20. Figure showing the rescaling of estimated density distribution to habitat risk for the species unit. Bottom left and right: species unit abundance and top-use areas as cumulative percentiles (up to 0.95 abundance, defining species unit range). Red polygons: SPAs designated for one or more species in the species unit. Purple polygons: low-risk areas identified in Figure 2.5. Blue symbols: existing wind turbines.

8.6 Great black-backed gull. Species unit “GBBG”

8.6.1 Aerial survey dataset

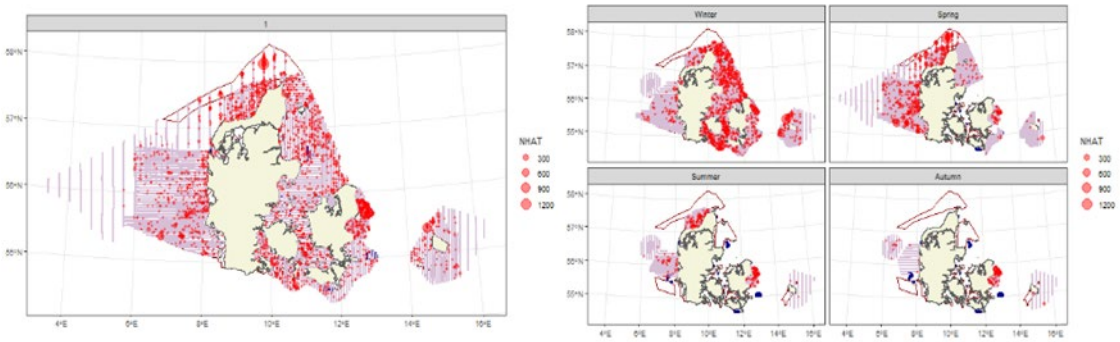

Figure 8.21. Maps showing observed counts (red) and effort segments (pink). Left panel: analyzed dataset for the species unit, pooled across those seasons the species unit was considered present (Table 1.4). Right panel: all data for the species unit, split across the seasons.

8.6.2 Spatial model outputs

Figure 8.22. Maps showing predicted counts (top) and boot-strapped uncertainty (bottom), overlaid with data. Data are shown as average counts in a grid of 20-km-wide hexagons.

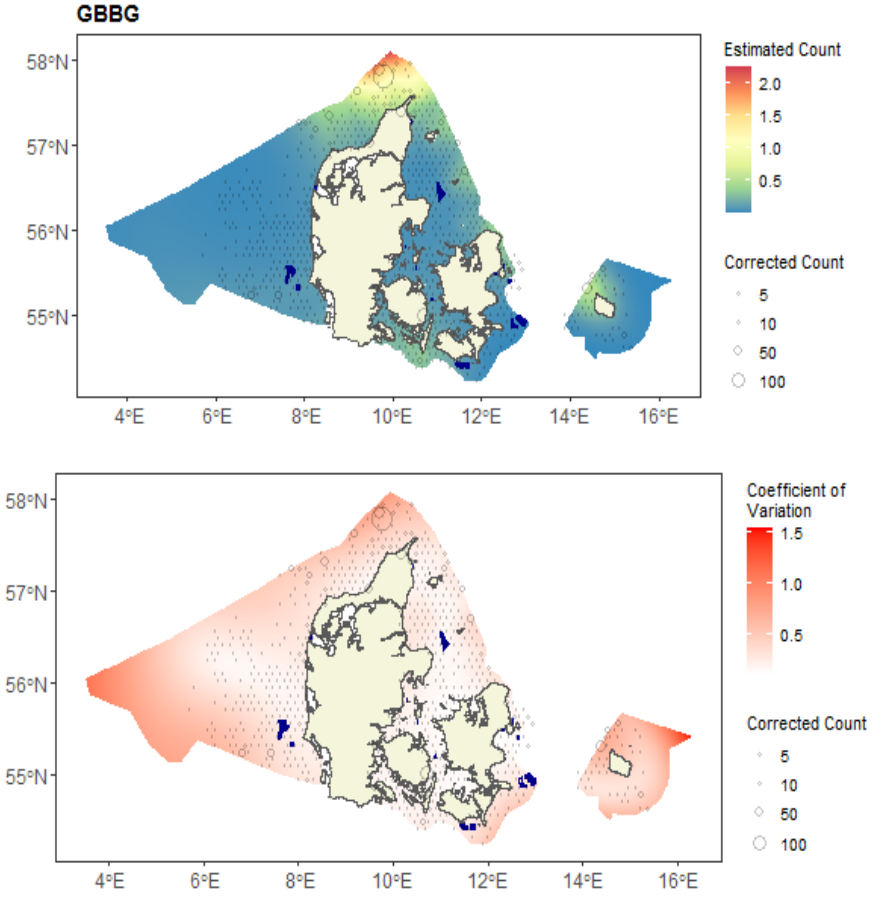

8.6.3 Diagnostics for the spatial model

Var. 1D	Var. 2D	# Pars.	Dispersion par.	CV score
distcoast, df=1	s(x,y, df=11)	13	130.2	18.5

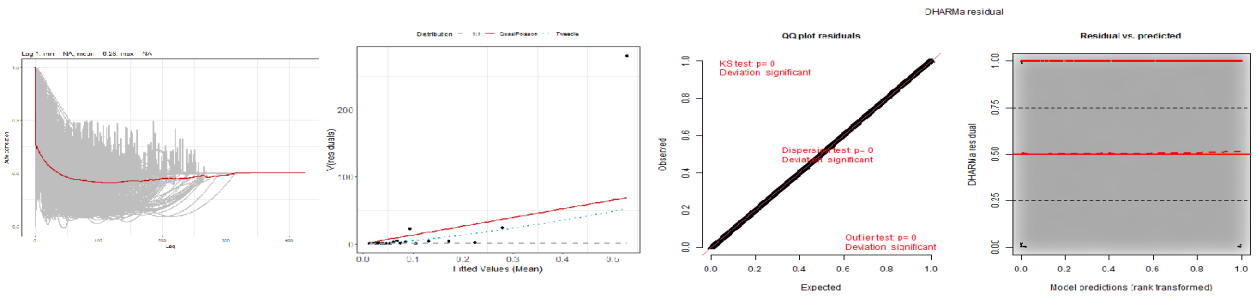

Figure 8.23. Figure showing diagnostics for the selected best spatial model. Left-most panel: within-block autocorrelation function, with the grey lines representing the residual correlation observed in each transect and the red line the average of these values across transects. Second panel: the estimated Tweedie mean-variance relationship (red line) against observed values (black symbols), with grey dashed line showing 1:1 relationship for reference. Third and right-most panel: QQplot and residuals against predicted values. The red stars are outliers and the red line is a smooth spline around the mean of the residuals.

8.6.4 Risk-mapping

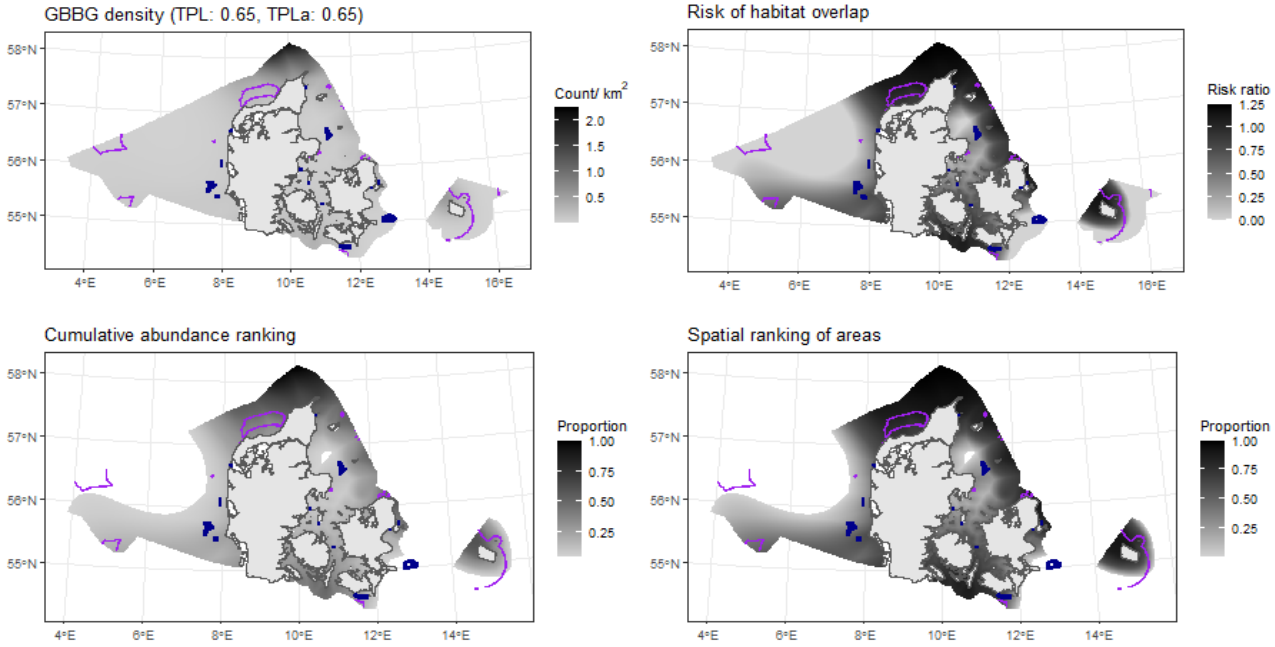

Figure 8.24. Figure showing the rescaling of estimated density distribution to habitat risk for the species unit. Bottom left and right: species unit abundance and top-use areas as cumulative percentiles (up to 0.95 abundance, defining species unit range). Red polygons: SPAs designated for one or more species in the species unit. Purple polygons: low-risk areas identified in Figure 2.5. Blue symbols: existing wind turbines.

8.7 Common Goldeneye. Species unit “Goldeneye”

8.7.1 Aerial survey dataset

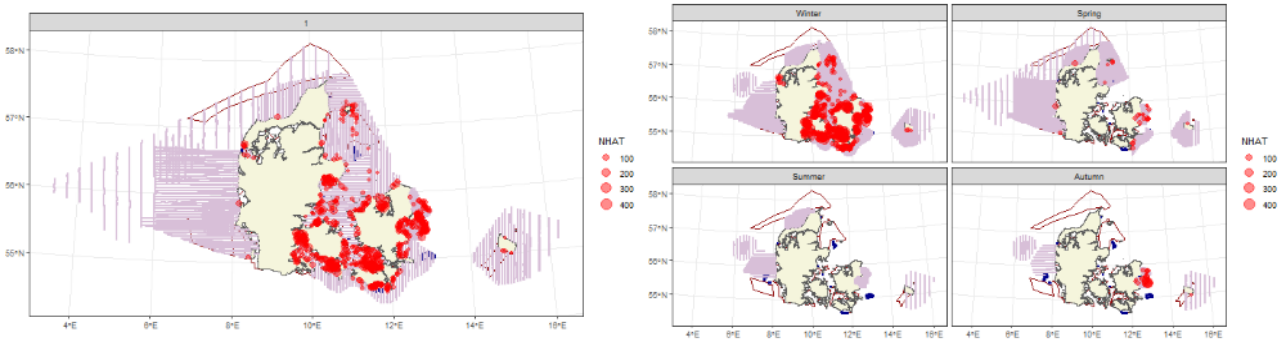

Figure 8.25. Maps showing observed counts (red) and effort segments (pink). Left panel: analyzed dataset for the species unit, pooled across those seasons the species unit was considered present (Table 1.4). Right panel: all data for the species unit, split across the seasons.

8.7.2 Spatial model outputs

Figure 8.26. Maps showing predicted counts (top) and boot-strapped uncertainty (bottom), overlaid with data. Data are shown as average counts in a grid of 20-km-wide hexagons.

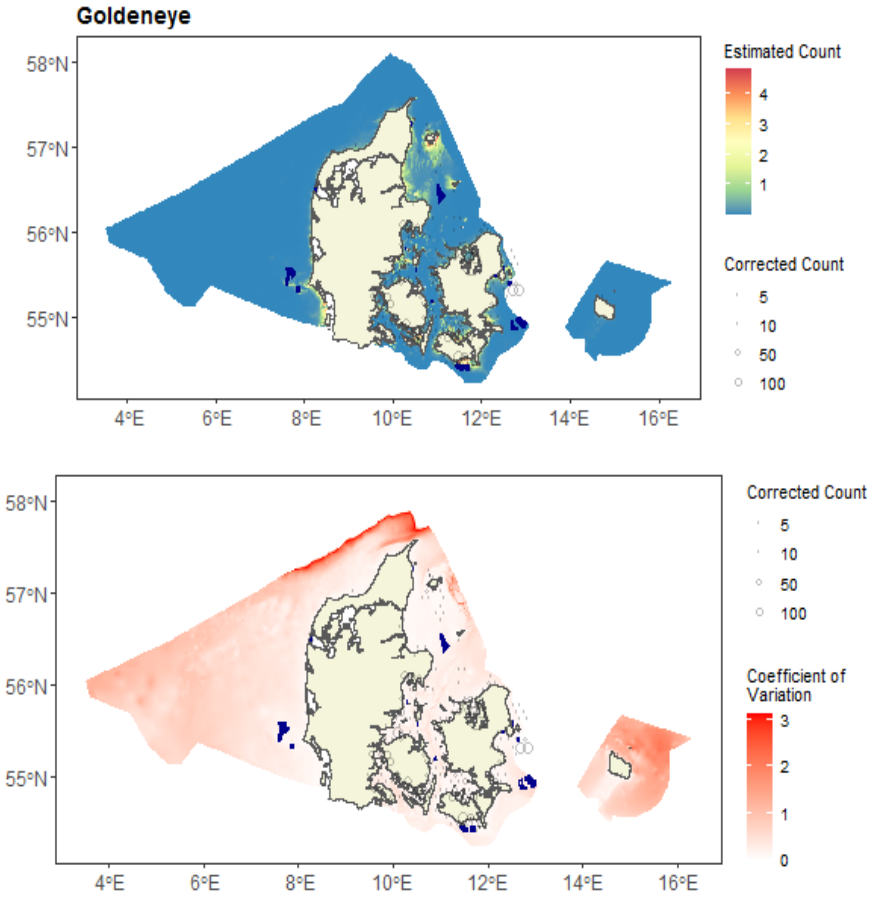

8.7.3 Diagnostics for the spatial model

Var. 1D	Var. 2D	# Pars.	Dispersion par.	CV score
depth, df=1	NA	2	260.1	22

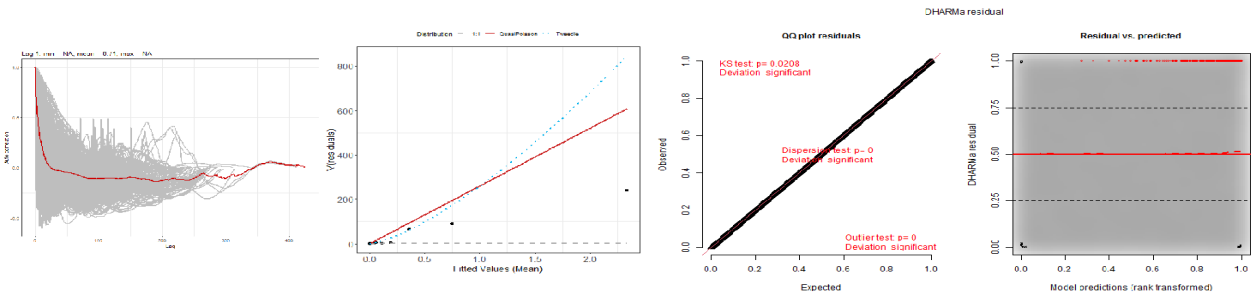

Figure 8.27. Figure showing diagnostics for the selected best spatial model. Left-most panel: within-block autocorrelation function, with the grey lines representing the residual correlation observed in each transect and the red line the average of these values across transects. Second panel: the estimated Tweedie mean-variance relationship (red line) against observed values (black symbols), with grey dashed line showing 1:1 relationship for reference. Third and right-most panel: QQplot and residuals against predicted values. The red stars are outliers and the red line is a smooth spline around the mean of the residuals.

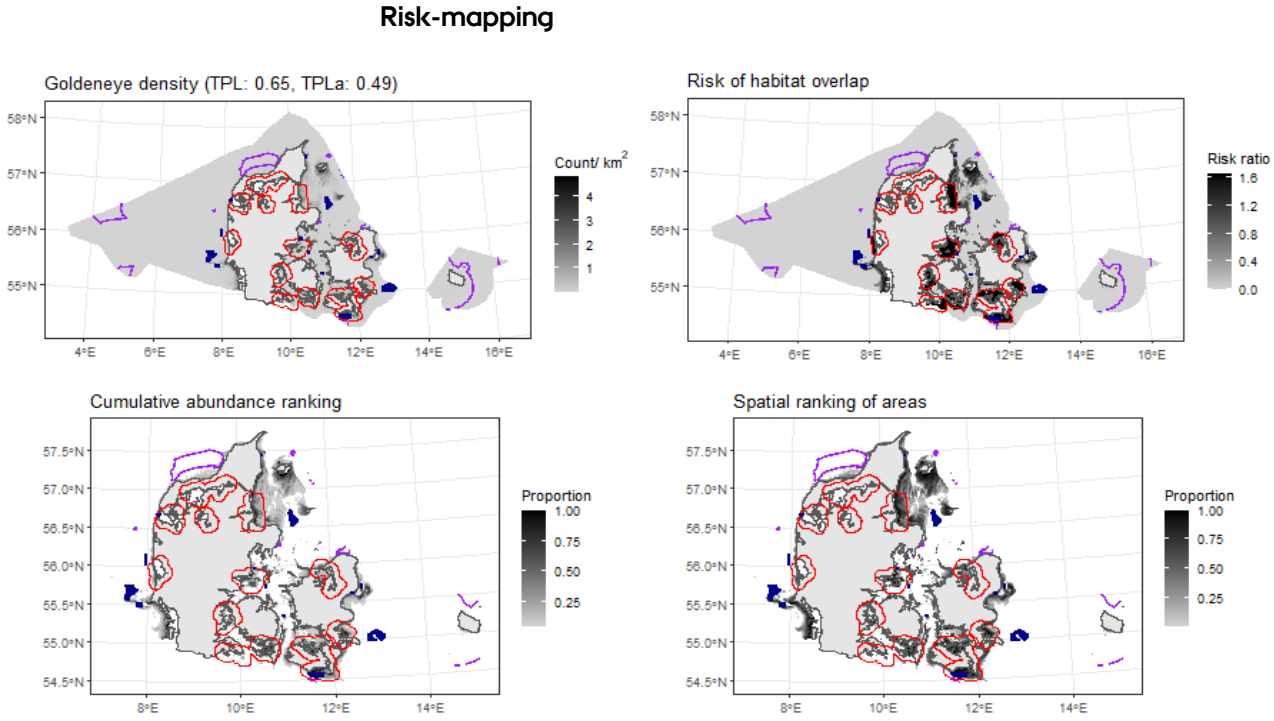

Figure 8.28. Figure showing the rescaling of estimated density distribution to habitat risk for the species unit. Bottom left and right: species unit abundance and top-use areas as cumulative percentiles (up to 0.95 abundance, defining species unit range). Red polygons: SPAs designated for one or more species in the species unit. Purple polygons: low-risk areas identified in Figure 2.5. Blue symbols: existing wind turbines.

8.8 Crested grebe/ red-necked grebe. Species unit “Grebe”

8.8.1 Aerial survey dataset

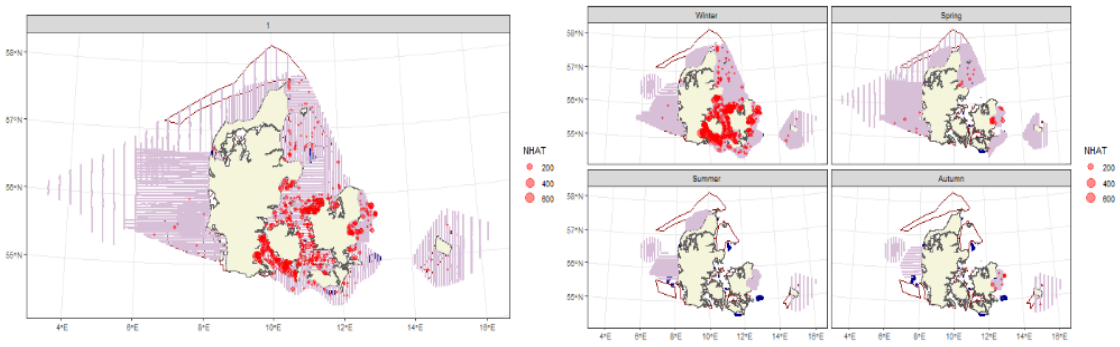

Figure 8.29. Maps showing observed counts (red) and effort segments (pink). Left panel: analyzed dataset for the species unit, pooled across those seasons the species unit was considered present (Table 1.4). Right panel: all data for the species unit, split across the seasons.

8.8.2 Spatial model outputs

Figure 8.30. Maps showing predicted counts (top) and boot-strapped uncertainty (bottom), overlaid with data. Data are shown as average counts in a grid of 20-km-wide hexagons.

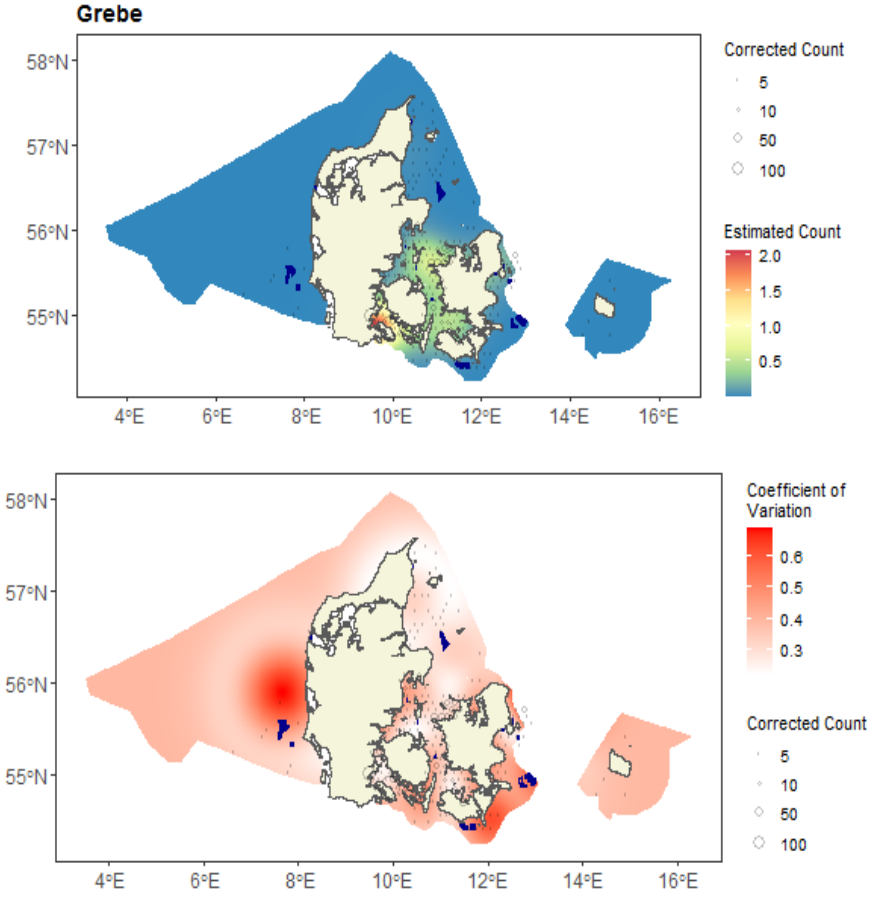

8.8.3 Diagnostics for the spatial model

Var. 1D	Var. 2D	# Pars.	Dispersion par.	CV score
NA	s(x,y, df=13)	14	159.1	6.9

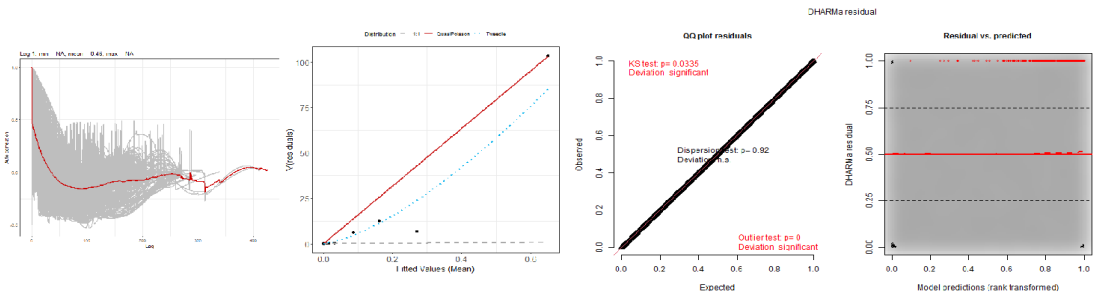

Figure 8.31. Figure showing diagnostics for the selected best spatial model. Left-most panel: within-block autocorrelation function, with the grey lines representing the residual correlation observed in each transect and the red line the average of these values across transects. Second panel: the estimated Tweedie mean-variance relationship (red line) against observed values (black symbols), with grey dashed line showing 1:1 relationship for reference. Third and right-most panel: QQplot and residuals against predicted values. The red stars are outliers and the red line is a smooth spline around the mean of the residuals.

8.8.4 Risk-mapping

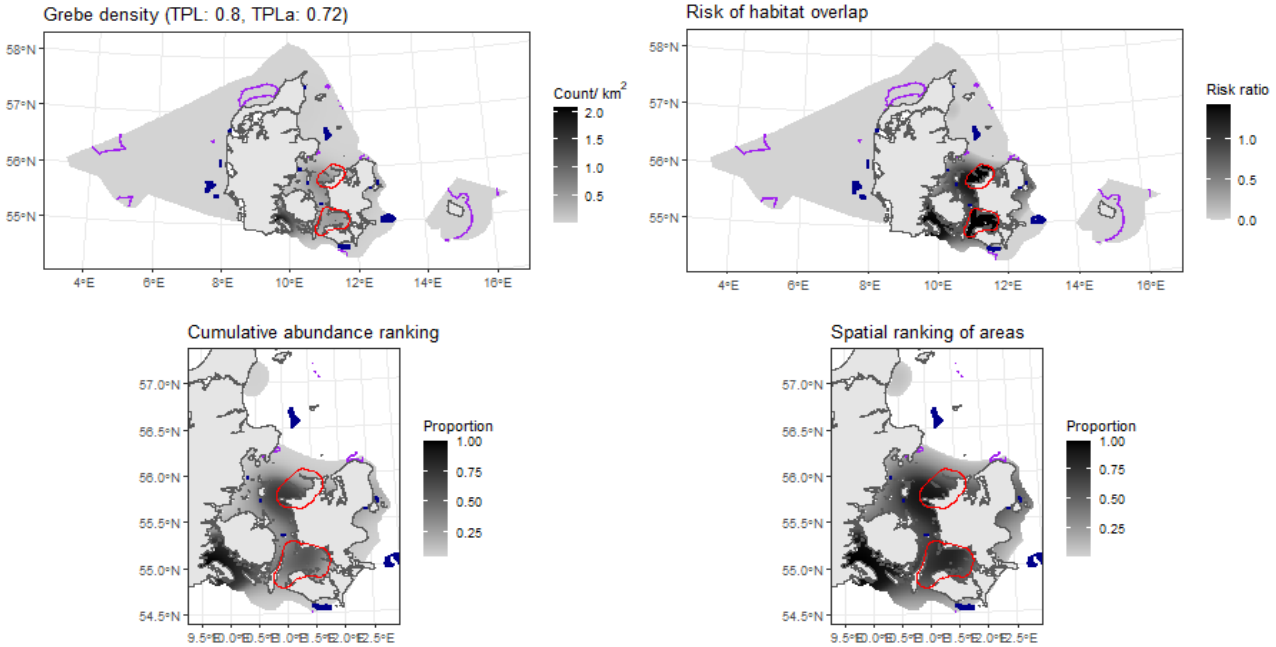

Figure 8.32. Figure showing the rescaling of estimated density distribution to habitat risk for the species unit. Bottom left and right: species unit abundance and top-use areas as cumulative percentiles (up to 0.95 abundance, defining species unit range). Red polygons: SPAs designated for one or more species in the species unit. Purple polygons: low-risk areas identified in Figure 2.5. Blue symbols: existing wind turbines.

8.9 Herring gull/ common gull. Species unit “Gull”

8.9.1 Aerial survey dataset

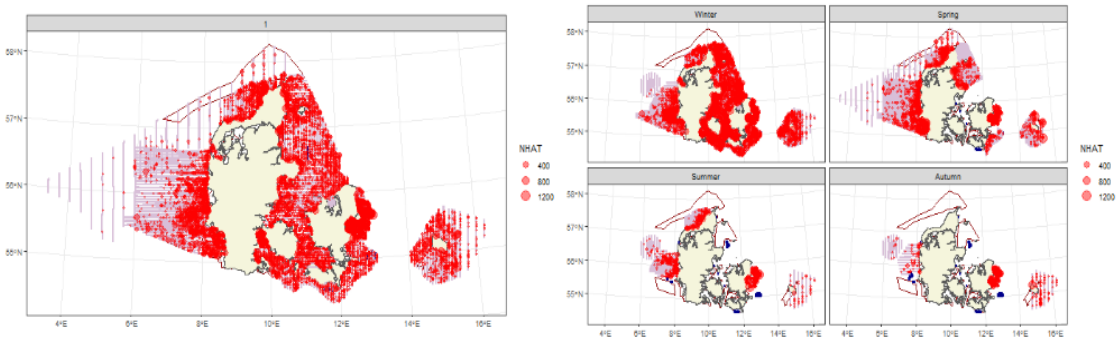

Figure 8.33. Maps showing observed counts (red) and effort segments (pink). Left panel: analyzed dataset for the species unit, pooled across those seasons the species unit was considered present (Table 1.4). Right panel: all data for the species unit, split across the seasons.

8.9.2 Spatial model outputs

Figure 8.34. Maps showing predicted counts (top) and boot-strapped uncertainty (bottom), overlaid with data. Data are shown as average counts in a grid of 20-km-wide hexagons.

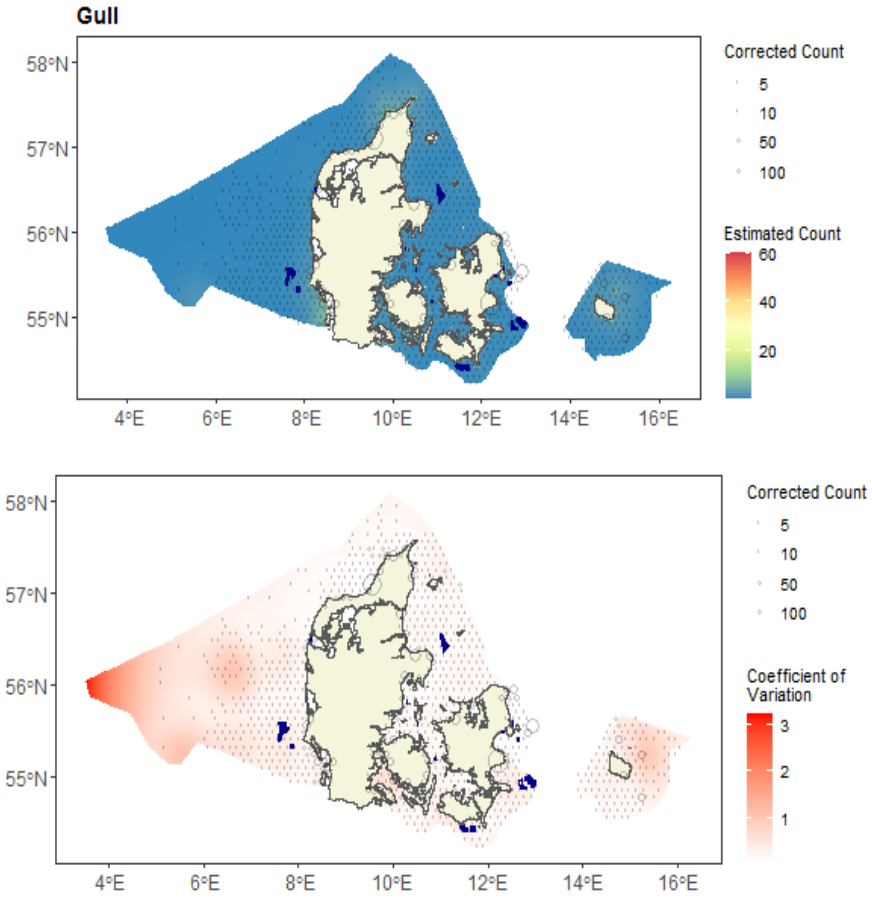

8.9.3 Diagnostics for the spatial model

Var. 1D	Var. 2D	# Pars.	Dispersion par.	CV score
s(distcoast, df=4)	s(x,y, df=20)	25	205.3	239.1

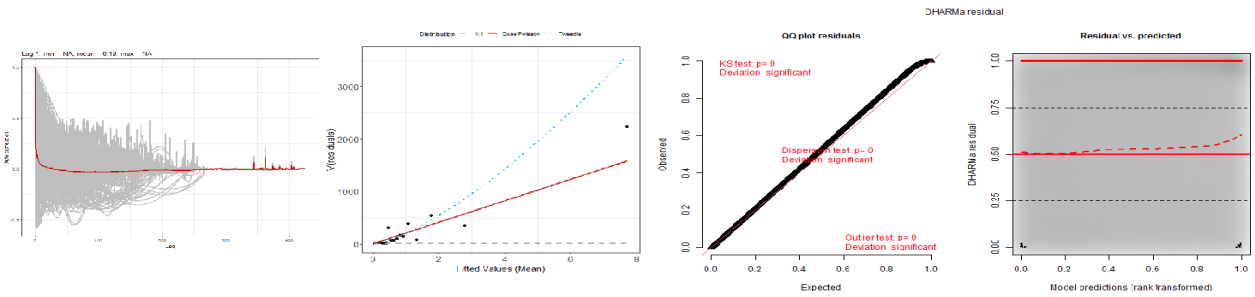

Figure 8.35. Figure showing diagnostics for the selected best spatial model. Left-most panel: within-block autocorrelation function, with the grey lines representing the residual correlation ob-served in each transect and the red line the average of these values across transects. Sec-ond panel: the estimated Tweedie mean-variance relationship (red line) against observed values (black symbols), with grey dashed line showing 1:1 relationship for reference. Third and right-most panel: QQplot and residuals against predicted values. The red stars are out-liers and the red line is a smooth spline around the mean of the residuals.

8.9.4 Risk-mapping

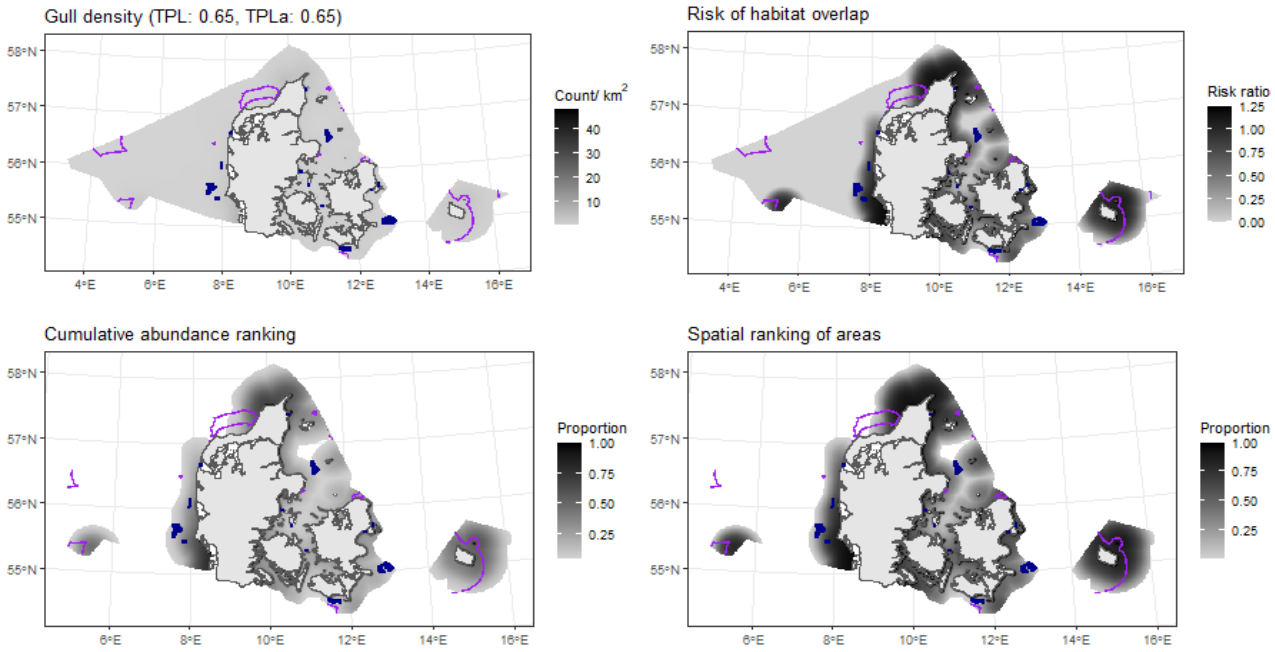

Figure 8.36. Figure showing the rescaling of estimated density distribution to habitat risk for the species unit. Bottom left and right: species unit abundance and top-use areas as cumulative percentiles (up to 0.95 abundance, defining species unit range). Red polygons: SPAs designated for one or more species in the species unit. Purple polygons: low-risk areas identified in Figure 2.5. Blue symbols: existing wind turbines.

8.10 Black-legged kittiwake. Species unit “Kittiwake”

8.10.1 Aerial survey dataset

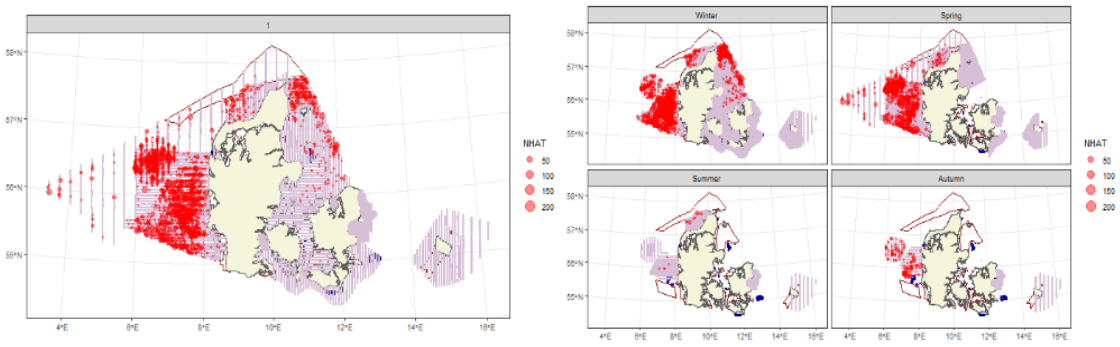

Figure 8.37. Maps showing observed counts (red) and effort segments (pink). Left panel: analyzed dataset for the species unit, pooled across those seasons the species unit was considered present (Table 1.4). Right panel: all data for the species unit, split across the seasons.

8.10.2 Spatial model outputs

Figure 8.38. Maps showing predicted counts (top) and boot-strapped uncertainty (bottom), overlaid with data. Data are shown as average counts in a grid of 20-km-wide hexagons.

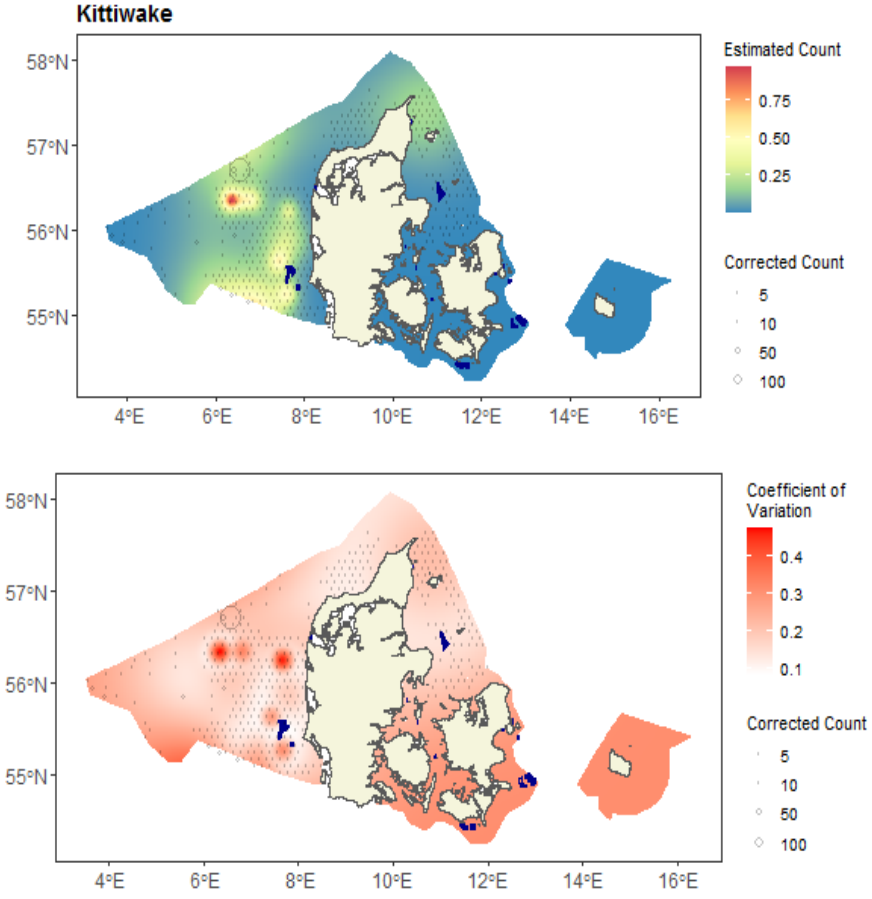

8.10.3 Diagnostics for the spatial model

Var. 1D	Var. 2D	# Pars.	Dispersion par.	CV score
NA	s(x,y, df=11)	12	37.3	1.9

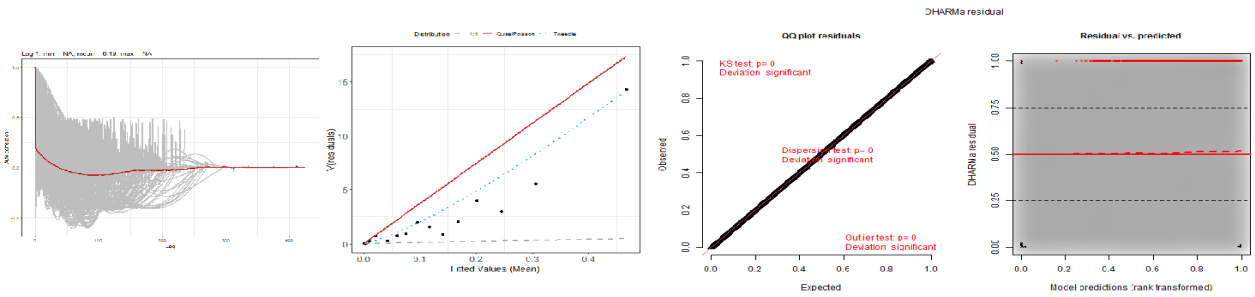

Figure 8.39. Figure showing diagnostics for the selected best spatial model. Left-most panel: within-block autocorrelation function, with the grey lines representing the residual correlation observed in each transect and the red line the average of these values across transects. Second panel: the estimated Tweedie mean-variance relationship (red line) against observed values (black symbols), with grey dashed line showing 1:1 relationship for reference. Third and right-most panel: QQplot and residuals against predicted values. The red stars are outliers and the red line is a smooth spline around the mean of the residuals.

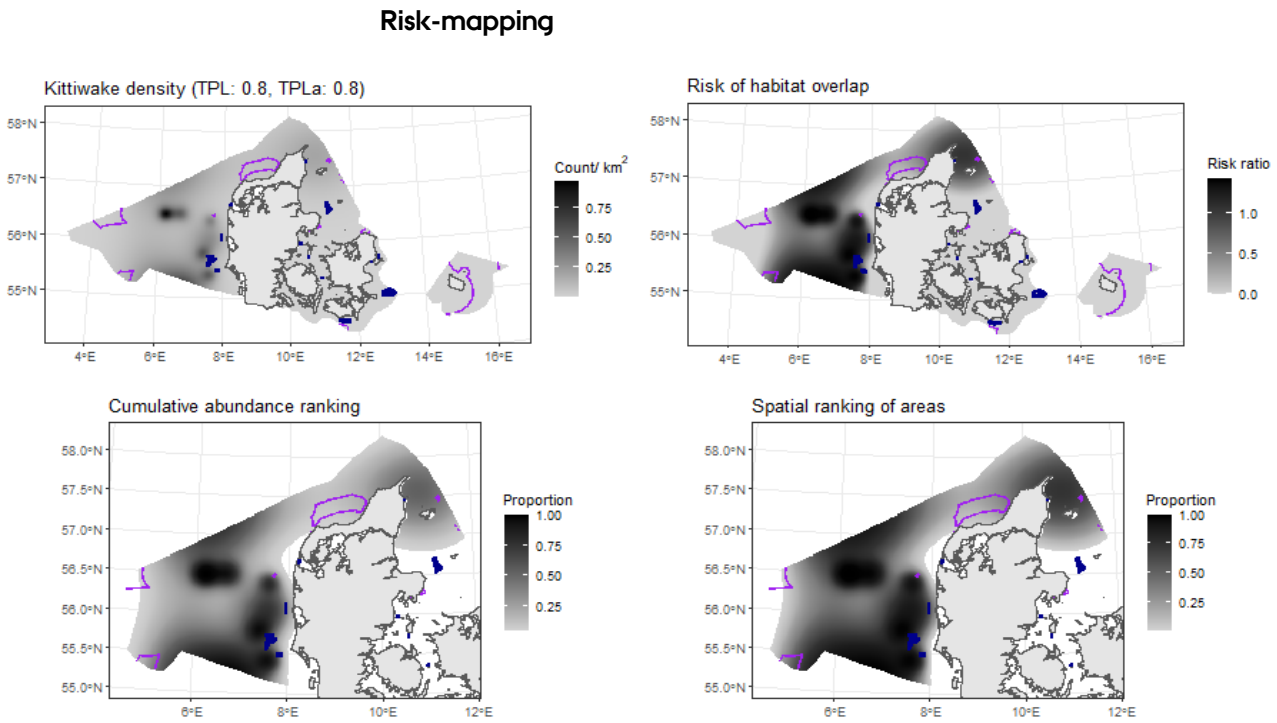

Figure 8.40. Figure showing the rescaling of estimated density distribution to habitat risk for the species unit. Bottom left and right: species unit abundance and top-use areas as cumulative percentiles (up to 0.95 abundance, defining species unit range). Red polygons: SPAs designated for one or more species in the species unit. Purple polygons: low-risk areas identified in Figure 2.5. Blue symbols: existing wind turbines.

8.11 Lesser black-backed gull. Species unit “LBBG”

8.11.1 Aerial survey dataset

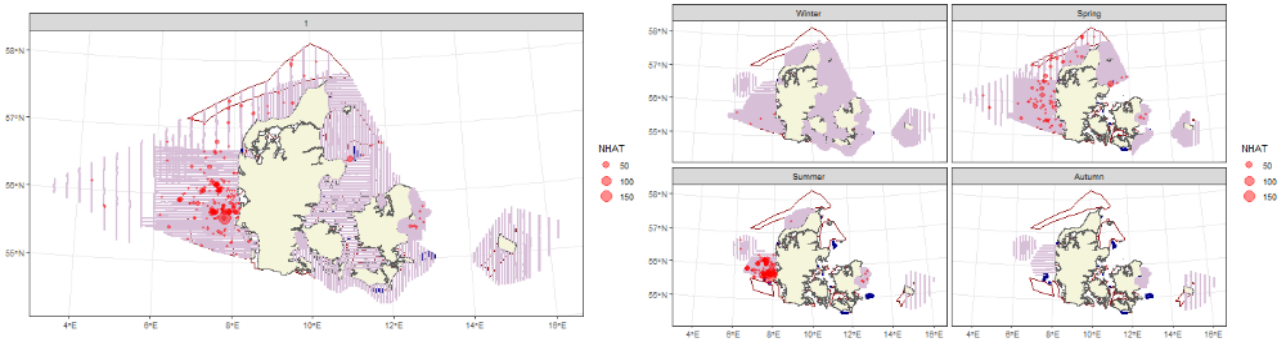

Figure 8.41. Maps showing observed counts (red) and effort segments (pink). Left panel: analyzed dataset for the species unit, pooled across those seasons the species unit was considered present (Table 1.4). Right panel: all data for the species unit, split across the seasons.

8.11.2 Spatial model outputs

Figure 8.42. Maps showing predicted counts (top) and boot-strapped uncertainty (bottom), overlaid with data. Data are shown as average counts in a grid of 20-km-wide hexagons.

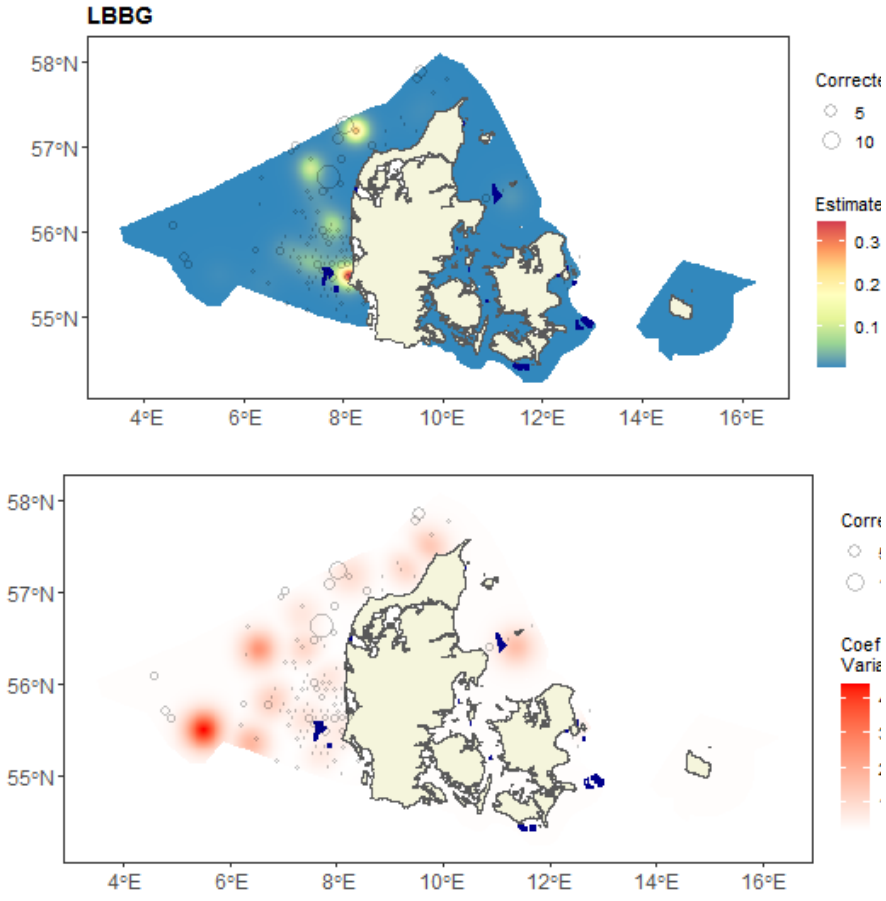

8.11.3 Diagnostics for the spatial model

Var. 1D	Var. 2D	# Pars.	Dispersion par.	CV score
NA	s(x,y, df=15)	16	59.5	0.3

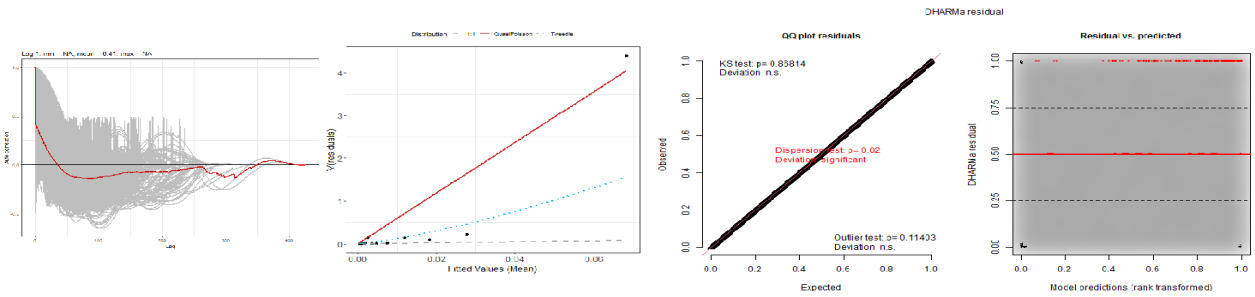

Figure 8.43. Figure showing diagnostics for the selected best spatial model. Left-most panel: within-block autocorrelation function, with the grey lines representing the residual correlation observed in each transect and the red line the average of these values across transects. Second panel: the estimated Tweedie mean-variance relationship (red line) against observed values (black symbols), with grey dashed line showing 1:1 relationship for reference. Third and right-most panel: QQplot and residuals against predicted values. The red stars are outliers and the red line is a smooth spline around the mean of the residuals.

8.11.4 Risk-mapping

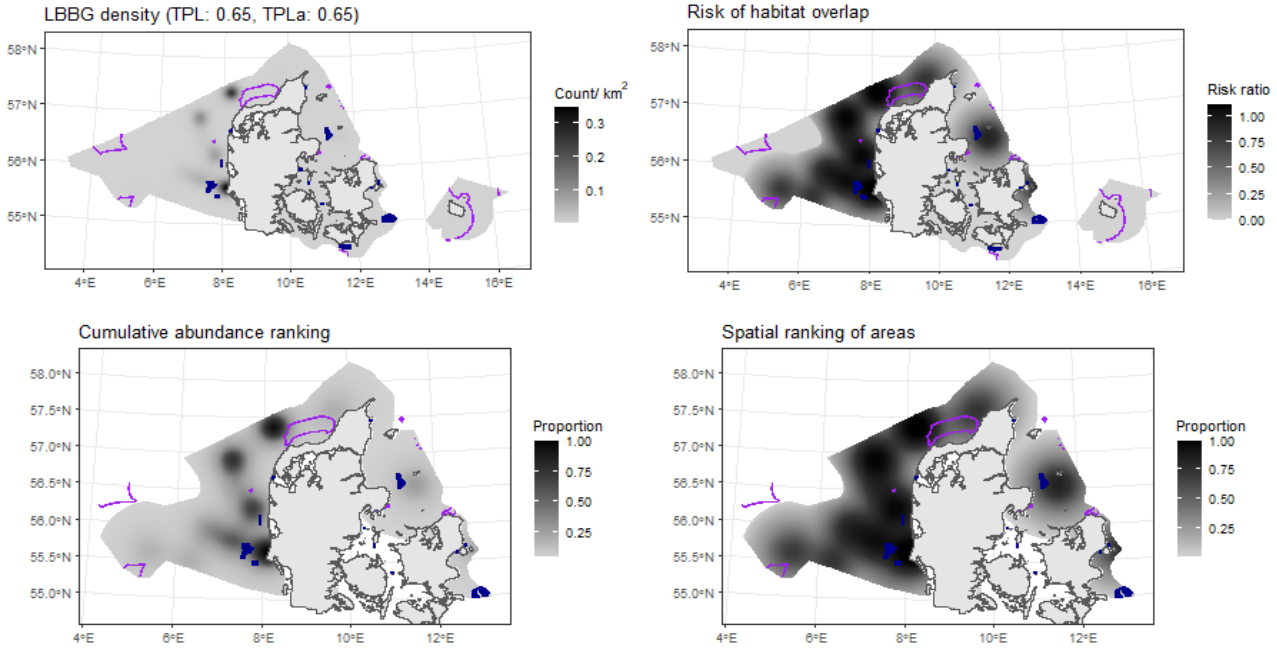

Figure 8.44. Figure showing the rescaling of estimated density distribution to habitat risk for the species unit. Bottom left and right: species unit abundance and top-use areas as cumulative percentiles (up to 0.95 abundance, defining species unit range). Red polygons: SPAs designated for one or more species in the species unit. Purple polygons: low-risk areas identified in Figure 2.5. Blue symbols: existing wind turbines.

8.12 Little gull. Species unit “Littlegull”

8.12.1 Aerial survey dataset

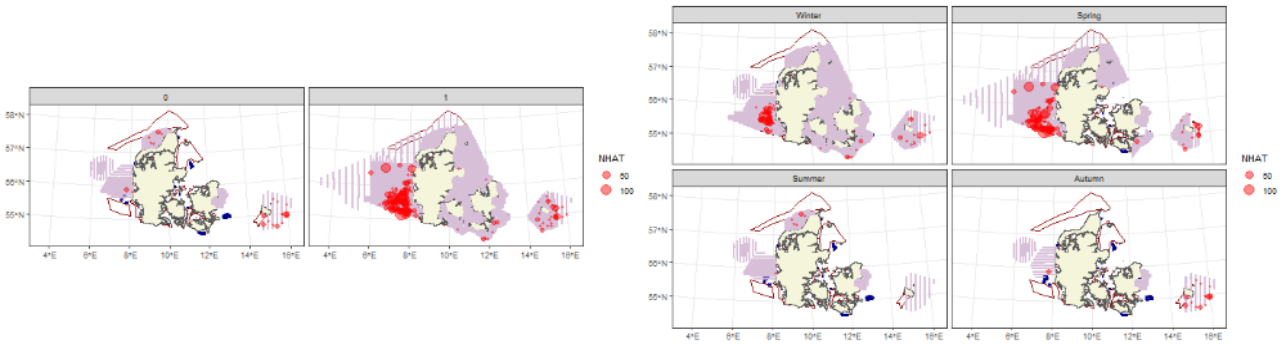

Figure 8.45. Maps showing observed counts (red) and effort segments (pink). Left panel: analyzed dataset for the species unit, pooled across those seasons the species unit was considered present (Table 1.4). Right panel: all data for the species unit, split across the seasons.

8.12.2 Spatial model outputs

Figure 8.46. Maps showing predicted counts (top) and bootstrapped uncertainty (bottom), overlaid with data. Data are shown as average counts in a grid of 20-km-wide hexagons.

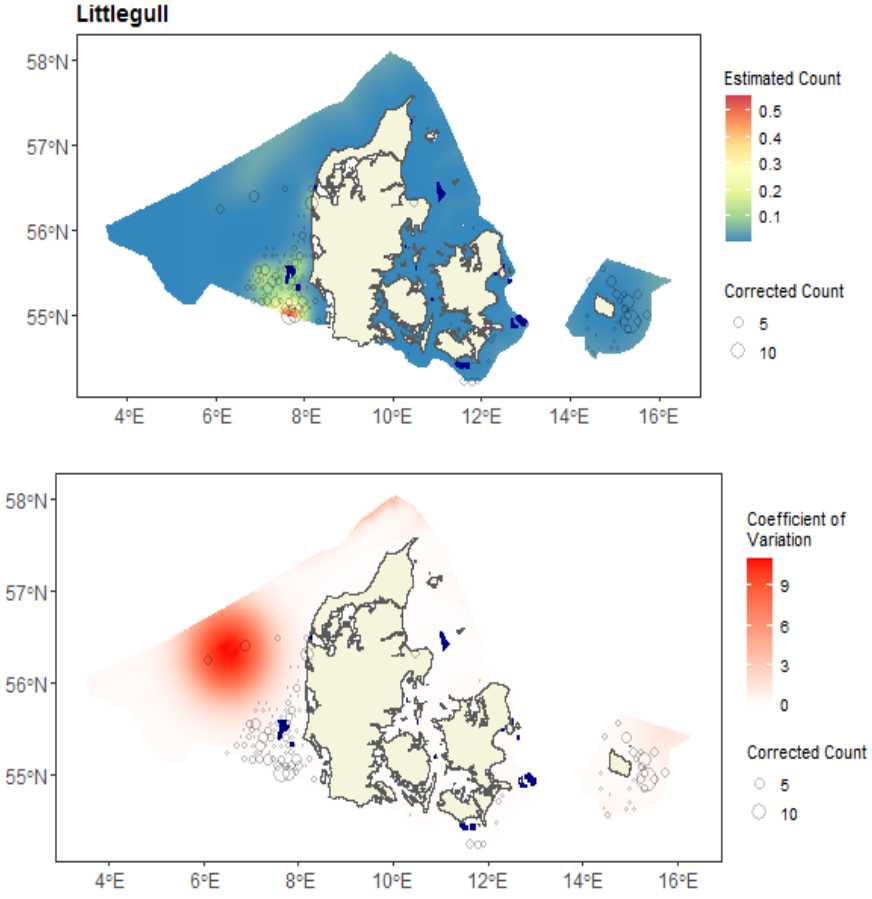

8.12.3 Diagnostics for the spatial model

Var. 1D	Var. 2D	# Pars.	Dispersion par.	CV score
s(distcoast, df=2)	s(x,y, df=11)	14	101.8	0.6

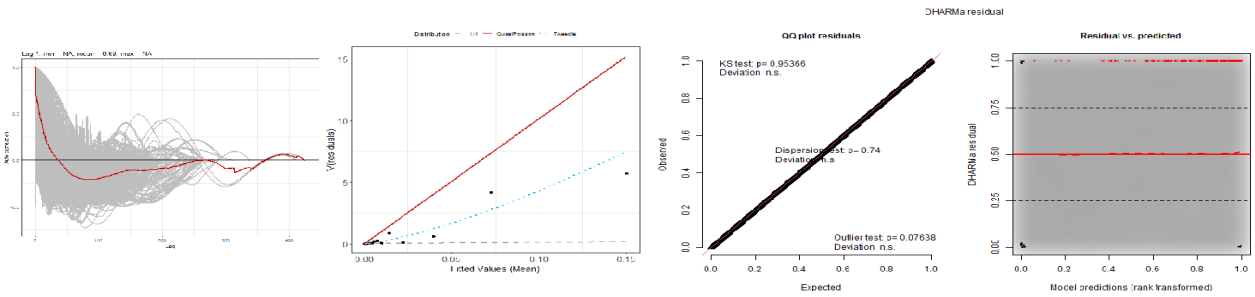

Figure 8.47. Figure showing diagnostics for the selected best spatial model. Left-most panel: within-block autocorrelation function, with the grey lines representing the residual correlation observed in each transect and the red line the average of these values across transects. Second panel: the estimated Tweedie mean-variance relationship (red line) against observed values (black symbols), with grey dashed line showing 1:1 relationship for reference. Third and right-most panel: QQplot and residuals against predicted values. The red stars are outliers and the red line is a smooth spline around the mean of the residuals.

8.12.4 Risk-mapping

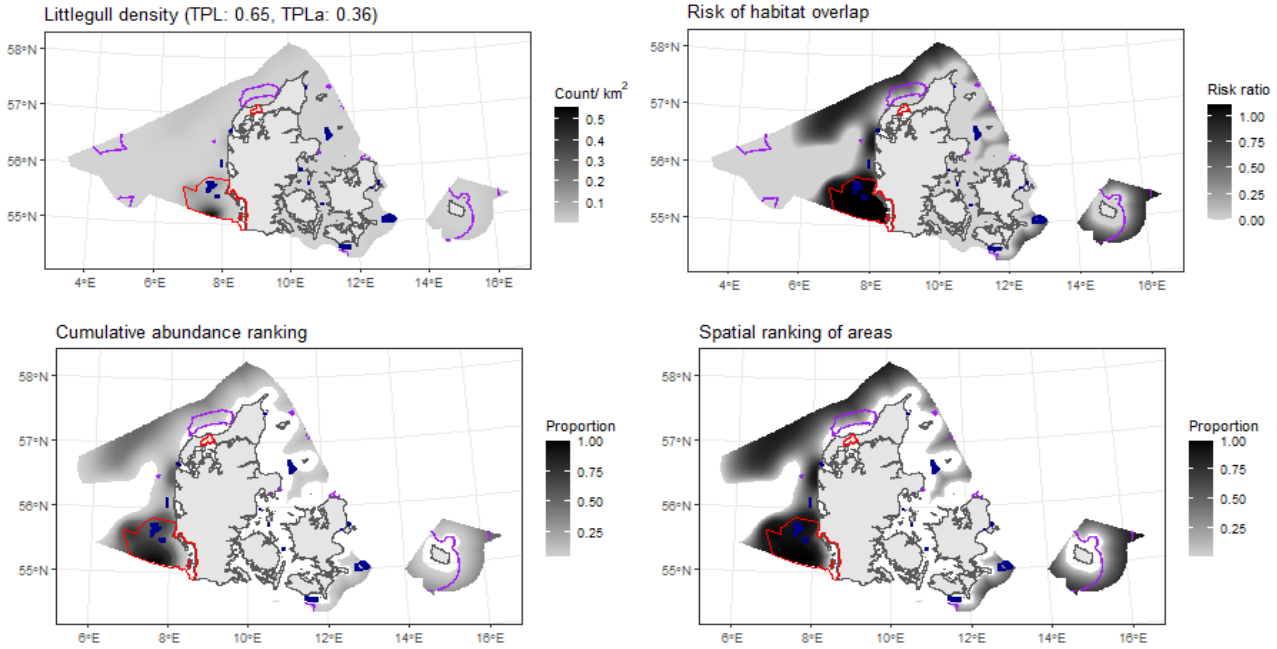

Figure 8.48. Figure showing the rescaling of estimated density distribution to habitat risk for the species unit. Bottom left and right: species unit abundance and top-use areas as cumulative percentiles (up to 0.95 abundance, defining species unit range). Red polygons: SPAs designated for one or more species in the species unit. Purple polygons: low-risk areas identified in Figure 2.5. Blue symbols: existing wind turbines.

8.13 Long-tailed duck. Species unit “Longtailed”

8.13.1 Aerial survey dataset

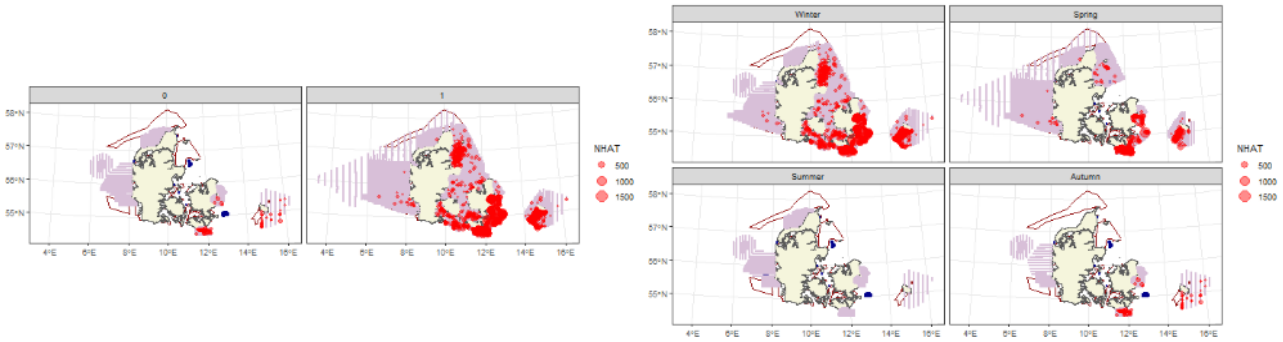

Figure 8.49. Maps showing observed counts (red) and effort segments (pink). Left panel: analyzed dataset for the species unit, pooled across those seasons the species unit was considered present (Table 1.4). Right panel: all data for the species unit, split across the seasons.

8.13.2 Spatial model outputs

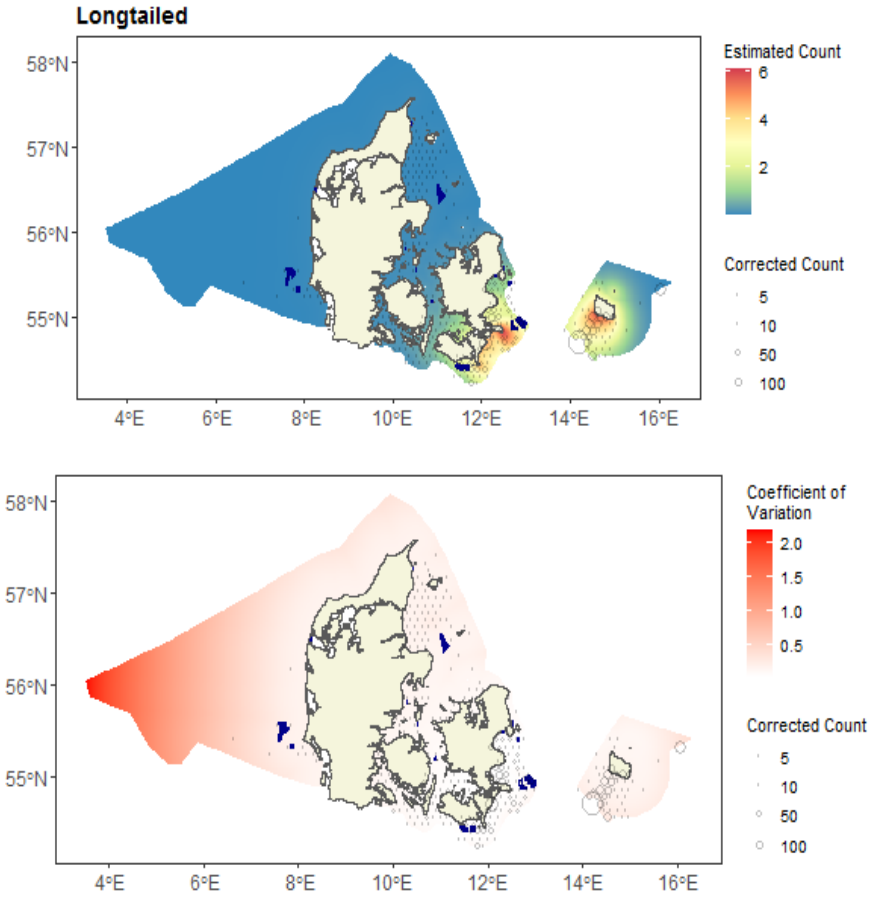

Figure 8.50. Maps showing predicted counts (top) and bootstrapped uncertainty (bottom), overlaid with data. Data are shown as average counts in a grid of 20-km-wide hexagons.

8.13.3 Diagnostics for the spatial model

Var. 1D	Var. 2D	# Pars.	Dispersion par.	CV score
s(distcoast, df=2)	s(x,y, df=2)	4	171.9	92.9

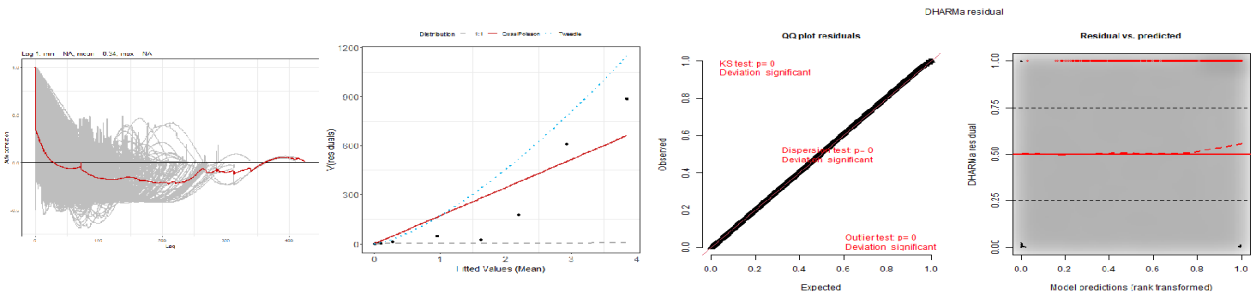

Figure 8.51. Figure showing diagnostics for the selected best spatial model. Left-most panel: within-block autocorrelation function, with the grey lines representing the residual correlation observed in each transect and the red line the average of these values across transects. Second panel: the estimated Tweedie mean-variance relationship (red line) against observed values (black symbols), with grey dashed line showing 1:1 relationship for reference. Third and right-most panel: QQplot and residuals against predicted values. The red stars are outliers and the red line is a smooth spline around the mean of the residuals.

8.13.4 Risk-mapping

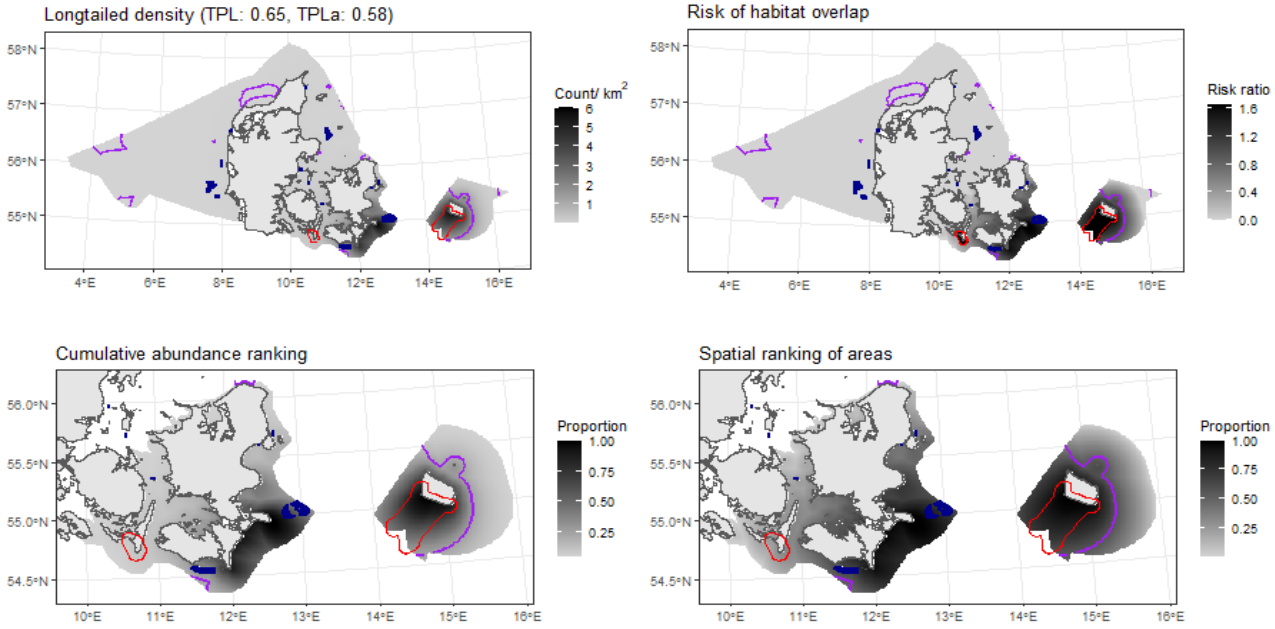

Figure 8.52. Figure showing the rescaling of estimated density distribution to habitat risk for the species unit. Bottom left and right: species unit abundance and top-use areas as cumulative percentiles (up to 0.95 abundance, defining species unit range). Red polygons: SPAs designated for one or more species in the species unit. Purple polygons: low-risk areas identified in Figure 2.5. Blue symbols: existing wind turbines.

8.14 Red-breasted merganser. Species unit “Merganser”

8.14.1 Aerial survey dataset

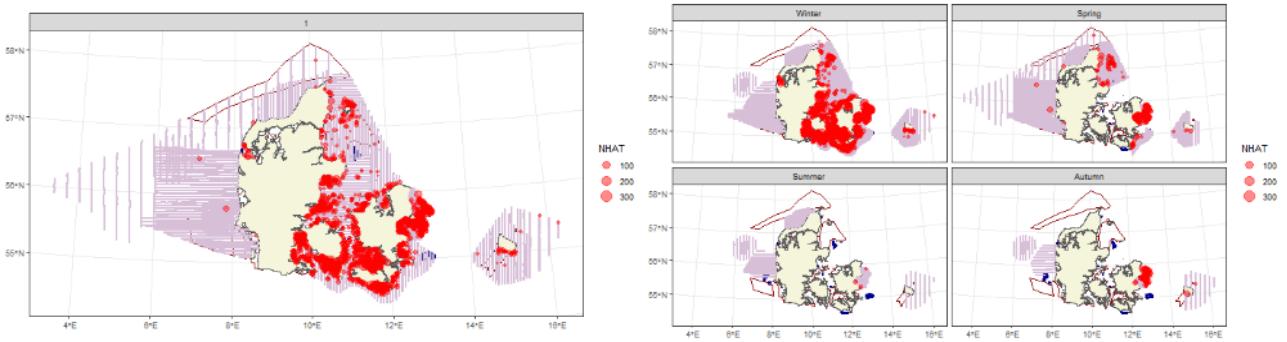

Figure 8.53. Maps showing observed counts (red) and effort segments (pink). Left panel: analyzed dataset for the species unit, pooled across those seasons the species unit was considered present (Table 1.4). Right panel: all data for the species unit, split across the seasons.

8.14.2 Spatial model outputs

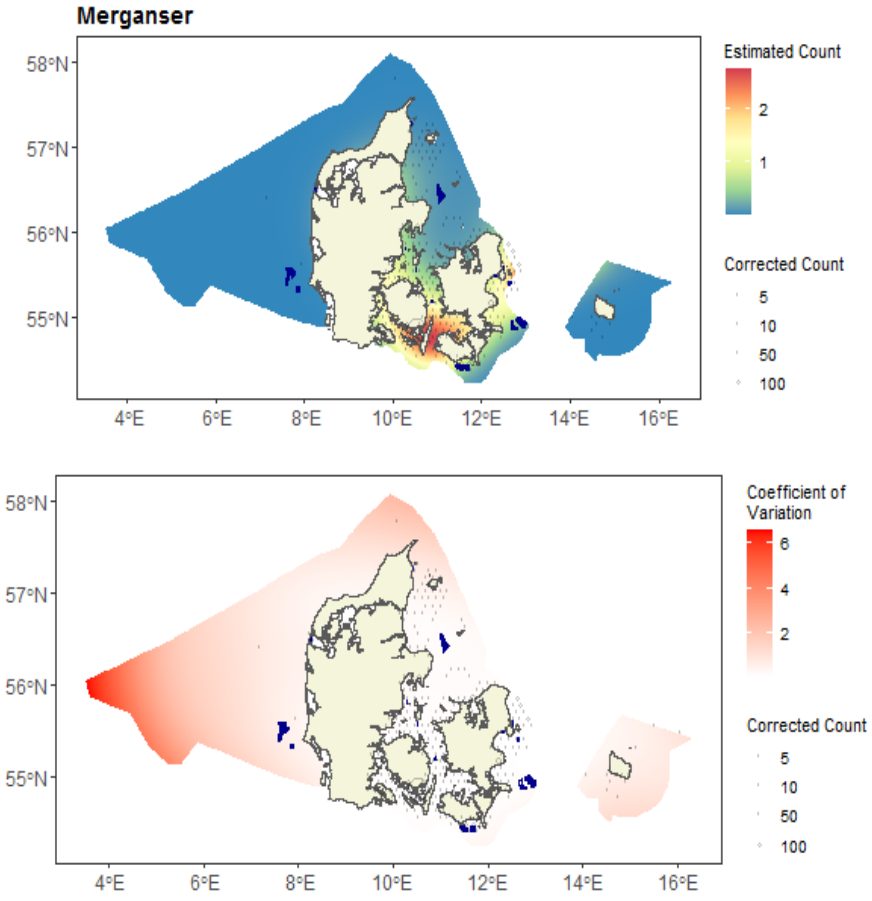

Figure 8.54. Maps showing predicted counts (top) and bootstrapped uncertainty (bottom), overlaid with data. Data are shown as average counts in a grid of 20-km-wide hexagons.

8.14.3 Diagnostics for the spatial model

Var. 1D	Var. 2D	# Pars.	Dispersion par.	CV score
NA	s(x,y, df=9)	10	64.1	15

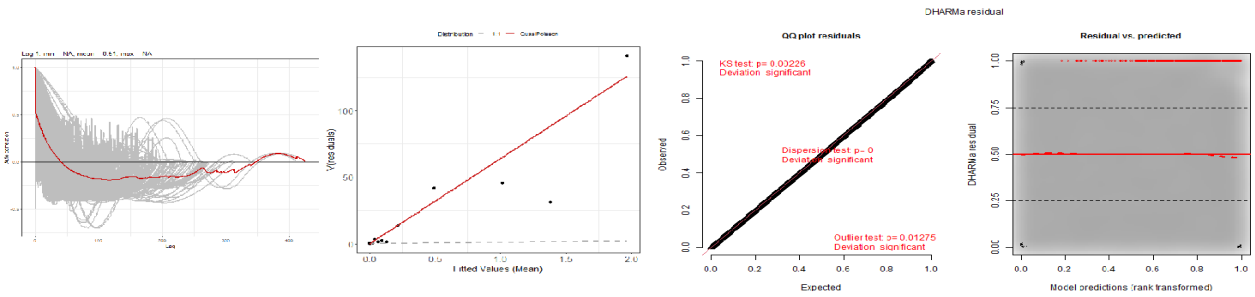

Figure 8.55. Figure showing diagnostics for the selected best spatial model. Left-most panel: within-block autocorrelation function, with the grey lines representing the residual correlation observed in each transect and the red line the average of these values across transects. Second panel: the estimated Tweedie mean-variance relationship (red line) against observed values (black symbols), with grey dashed line showing 1:1 relationship for reference. Third and right-most panel: QQplot and residuals against predicted values. The red stars are outliers and the red line is a smooth spline around the mean of the residuals.

8.14.4 Risk-mapping

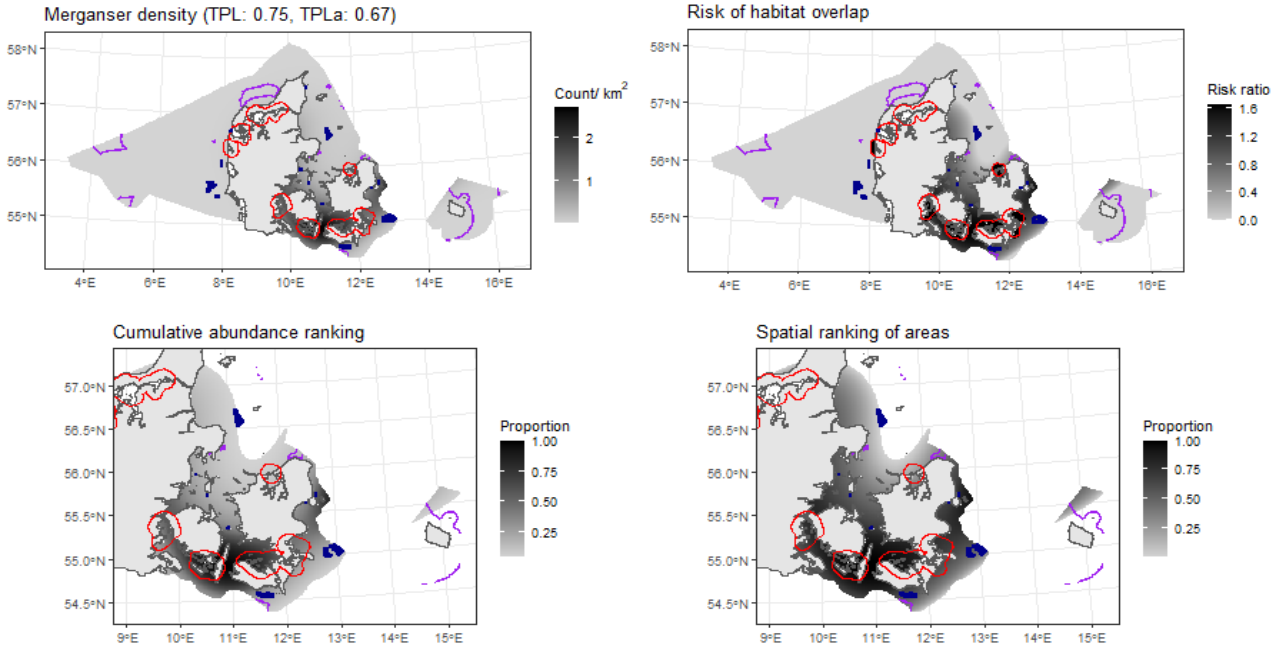

Figure 8.56. Figure showing the rescaling of estimated density distribution to habitat risk for the species unit. Bottom left and right: species unit abundance and top-use areas as cumulative percentiles (up to 0.95 abundance, defining species unit range). Red polygons: SPAs designated for one or more species in the species unit. Purple polygons: low-risk areas identified in Figure 2.5. Blue symbols: existing wind turbines.

8.15 Common scoter. Species unit “Scoter”

8.15.1 Aerial survey dataset

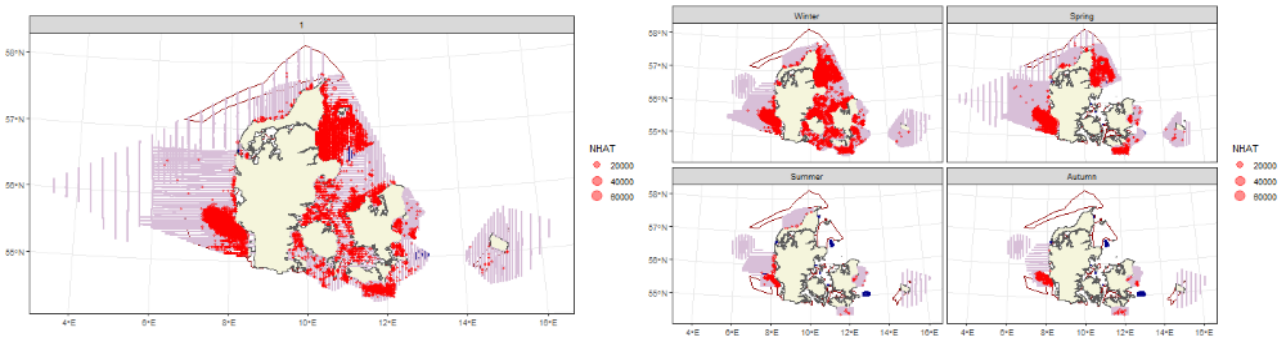

Figure 8.57. Maps showing observed counts (red) and effort segments (pink). Left panel: analyzed dataset for the species unit, pooled across those seasons the species unit was considered present (Table 1.4). Right panel: all data for the species unit, split across the seasons.

8.15.2 Spatial model outputs

Figure 8.58. Maps showing predicted counts (top) and boot-strapped uncertainty (bottom), overlaid with data. Data are shown as average counts in a grid of 20-km-wide hexagons.

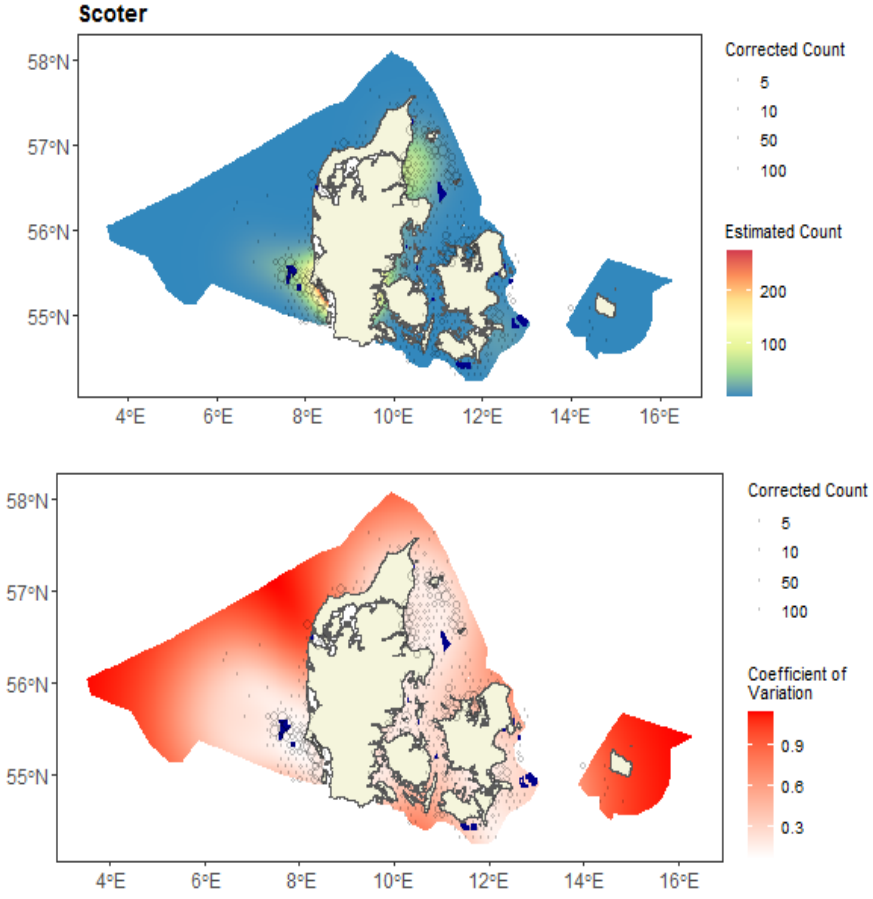

8.15.3 Diagnostics for the spatial model

Var. 1D	Var. 2D	# Pars.	Dispersion par.	CV score
NA	s(x,y, df=7)	8	5555.6	127899.2

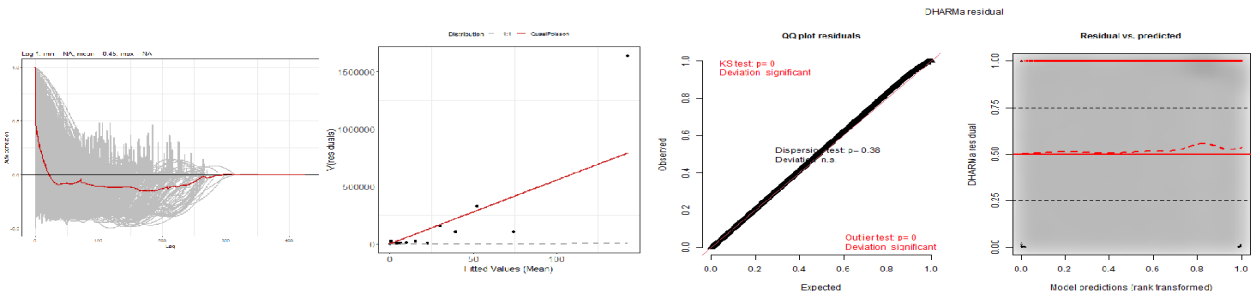

Figure 8.59. Figure showing diagnostics for the selected best spatial model. Left-most panel: within-block autocorrelation function, with the grey lines representing the residual correlation observed in each transect and the red line the average of these values across transects. Second panel: the estimated Tweedie mean-variance relationship (red line) against observed values (black symbols), with grey dashed line showing 1:1 relationship for reference. Third and right-most panel: QQplot and residuals against predicted values. The red stars are outliers and the red line is a smooth spline around the mean of the residuals.

8.15.4 Risk-mapping

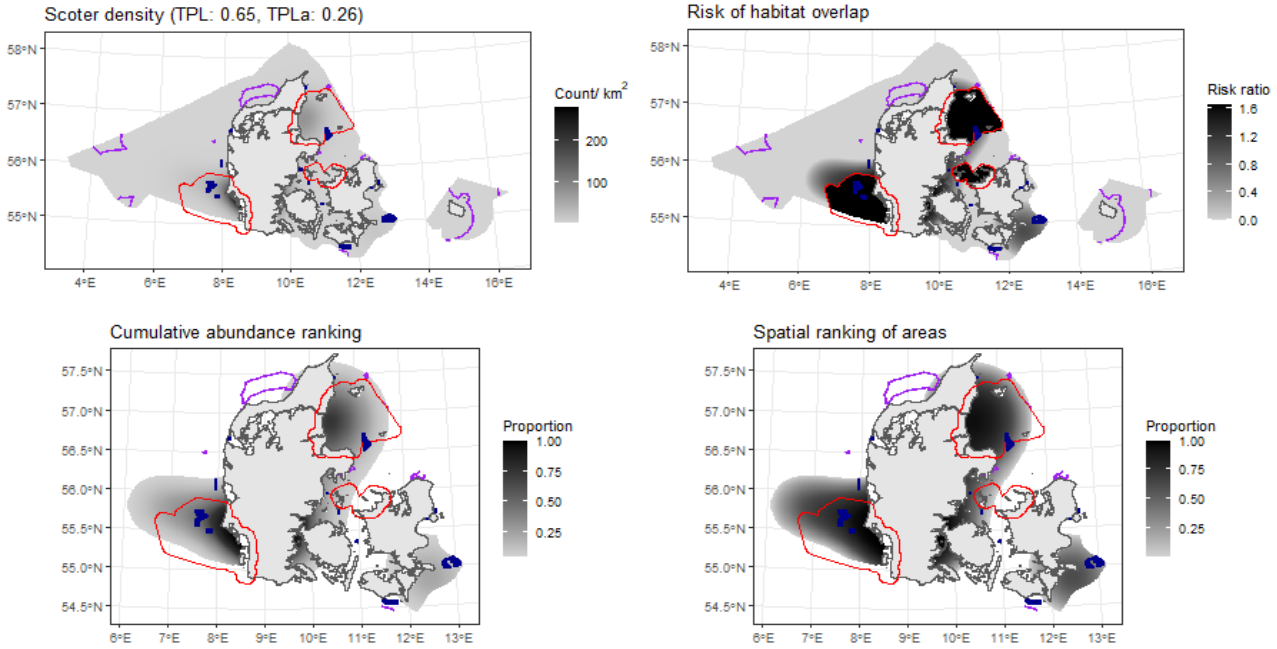

Figure 8.60. Figure showing the rescaling of estimated density distribution to habitat risk for the species unit. Bottom left and right: species unit abundance and top-use areas as cumulative percentiles (up to 0.95 abundance, defining species unit range). Red polygons: SPAs designated for one or more species in the species unit. Purple polygons: low-risk areas identified in Figure 2.5. Blue symbols: existing wind turbines.

8.16 Common tern/ arctic tern/ sandwich tern. Species unit "Tern"

8.16.1 Aerial survey dataset

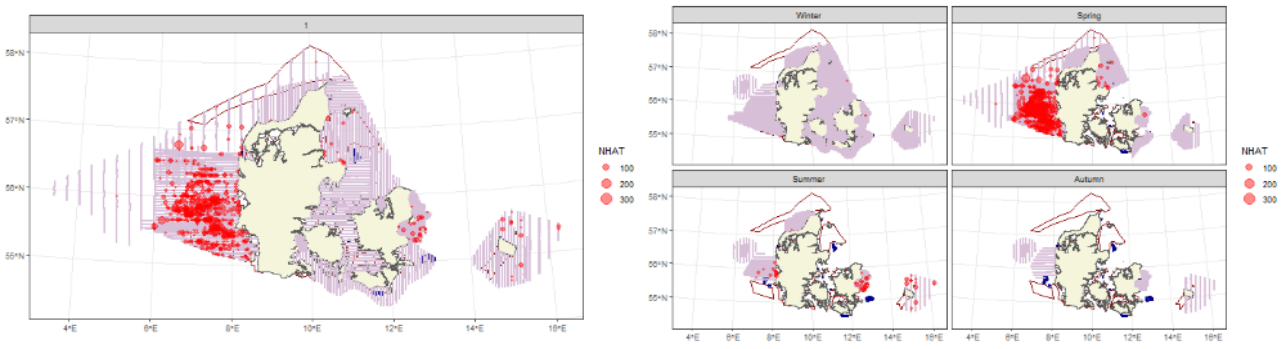

Figure 8.61. Maps showing observed counts (red) and effort segments (pink). Left panel: analyzed dataset for the species unit, pooled across those seasons the species unit was considered present (Table 1.4). Right panel: all data for the species unit, split across the seasons.

8.16.2 Spatial model outputs

Figure 8.62. Maps showing predicted counts (top) and bootstrapped uncertainty (bottom), overlaid with data. Data are shown as average counts in a grid of 20-km-wide hexagons.

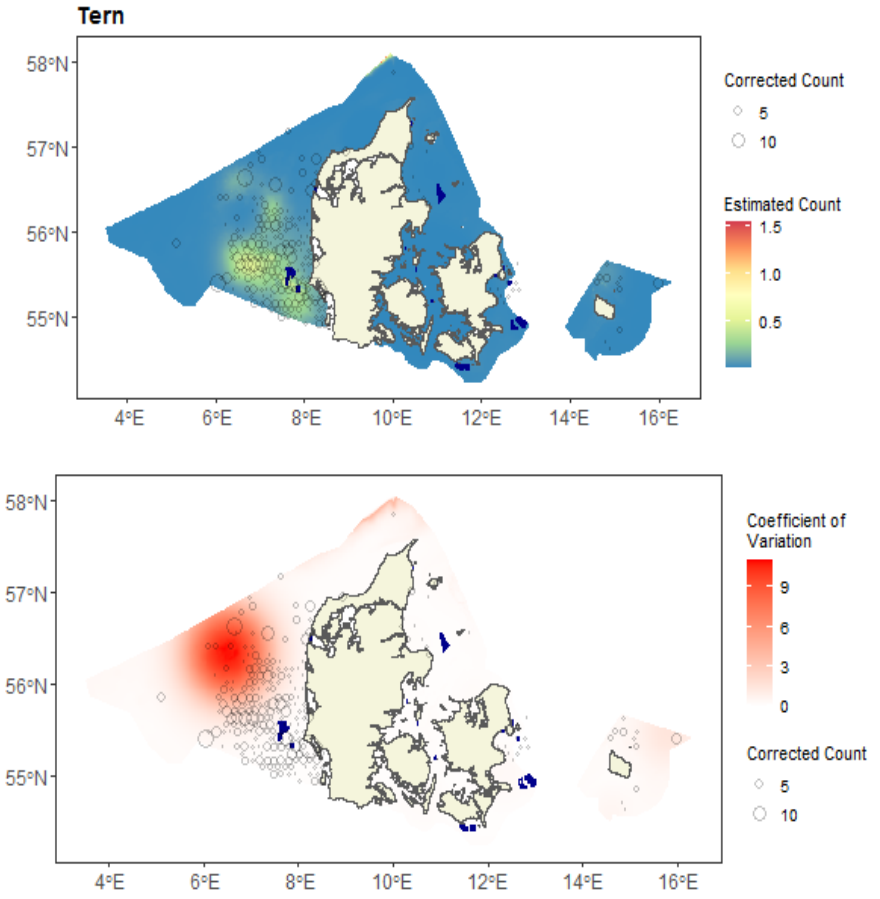

8.16.3 Diagnostics for the spatial model

Var. 1D	Var. 2D	# Pars.	Dispersion par.	CV score
s(depth, df=2)	s(x,y, df=12)	15	91.3	3.4

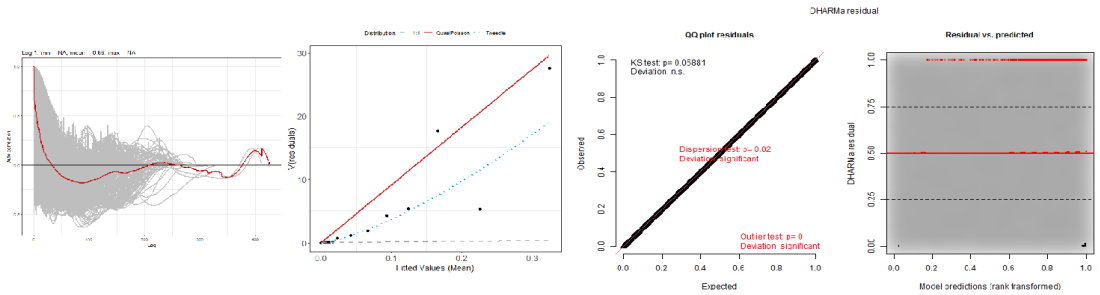

Figure 8.63. Figure showing diagnostics for the selected best spatial model. Left-most panel: within-block autocorrelation function, with the grey lines representing the residual correlation observed in each transect and the red line the average of these values across transects. Second panel: the estimated Tweedie mean-variance relationship (red line) against observed values (black symbols), with grey dashed line showing 1:1 relationship for reference. Third and right-most panel: QQplot and residuals against predicted values. The red stars are outliers and the red line is a smooth spline around the mean of the residuals.

8.16.4 Risk-mapping

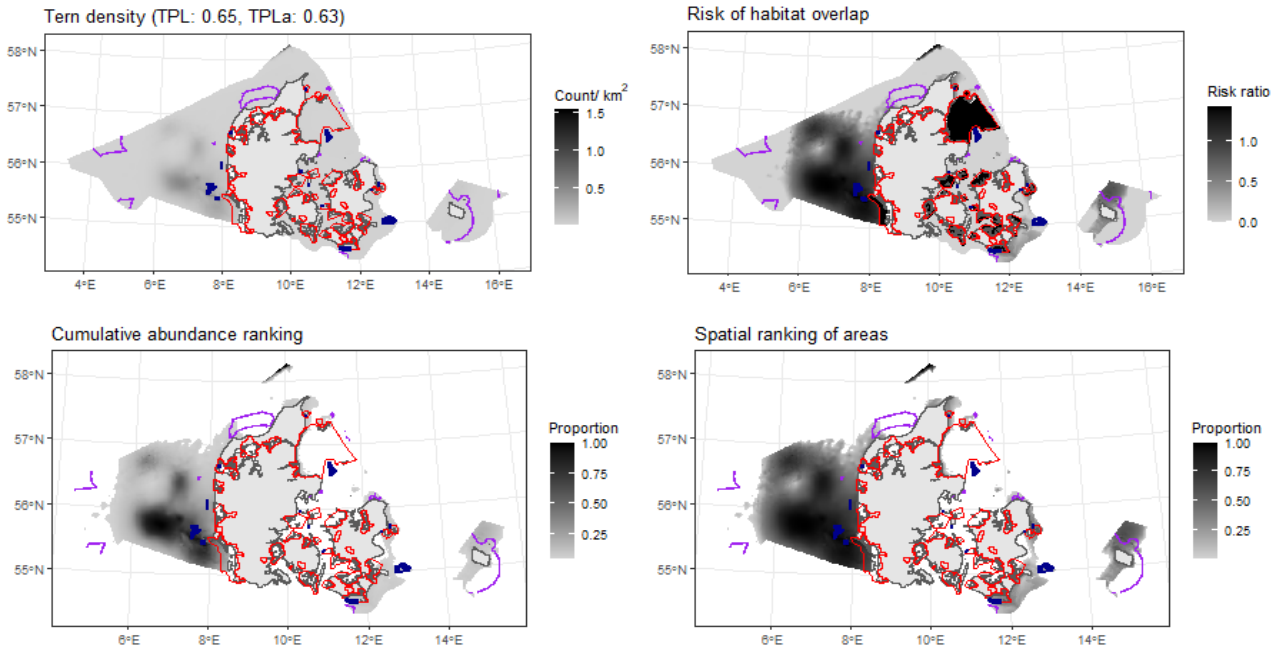

Figure 8.64. Figure showing the rescaling of estimated density distribution to habitat risk for the species unit. Bottom left and right: species unit abundance and top-use areas as cumulative percentiles (up to 0.95 abundance, defining species unit range). Red polygons: SPAs designated for one or more species in the species unit. Purple polygons: low-risk areas identified in Figure 2.5. Blue symbols: existing wind turbines.

8.17 Velvet scoter. Species unit “Velvetscoter”

8.17.1 Aerial survey dataset

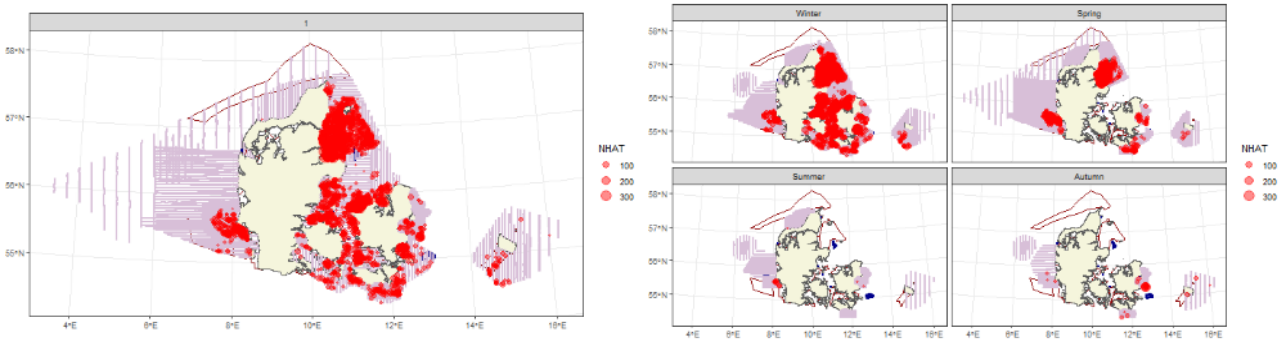

Figure 8.65. Maps showing observed counts (red) and effort segments (pink). Left panel: analyzed dataset for the species unit, pooled across those seasons the species unit was considered present (Table 1.4). Right panel: all data for the species unit, split across the seasons.

8.17.2 Spatial model outputs

Figure 8.66. Maps showing predicted counts (top) and boot-strapped uncertainty (bottom), overlaid with data. Data are shown as average counts in a grid of 20-km-wide hexagons.

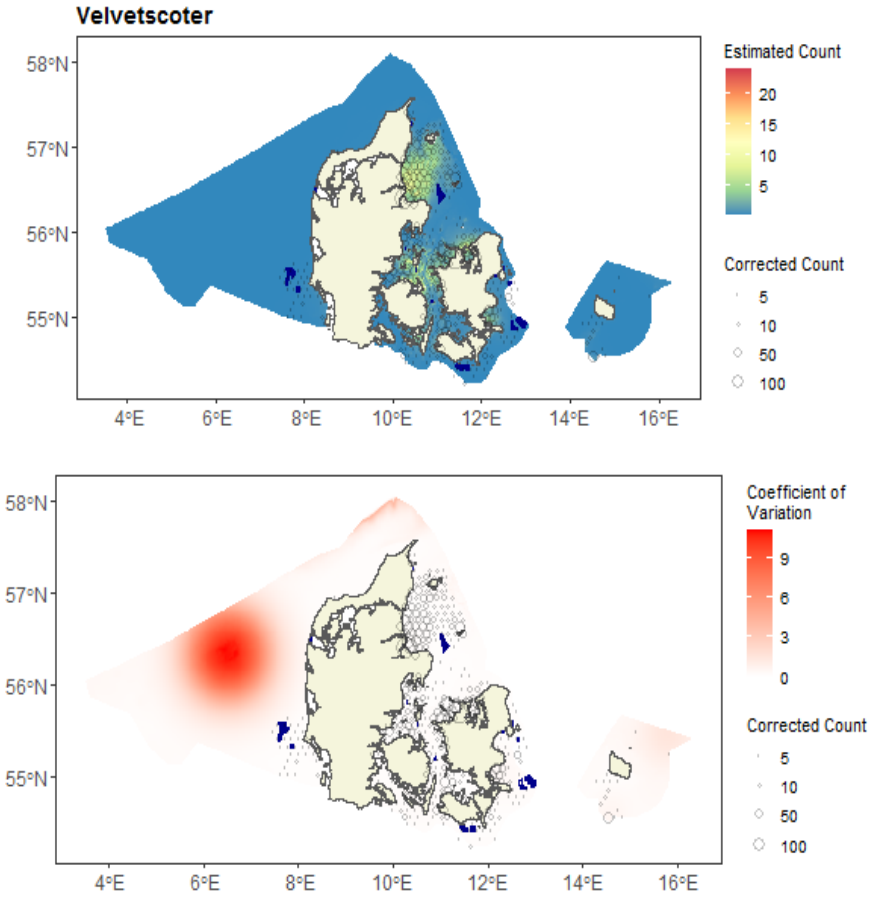

8.17.3 Diagnostics for the spatial model

Var. 1D	Var. 2D	# Pars.	Dispersion par.	CV score
depth, df=1	s(x,y, df=10)	12	91.7	15.6

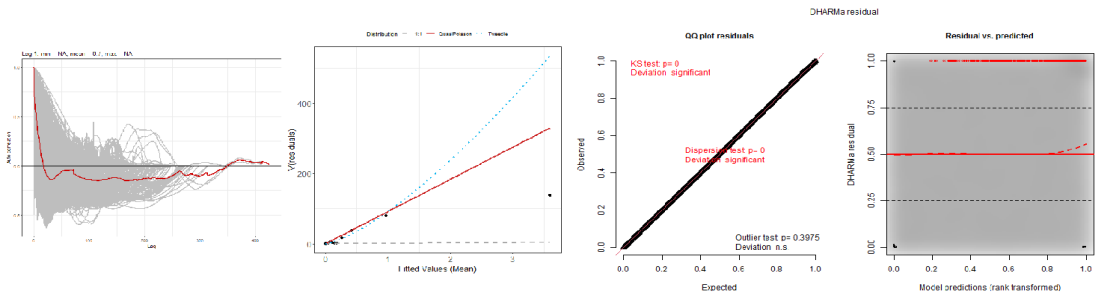

Figure 8.67. Figure showing diagnostics for the selected best spatial model. Left-most panel: within-block autocorrelation function, with the grey lines representing the residual correlation observed in each transect and the red line the average of these values across transects. Second panel: the estimated Tweedie mean-variance relationship (red line) against observed values (black symbols), with grey dashed line showing 1:1 relationship for reference. Third and right-most panel: QQplot and residuals against predicted values. The red stars are outliers and the red line is a smooth spline around the mean of the residuals.

8.17.4 Risk-mapping

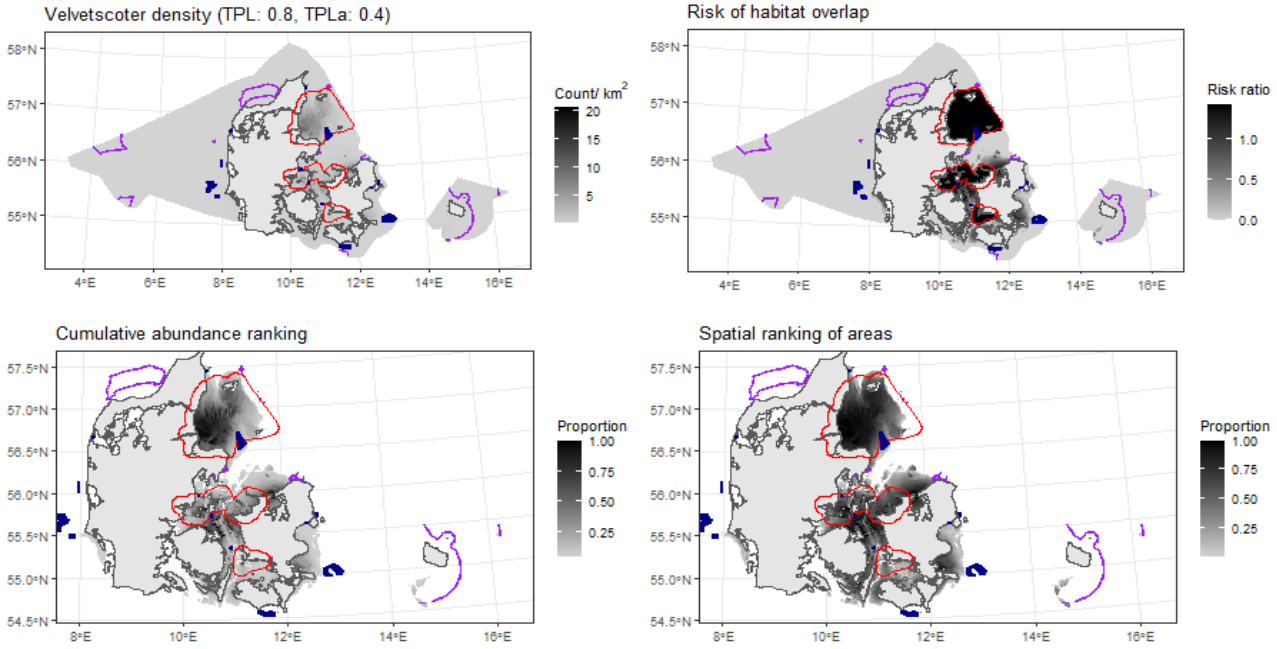

Figure 8.68. Figure showing the rescaling of estimated density distribution to habitat risk for the species unit. Bottom left and right: species unit abundance and top-use areas as cumulative percentiles (up to 0.95 abundance, defining species unit range). Red polygons: SPAs designated for one or more species in the species unit. Purple polygons: low-risk areas identified in Figure 2.5. Blue symbols: existing wind turbines.

9 Appendix 4: Overview of data input.

The access to data from aerial Distance Sampling line transect surveys for this risk assessment analysis was almost entirely built on survey data from Aarhus University. The data was a combination of surveys conducted in relation to the establishment of offshore wind farms in Denmark, supplied with data from the Danish national monitoring program (NOVANA) for migratory birds.

In the below Table 9.1 an overview of the data sets used for this analysis is presented. Data sets that are available, but has not been included in this analysis, is also listed below.

Table 9.1. Data summary for bird data, along with status for each dataset. Data status: Included: Data that has been included in the analysis; Excluded: Data that has been professionally assessed as not useful, e.g., due to age or collection method; Unavailable: Data that could not be obtained, e.g. because they have not been stored or not ready within the timeframe of the project; Unauthorized: Data for which permission to use could not be obtained. Data owner abbreviations: MST = Miljøstyrelsen, the Danish Environmental Protection Agency, ENS = Energistyrelsen, the Danish Energy Agency.

Data description	Project	Time period	Geographical area	Number of survey days	Transect Length (Km)	Data owner	Data Status*
Aerial line transect survey	Habitats directive related	2019	East Bornholm	1	608	MST	Included
Aerial line transect survey	Habitats directive related	2022	East of Bornholm	2	1168	MST	Included
Aerial line transect survey	HornsRev OWF	2000	Horns Rev	7	5055	Various	Included
Aerial line transect survey	HornsRev OWF	2001	Horns Rev	5	3988	Various	Included
Aerial line transect survey	HornsRev OWF	2002	Horns Rev	4	2780	Various	Included
Aerial line transect survey	HornsRev OWF	2003	Horns Rev	6	4583	Various	Included
Aerial line transect survey	HornsRev OWF	2004	Horns Rev	4	3398	Various	Included
Aerial line transect survey	HornsRev OWF	2005	Horns Rev	7	4696	Various	Included
Aerial line transect survey	HornsRev OWF	2006	Horns Rev	5	4244	Various	Included
Aerial line transect survey	HornsRev OWF	2007	Horns Rev	4	2891	Various	Included
Aerial line transect survey	HornsRev OWF	2011	Horns Rev	5	3150	Various	Included
Aerial line transect survey	HornsRev OWF	2012	Horns Rev	5	3158	Various	Included
Aerial line transect survey	HornsRev OWF	2023	Horns Rev	2	1131	Various	Included
Aerial line transect survey	HornsRev OWF	2024	Horns Rev	4	2364	Various	Included
Aerial line transect survey	OWF-related	2012	Jammer-bugten	4	2767	Vattenfall	Included

Aerial line transect survey	OWF-related	2013	Jammer-bugten	1	765	Vattenfall	Included
Aerial line transect survey	NOVANA	2008	Inner Danish waters 2008	13	6761	MST	Included
Aerial line transect survey	NOVANA	2013	Inner Danish waters 2013	15	8453	MST	Included
Aerial line transect survey	NOVANA	2016	Inner Danish waters 2016	14	7082	MST	Included
Aerial line transect survey	NOVANA	2019	Inner Danish waters 2020	2	1020	MST	Included
Aerial line transect survey	NOVANA	2020	Inner Danish waters 2020	12	6844	MST	Included
Aerial line transect survey	NOVANA	2023	Inner Danish waters 2023	13	8150	MST	Included
Aerial line transect survey	Energinet, North Sea I	2023	North Sea I survey area	10	6236	Energinet	Included
Aerial line transect survey	NOVANA	2024	North Sea I survey area	6	3711	Energinet	Included
Aerial line transect survey	Habitat Directive related	2019	Entire Danish North Sea 2019	5	3982	MST	Included
Aerial line transect survey	Habitat Directive related	2009	Eastern Danish North Sea	1	1062	MST	Included
Aerial line transect survey	Habitat Directive related	2016	Eastern Danish North Sea	4	2269	MST	Included
Aerial line transect survey	Habitat Directive related	2017	Eastern Danish North Sea	3	2342	MST	Included
Aerial line transect survey	Energinet, North Sea Energy Island	2022	North Sea Energy Island survey area	6	3581	Energinet	Included
Aerial line transect survey	Energinet, North Sea Energy Island	2023	North Sea Energy Island survey area	6	3563	Energinet	Included
Aerial line transect survey	North Sea South project	2003	Southern Danish North Sea	3	2557	MST	Included
Aerial line transect survey	North Sea South project	2004	Southern Danish North Sea	1	819	MST	Included
Aerial line transect survey	North Sea South project	2007	Southern Danish North Sea	1	872	MST	Included

Aerial line transect survey	North Sea South project	2008	Southern Danish	1	878	MST	Included
Aerial line transect survey	OWF-related	2019	North Sea Øresund/ Køge Bugt	2	1246	HOFOR	Included
Aerial line transect survey	OWF-related	2020	Øresund/ Køge Bugt	6	3769	HOFOR	Included
Aerial line transect survey	Rødsand/Nysted OWF related	1999	Rødsand/Nysted OWF Survey area	3	1730	Various	Included
Aerial line transect survey	Rødsand/Nysted OWF related	2000	Rødsand/Nysted OWF Survey area	7	3713	Various	Included
Aerial line transect survey	OWF related	2001	Rødsand/Nysted OWF Survey area	7	3704	Various	Included
Aerial line transect survey	Rødsand/Nysted OWF related	2002	Rødsand/Nysted OWF Survey area	4	2324	Various	Included
Aerial line transect survey	OWF related	2003	Rødsand/Nysted OWF Survey area	4	2203	Various	Included
Aerial line transect survey	Rødsand/Nysted OWF related	2004	Rødsand/Nysted OWF Survey area	4	2330	Various	Included
Aerial line transect survey	OWF related	2005	Rødsand/Nysted OWF Survey area	5	2908	Various	Included
Aerial line transect survey	Rødsand/Nysted OWF related	2007	Rødsand/Nysted OWF Survey area	3	1749	Various	Included
Aerial line transect survey	OWF related	2011	Rødsand/Nysted OWF Survey area	5	2915	Various	Included
Aerial line transect survey	Thor OWF-related	2019	Thor OWF survey area	8	4659	ENS	Included
Aerial line transect survey	NOVANA	2022	Aalborg Bugt	2	1374	MST	Included
Aerial line transect survey	NOVANA	2006	Inner Danish waters				Unavailable
Aerial line transect survey	NOVANA	2012	Inner Danish waters				Unavailable
Aerial line transect survey	NOVANA	2018	Inner Danish waters				Unavailable

Aerial line transect survey	OWF-related	Smålandsfar-vand/ Omø Staalgrunde	European Energy	Unavailable
Aerial line transect survey	OWF-related	Jammerland Bugt	European Energy	Unauthorized
Aerial line transect survey	OWF-related	Anholt OWF	Ørsted	Unavailable
Aerial line transect survey	Femern Baelt Project	Femern Bælt	Sund og Bælt A/S	Unavailable
Aerial line transect survey	Bornholm Energy Island	Rønne Banke	Energinet	Unavailable
Aerial line transect survey	Kriegers Flak OWF-related	Kriegers Flak	Energinet	Unavailable
Aerial line transect survey	Kattegat OWF-related	Central Kattegat	Energinet	Unavailable

MAPPING RELATIVE RISK TO SEABIRDS FROM OFFSHORE WIND ENERGY DEVELOPMENTS IN DANISH WATERS

To identify the most suitable areas for development of offshore wind energy in Danish marine areas, the Danish Energy Agency, in 2022, initiated a project to support the long-term planning of future offshore wind farms in Denmark. This report evaluates the relative risks to seabirds posed by offshore wind energy developments in Danish waters, focusing on habitat alteration, displacement, and collision risks.

Using a spatial risk-ranking algorithm, this report aims to identify the highest- versus lowest-sensitivity areas based on seabird distributions and abundances derived from aerial surveys conducted between 2000 and 2024. The algorithm combines species density distribution estimates with species-specific assessment targets and susceptibility to risks (habitat alteration, collision, displacement), producing maps highlighting zones where future offshore wind development could have relatively high impacts. Data on bird distributions and abundances were collected using the Distance Sampling line transect method (Buckland et al., 2001), comprising 243 aerial surveys conducted over 203 different days and covering more than 150,000 km of transects and more than 230,000 species detections. These surveys focused on capturing distributions of non-breeding birds. An overview of the data set is provided in Appendix 4.

Coastal and shallow areas showed the highest sensitivity in terms of potential habitat alteration and displacement risk in case of future wind energy development. These areas had high concentrations of divers, grebes and seaducks, and contained core habitats that wind farm structures and associated activities may disrupt. Seabirds susceptible to displacement, such as divers and some species of sea ducks, were particularly at risk, as these species tended to avoid areas around wind farms. These findings underscore the importance of protecting coastal and shallow areas with high seabird density, especially those designated as Special Protection Areas (SPAs).

Furthermore, offshore areas were identified as having higher relative collision risk, especially for species such as kittiwakes and other gull species, which are more prone to flying at heights within turbine blade sweep areas. The mapping identified particular offshore regions as high-risk zones for these species.

Additional data can provide extra information for the risk mapping exercise. For example, the current version of this work uses previously published expert assessment of collision risk for each species. However, GPS tracking data from birds can provide empirical information on migration routes and foraging activity. Such data from key species of colonial breeding birds during the 2023-2024 breeding seasons highlighted additional areas that could be at risk by illustrating marine area use patterns for sensitive species.

In conclusion, this relativistic risk assessment framework, grounded in quantitative assessment targets and species-specific susceptibility to risks, provides a decision-making tool for future wind farm planning to minimise ecological impacts on Denmark's seabird populations. Recommendations emphasise continued data collection and refinement of species-specific input parameters to enhance reliability of the algorithm, ultimately supporting a balanced approach to wind energy expansion and seabird conservation in Danish waters.

ISBN: 978-87-7156-929-2
ISSN: 2244-999X